3.4 Cooperative Phenomena in Complex Macroscopic Systems

Tensor-Network Representation of Gapless Kitaev Spin Liquids[1]

Naoki KAWASHIMA
Institute for Solid State Physics, University of Tokyo
Kashiwa-no-ha, Kashiwa, Chiba 277-8581

While the tensor network (TN) representation is recently used as the variational ansatz for various quantum many-body problems, it is also useful in capturing essence of novel quantum states, with the AKLT state as a well-known example. The Kitaev honeycomb model (KHM) is an exactly soluble model which exhibits gapless and gapped KSL ground states with fractionalized excitations. Recent successful realizations of Kitaev materials triggered a burst of theoretical investigations on it. In the present work, we propose a compact TN representation for KHM. Our variational wave function has the form $|\psi_n\rangle \equiv P_{\rm LG} R_{\rm DG}(\phi_n)$ $R_{\rm DG}(\phi_{n-1}) \cdots R_{\rm DG}(\phi_1)|(111)\rangle$ where $|(111)\rangle$ is the state where all spins are aligned to the (111) direction. The two operators $P_{\rm LG}$ and $R_{\rm DG}$ are essential in constructing the series of ansatze. The first one, $P_{\rm LG}$, is the 'loop-gas operator', which is defined as the sum of all TN operators (TPOs), each corresponding to a loop gas configuration. The second operator $R_{\rm DG}(\phi)$ is defined in a similar fashion, i.e., the sum of all TPOs corresponding to dimer-gas configurations. The parameter ϕ is such that $\tan\phi$ is the fugasity of the dimers.

The zero-th order ansatz ϕ_0, which is just a 'loop-gas state',

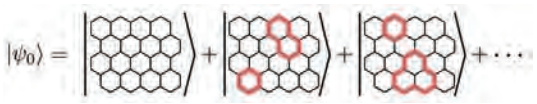

It has a remarkable feature that it is exactly identical to the classical loop-gas model. Therefore, without numerical calculation, we can say that it belongs to the Ising universality class. By optimizing $|\psi_1\rangle$, we can achieve much more accurate estimate (0.2% relative error in energy). Since the state is not exactly solvable any more, we must verify its critical properties. Our calculation shows, with more than 2 digit accuracy, that ψ_1 have the same critical properties regardless of the value of ϕ_1. Going to the even higher order approximation, ϕ_2, we can obtain very accurate result (0.007% error). From these results, we strongly believe

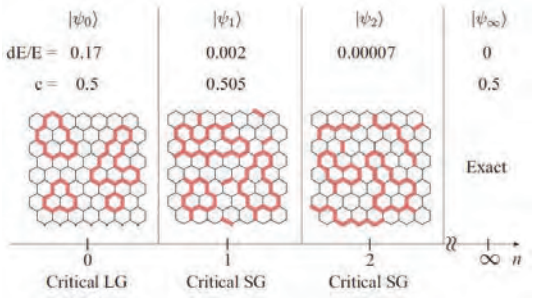

Figure 1: Comparison among the k-th order ansatze. While all belong to the same universality class, the energy converges quickly to the exact ground state energy of KHM.

that the present series of ansatze quickly converge to the exact ground state of the KHM (Fig.1), while retaining the essential properties of the KHM from the beginning ϕ_0.

[1] This report is based on H.-Y. Lee (ISSP), R. Kaneko (ISSP), T. Okubo (U. Tokyo) and N. Kawashima (ISSP), arXiv:1901.05786

Molecular Dynamics Simulation of a Kármán-Vortex Cavitation

Yuta ASANO, Hiroshi WATANABE, and Hiroshi NOGUCHI
Institute for Solid State Physics, University of Tokyo
Kashiwa-no-ha, Kashiwa, Chiba 277-8581

Cavitation is a flow phenomenon which is accompanied by a formation and growth of bubbles generated by a local pressure reduction by a high flow rate in a liquid [1]. The elucidation of the mechanism is very important in engineering fields because the cavitation causes various influences on fluid machinery. However, the mechanism of the cavitation inception remains unclear due to the difficulty to discuss the dynamics of microscopic bubble nuclei in a macroscopic flow field.

Therefore, in order to elucidate the mechanism of the cavitation from the molecular scale, we performed a molecular dynamics (MD) simulation of the Kármán-vortex cavitation using ISSP supercomputer.

In the present study, we investigated the cavitation effects on the Kármán vortex behind a circular cylinder by an MD simulation. To generate a multiphase flow, the interaction between fluid particles is employed by the Lennard-Jones (LJ) potential. The circular cylinder is modeled by a set of LJ particles whose positions are fixed on the surface of the cylinder. The computational cell is subjected to the periodic boundary condition. The temperature and the velocity in the downstream region of the cylinder are controlled by the Langevin thermostat [2]. In this way, uniform fluid can be re-introduced from the upstream side of the cylinder through the periodic boundary.

The top panel in Fig. 1 shows a snapshot of the density field at $T \simeq 1.4T_c$ (T_c: critical temperature). White color indicates a gas phase. The bubbles generated near the cylinder are caught into the Kármán vortex. Furthermore, at this temperature, it is also found that the bubbles are generated periodically in conjunction with the shedding period of the Kármán vortex. The bottom panel in Fig. 1 is a snapshot of the density field of a single-phase flow generated by using the Weeks-Chandler-Andersen potential for the interparticle interaction between fluid particles.

In order to investigate the influence of cavitation on the shedding frequency of Kármán vortex, the Strouhal number St is estimated. In the case of Fig. 1, $St \simeq 0.2$ is obtained both multiphase and single-phase flows. However, in the case of the multiphase flow, the oscillation of the lifting force caused

by vortex shedding disappear with decreasing temperature. This is because the generation of bubbles inhibits the formation of vortices and the vortex formation length significantly increases. On the other hand, in the case of single-phase flow, such a change does not occur because the decreasing temperature only causes a slight reduction in the viscosity. Therefore, we conclude that the cavitation inhibits the formation of the Kármán vortex.

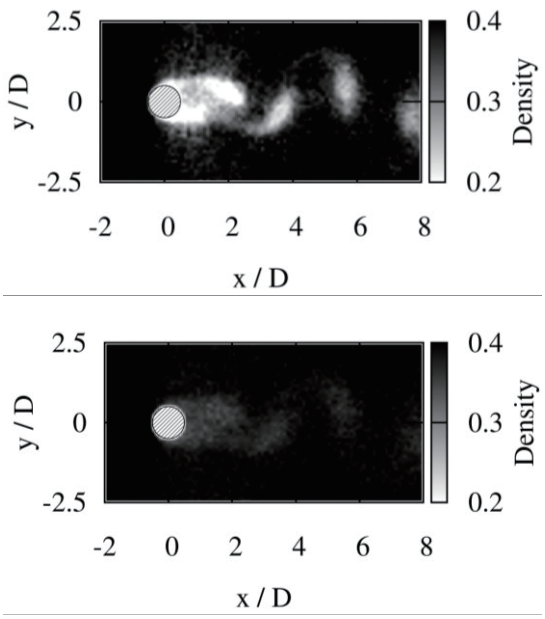

Figure 1: Snapshot of the density field of Lennard-Jones fluid (top) and Weeks—Chandler—Andersen fluid (bottom) at $T \simeq 1.4T_c$. The shaded area represents a cylinder of diameter D.

References

[1] R. E. A. Arndt: Annu. Rev. Fluid Mech. **34** (2002) 143.

[2] Y. Asano, H. Watanabe, and H. Noguchi, J. Chem. Phys. **148** (2018) 144901.

Spin and chiral orderings of the three-dimensional Heisenberg spin glass

Hikaru Kawamura and Takumi Ogawa

Graduate School of Science, Osaka University, Toyonaka 560-0043

The nature of the ordering of the three-dimensional isotropic Heisenberg spin glass (SG), a typical model of the so-called canonical SG, has been studied for years. Main issue has been whether the model exhibits the spin-chirality decoupling, i.e., exhibits two separate transitions, each associated with the glass ordering of the spin and of the chirality, $T_{SG} < T_{CG}$ [1]. The numerical situation, however, remains controversial: Some groups claimed $T_{SG} < T_{CG}$ [2], while some others $T_{SG} = T_{CG}$.

In this year`s project, we study the spin and chiral orderings of the 3D Heisenberg SG model with the nearest-neighbor random Gaussian coupling by extensive Monte Carlo simulations, to shed further light to the controversy. Larger system sizes up to $L=48$ (L the linear size) are studied both for periodic and open boundary conditions, and several independent physical quantities are computed including the correlation-length ratio and the Binder ratio are measured both for the spin and for the chirality, all of which are combined to give better estimates of T_{SG} and T_{CG} with higher precision than the preceding works. Indeed, we succeed in obtaining estimates of T_{SG} and T_{CG} as $T_{SG} = 0.130 \pm 0.001$ and $T_{CG} = 0.143 \pm 0.001$, with significantly less error bars than the previous works. The extrapolation of the finite-L data to $L=\infty$ is shown in the figure both for the spin and the chirality. The result gives a strong numerical support to the spin-chirality decoupling. The chiral-glass exponents are estimated to be $\nu_{CG}=1.39$ and $\eta_{CG}=0.43$, which supports the chirality scenario.

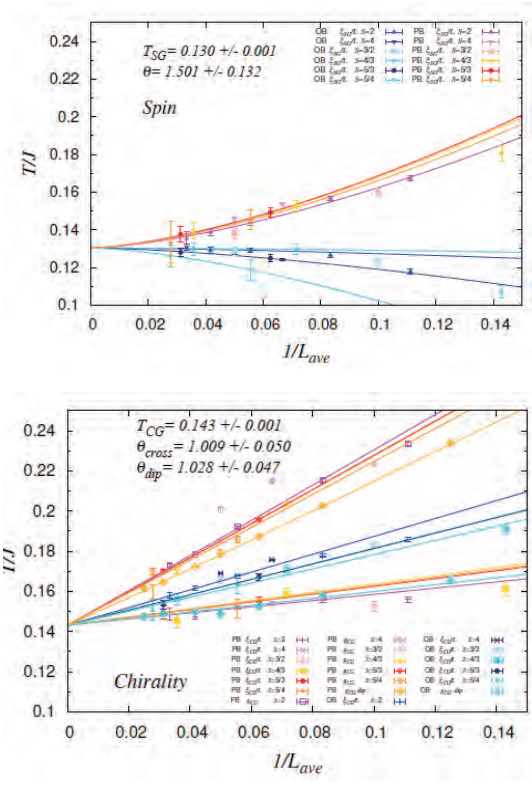

[1] H. Kawamura, Phys. Rev. Lett. **68**, 3785 (1992).

[2] D.X. Viet and H. Kawamura, Phy.s Rev. Lett. **102**, 027202 (2009).

Nature of the high-speed rupture of the two-dimensional Burridge-Knopoff model of earthquakes

Hikaru Kawamura, Koji Yoshimura and Shingo Kakui

Graduate School of Science, Osaka University, Toyonaka, Osaka 560-0043

Statistical physical study of earthquakes is often based on simplified models of various levels of simplification [1]. One of the standard models widely employed in statistical physical study of earthquakes might be the Burridge-Knopoff (BK) spring-block model. In the BK model, an earthquake fault is simulated by an assembly of blocks which is subject to the frictional force. More or less "realistic" friction law now standard in seismology might be the rate-and-state dependent friction (RSF) law. Then, it would be highly interesting to clarify the properties of the BK model obeying the RSF law. Though the statistical properties of the 1D BK model under the RSF law have been studied by the present authors' group [2], they have been limited so far to the 1D model. Under such circumstances, it is desirable to investigate the properties of the 2D BK model. In this year's project, we have tried such simulations on the 2D BK model under the RSF law, by concentrating on the high-speed rupture of main shocks [3].

The model consists of a 2D array of $N=L*L$ blocks which are subject to a RSF force. An obvious difference of the 2D model from the 1D counterpart might be its geometrical aspect. In fact, the 2D model exhibits in its stationary state a sequence of earthquake-like events of various sizes, among which very large events turn out to exhibit characteristic features. To illustrate this, we show in the above figure the way of the rupture propagation for a typical large event for $L=500$ system as color plots of the block sliding velocity. Indeed, the way of the rupture propagation is highly asymmetric and irregular in shape, a characteristic of the 2D system. For further details, please refer to ref. [3].

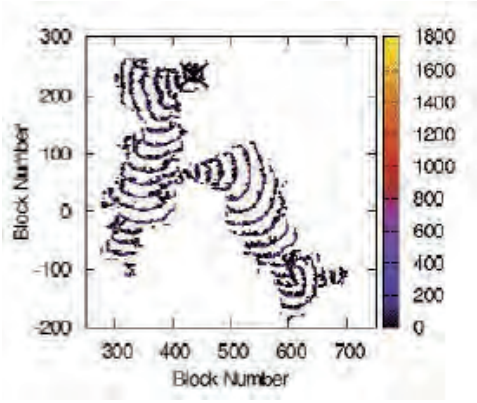

[1] For review, see, H. Kawamura, T. Hatano, N. Kato, S. Biswas and B.K. Chakrabarti, Rev. Mod. Phys. **84**, 839 (2012).

[2] H. Kawamura et al, Phys. Rev. E **95**, 04212 (2017).

[3] H. Kawamura et al, Phil. Trans. R. Soc. A **377** 20170391 (2018).

Numerical analysis of non-equilibrium dynamics of polymeric liquid and solid

Takahiro MURASHIMA

Department of Physics, Tohoku University,

6-3, Aramaki-Aza-Aoba, Aoba-Ku, Sendai, Miyagi 980-8578

We have developed two codes [1,2] implemented to massively parallel code, LAMMPS [3]. The one is for elongational flow successful in molecular dynamics simulation [1]. The other is multiscale simulation code coupling finite element method and molecular dynamics simulation [2].

Elongational flow was difficult on molecular dynamics simulation because the simulation box was collapsed within a finite simulation time. We can avoid this collapse if we set the initial simulation box not parallel to elongational direction. We have succeeded in obtaining the elongational viscosities on molecular dynamics simulation. The details are found in Ref [1].

Multiscale simulation coupling macroscopic continuum simulation and molecular dynamics simulation was difficult because the general deformation or strain was not dealt within the conventional technique on molecular dynamics simulation. The general strain can be decomposed to a rotation tensor and a stretch tensor by using QR decomposition. Using this technique, we have succeeded in coupling finite element method and molecular dynamics simulation and investigated a uniaxial loading of polymeric solid. The details are found in Ref [2].

References

[1] T. Murashima, K. Hagita, T. Kawakatsu: J. Soc. Rheol. Jpn. **46** (2018) 207.

[2] T. Murashima, S. Urata, S. Li: arXiv: 1902.09171.

[3] S. Plimpton: J. Comp. Phys. **117** (1995) 1.

How to conserve angular-momentum in discretization of Navier-Stokes equation for viscous fluids

Hiroshi NOGUCHI
Institute for Solid State Physics, University of Tokyo, Kashiwa, Chiba 277-8581

Although the Navier-Stokes equation (NSE) is derived under angular-momentum conservation (AMC), numerical simulation methods often lack it. We revealed how AMC is lost in the discretization of Navier-Stokes equation and how to recover it [1].

In conventional viscous fluids that do conserve angular momentum, the stress is expressed by a symmetric tensor: $\boldsymbol{\sigma} = -P\mathbf{I} + \eta(\nabla\mathbf{v} + (\nabla\mathbf{v})^{\mathrm{T}}) + \lambda(\nabla\cdot\mathbf{v})\mathbf{I}$. NSE is derived from this stress and $\rho D\mathbf{v}/Dt = \nabla\boldsymbol{\sigma}$:

$$\rho\frac{D\mathbf{v}}{Dt} = -\nabla P + \eta\nabla^2\mathbf{v} + (\eta+\lambda)\nabla(\nabla\cdot\mathbf{v}), \quad (1)$$

where D/Dt is the Lagrangian derivative. The second term in the shear stress, $\eta(\nabla\mathbf{v})^{\mathrm{T}}$, and compression stress, $\lambda(\nabla\cdot\mathbf{v})\mathbf{I}$, degenerately gives the last term in NSE. When the second shear stress is removed, it still results in the same equation if the coefficient is adjusted as $\lambda^{(-)} = \eta + \lambda$. Thus, the NSE can be obtained in the absence of AMC: *i.e.*, NSE by itself does not guarantee AMC. The AMC violation is caused by the implementation of these degenerated viscous terms.

We clarified how AMC is lost using Lagrangian finite volume method (LFVM). The velocity evolution of a FVM cell of volume V_i is given by

$$M_i\frac{D\mathbf{v}_i}{Dt} = \int_{V_i}\nabla\boldsymbol{\sigma}\,dV = \int_{S_i}\boldsymbol{\sigma}\hat{\mathbf{n}}\,dS \quad (2)$$

$$= \int_{S_i} -P\hat{\mathbf{n}} + \eta(\hat{\mathbf{n}}\cdot\nabla)\mathbf{v}_i + \eta\nabla v_{\mathrm{n}} + \lambda(\nabla\cdot\mathbf{v})\hat{\mathbf{n}}\,dS, \quad (3)$$

where $v_{\mathrm{n}} = \mathbf{v}\cdot\hat{\mathbf{n}}$ is the velocity normal to the interface. The momenta of the neighboring cells are transported via the stress on the interface surface between the cells. On the other hand, the integration of NSE using the divergence theorem can give a velocity evolution that DOES NOT conserve the angular momentum:

$$M_i\frac{D\mathbf{v}_i}{Dt} = \int_{S_i} -P\hat{\mathbf{n}} + \eta(\hat{\mathbf{n}}\cdot\nabla)\mathbf{v}_i + (\eta+\lambda)(\nabla\cdot\mathbf{v})\hat{\mathbf{n}}\,dS. \quad (4)$$

Because the third term in Eq. (3) is missing, the stress is asymmetric. To maintain AMC, the degenerated terms must be separately integrated in accordance with their stress origins. This relation holds in the other discretized NSE methods such as smoothed particle hydrodynamics.

The violation causes artificial rotations in multi-component fluids with different viscosities, although correct velocity evolutions are obtained for single-component fluids in the case that the boundary condition is given by the velocity. At the interface between two fluids or with a mobile solid object, AMC must be satisfied, whereas AMC can be neglected in bulk fluids. We also clarified that the condition for constant fluid rotation as a rigid body in a container rotating at a constant speed is not the AMC of the stresses, but the invariance of the viscous forces under a global rotation. To confirm our theory, we simulated the circular laminar flows of single- and binary-component fluids using two-dimensional LFVM. The results show excellent agreement with the analytical predictions for fluids with and without AMC.

References

[1] H. Noguchi: Phys. Rev. E **99**, 023307 (2019).

Designing Thermal Functional Materials via Materials Informatics

Junichiro SHIOMI

Department of Mechanical Engineering, The University of Tokyo

7-3-1 Hongo, Bunkyo, 113-8656

Heat transport plays an important role in thermal management applications. However, it is challenging to design the detail thermal functional materials due to various degrees of freedom. Materials informatics (MI), which has been considered as the fourth paradigm of science in addition to theory, simulation, and experiment, is now a promising way to accelerate the discovery and design of materials with desired thermal property.

This year we have successfully realized the wavelength-selective thermal emitter with ultra-narrow band based on aperiodic multilayer metamaterials designed by Bayesian optimization, as shown in Fig. 1. This is the first time to demonstrate the possibility of using simple multilayer structure for extremely high Q-factor.

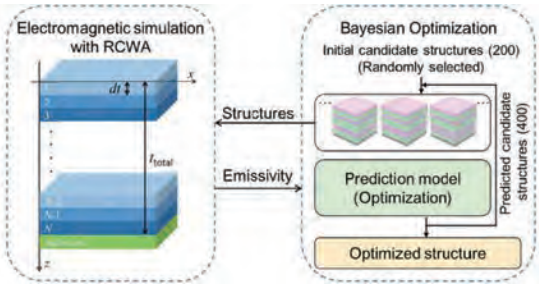

Figure 1: Schematics of Bayesian optimization for thermal radiation design.

The general optimization process can be easily understood from Fig. 1. After learning from the initial randomly-chosen training data, predictive thermal radiation property distribution can be estimated. Then it suggests new candidate structures which have high possibility to be high thermal radiation property. Those selected candidate structures were further evaluated by accurate calculation and added in training data for Bayesian optimization. After several iterations, the optimal structure can be identified. As shown in Figure 2 (a), the peaks for designed optimal structures were targeted 5, 6, 7 μm with high Q-factor of 217, 273 and 233.

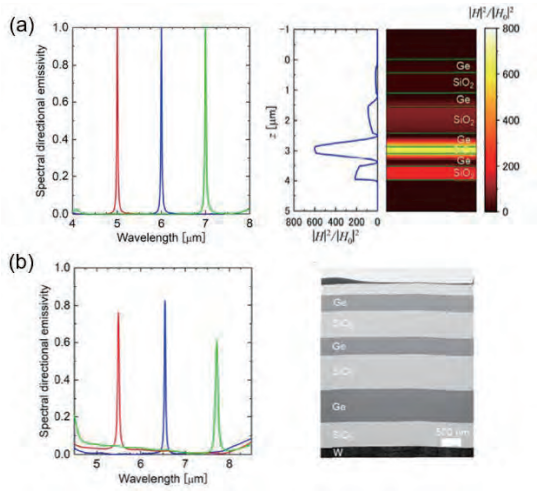

Figure 2: Thermal emitter design by Bayesian optimization, (a) Simulation, and (b) experiment.

For experimental structures show in Fig. 2 (b), a slight red shift for the targeted wavelength was observed and the amplitude for peak emissivity values were 0.76, 0.83 and 0.61 μm respectively with Q-factor of 132, 188, and 109 because the layer thicknesses of the actual fabricated samples somewhat deviated from the designed optimal case. Still, the obtained Q-factor 188 is very high and is the best experimental value among the multilayered metamaterials reported so far.

Besides the thermal radiation design, we also applied Monte Carlo tree search (MCTS) to optimize the interfacial Si-Ge roughness [2-4] for heat transport as shown in Fig. 3 (a). During the optimization, we divide the design region to 10 tree layers, the thickness of each layer is 5.43 Å, and each node in the tree has four child (0, 1, 2, 3), this gives the total number of candidates of 1048576.

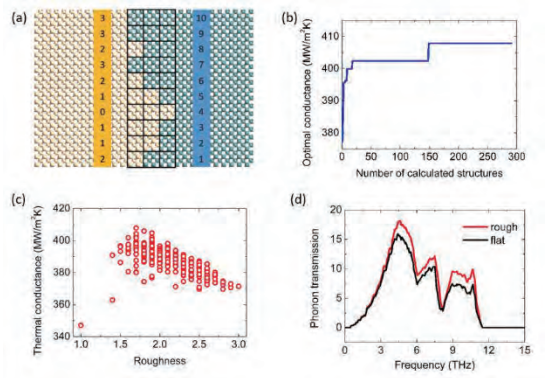

Figure 3: Interfacial roughness design by Monte Carlo tree search

As shown in Fig. 3 (b), within around 300 structures calculation, the interfacial thermal conductance quickly increases from 377 $MWm^{-2}K^{-1}$ to 408 $MWm^{-2}K^{-1}$. Figure 3 (c) shows the interfacial thermal conductance versus the roughness. The result indicates that the maximum interfacial thermal conductance appears in the middle value of interfacial roughness, which is not intuitive. By comparing the phonon transmission of the optimal and flat interface shown in Fig. 3 (d), we can find that the transmission in the middle frequency range from 4 to 10 THz is obviously enhanced.

In summary, (1) we have demonstrated the possibility of using simple multilayer structure for extremely high Q-factor based on Bayesian optimization, (2) we have designed non-intuitive rough interfacial structure to enhance heat transport via Monte Carlo tree search.

References

[1] A. Sakurai, K. Yada, T. Simomura, S. Ju, M. Kashiwagi, H. Okada, T. Nagao, K. Tsuda, J. Shiomi, ACS Central Science 5, 319, 2019.

[2] S. Ju, T. M. Dieb, K. Tsuda, J. Shiomi, Optimizing interface/surface roughness for thermal transport. NIPS 2018 Workshop: Machine Learning for Molecules and Materials, Montréal, Canada, 2018.

[3] T. M. Dieb, S. Ju, J. Shiomi, K. Tsuda, Monte Carlo tree search for materials design and discovery, MRS Communications, accepted, 2019.

[4] S. Ju, J. Shiomi, Nanoscale and Microscale Thermophysical Engineering **23**, 157-172, 2019.

Control of Phonon and Electron Transport Properties Using Mechanical Strain

Junichiro SHIOMI

Department of Mechanical Engineering, The University of Tokyo

7-3-1 Hongo, Bunkyo, 113-8656

A recent advance of nanotechnology allows us to design materials in nanoscale. When the length scale of nanostructures in materials reaches in the order of phonon wavelength, wave nature is expected to dominate their thermal transport properties. Despite many attempts to observe such coherent wave nature of phonons in experiments, very few studies have been reported the observation of coherent phonons except for at low temperature (< 10 K) or low frequency (< 1 THz) because phonons easily lose their phase information during scattering processes. Recently, Kodama *et al*. [1] have revealed that thermal conductivity of carbon nanotubes (CNTs) decreases by ≈ 60% and peak temperature of temperature dependent thermal conductivity decreases by ≈ 50 K due to encapsulation of fullerenes (top of Fig. 1). These results indicate that the encapsulated fullerenes act not as simple phonon scatterers like impurities but modulate phonon dispersion of outer single-walled CNTs (SWNTs). In this study, we show that fullerene encapsulation modulates coherent wave nature of outer SWNTs due to the periodic radial expansion. The radial expansion leads to softening and hardening of axial and radial modes, respectively, that should be caused by variation of force constants due to the induced strain. Moreover, the periodic strain leads to zone-folding effect and hybridization effect of phonon modes in outer SWNT and encapsulated fullerenes as shown in the closeup of Fig. 1. Our simulations reveal that the encapsulation-induced periodic strain makes an artificial superlattice of CNTs, which provides a new concept of tuning of microscopic thermal transport and strain-thermal engineering.

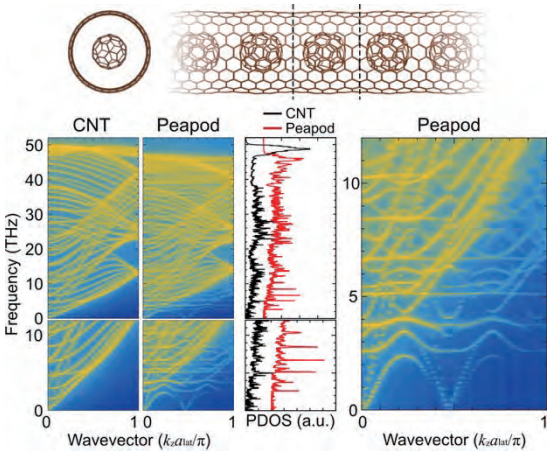

Fig. 1. Strain-induced zone-folding effects of carbon nanotubes (CNTs). [1,2] Periodicity of C_{60} fullerenes correspond to approximately four primitive unit cells of a SWNT. Bottom panels show spectral energy density and density of states (DOS) of a (10, 10) single-walled CNT (SWNT) and a C_{60}@(10, 10)SWNT peapod. k_z and a_{lat} are wavevector along the axis direction and the length of the primitive unit cell of the SWNT, respectively.

References

[1] T. Kodama, M. Ohnishi, W. Park, T. Shiga, J. Park, T. Shimada, H. Shinohara, J. Shiomi, and K. E. Goodson, Nat. Mater. **16**, 892 (2017).

[2] M. Ohnishi, T. Shiga, and J. Shiomi, Phys. Rev. B **95**, 155405 (2017).

Thermal Conduction Analysis of Cellulose Nanofibers by Molecular Dynamics

Junichiro SHIOMI

Department of Mechanical Engineering,

The University of Tokyo, 7-3-1 Hongo, Bunkyoku, 113-8656

The control of thermal energy is essential in advancing technology and preserving the environment. Cellulose nanomaterial thermal insulators have been shown to be superior to commonly-used thermal insulation materials such as silica in terms of affinity for environment and human body and thermal insulation performance. In order to get insight into the knowledge on heat conduction in cellulose nanomaterials, we have performed non-equilibrium molecular dynamics simulations for cellulose nanocrystal (CNC) and cellulose single-chain. Reedbush, Tsubame and Sekirei were used to conduct the simulations using LAMMPS and an in-house code to conduct the analysis on the thermal conductivity.

We found that thermal conductivities of CNC and cellulose single-chain range from 1.62 to 3.78 W/mK with increasing fiber lengths and the thermal conductivity of bulk CNC is calculated to be around 4.50 W/mK. Quasi-ballistic phonon transport in CNC is revealed and it suggests that shortening the length of CNC can lead to further reduction of the thermal conductivity.

The maximum length calculated in this study was only 30nm and this needs to extended to micron scale to be applied in industry, so further computational resources will be required.

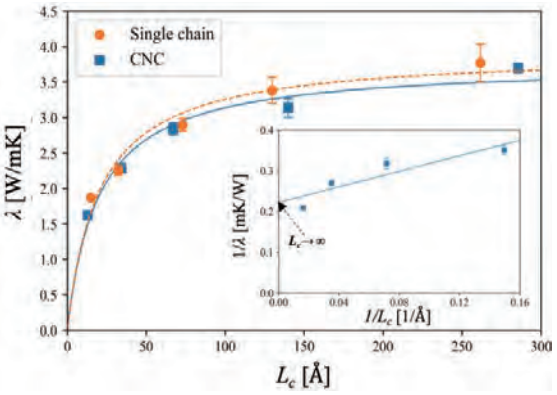

Fig. 1 Thermal conductivities of CNC and cellulose single chains as a function of the conduction region length. The inset shows extrapolation of thermal conductivity to infinite conduction-region length assuming the inverse proportionality.

Achievements

[1] M. Obori, D. Suh, S. Yamasaki, T. Kodama, T. Saito, A. Isogai, J. Shiomi: Phys. Rev. Appl. **11** (2019) 024044.

[2] M. Furuta, Bachelor's thesis (2019) the University of Tokyo.

Dynamics of fractional excitations in quantum spin liquid

Masafumi UDAGAWA
Gakushuin University
Mejiro, Toshima-ku, 171-8588

An experimental identification of quantum spin liquid (QSL) has been a central issue of condensed matter physics for decades. Since the QSL state is featureless in terms of local observables in its ground state, the excitations give the only possible route to its experimental identification. Accordingly, it is of crucial importance to clarify the nature of elementary excitations in this phase.

In this project, we focused on the two theoretical models of the QSL. One is Kitaev's honeycomb model. This model is an exactly solvable two dimensional model with QSL ground state. The Kitaev's spin liquid supports two species of fractional excitations: fermion and Vison. The dynamics of these excitations affects the observable dynamical response of this QSL. To clarify the dynamical response, we first developed an analytical solution of dynamical spin correlation for each sector of Vison configuration. By combining this solution with classical Monte Carlo method, we could obtain a solid theoretical scheme that allows an access to dynamical magnetic response at arbitrary temperatures. The advantage of this scheme is that a direct access to real-frequency representation is possible, without analytical continuation. In this project, we applied this scheme to the impurity problem, and obtained an anomalous zero-energy resonance due to the complex excitation of Vison and fermion [1].

As a second model, we also addressed the quantum spin ice model. This model is famous for its fractional excitations called magnetic monopole [2]. The nature of quantum magnetic monopole remains unclear. While they are expected to dominate the thermodynamic and transport properties of the system, the understanding of their basic properties, such as dispersion relations, is not well established. In this project, we combined degenerate first-order perturbation theory and exact diagonalization to obtain the excitation spectrum of quantum spin ice. The coupling to background spin ice manifold complicates the problem, and enlarge the Hilbert space even in a sector with small number of monopoles. We first made the breadth first search to set up Hilbert space of the two-monopole sector which satisfies the 2-in 2-out rule in all the tetrahedra except for those with monopoles. We then diagonalize the Hamiltonian on a lattice with 32 spins and obtain the two-monopole density of states. The obtained energy spectrum shows interesting phenomenon of dimensional transmutation, which leads to a steep "one-dimensional" Van-Hove singularity. This singularity is observable as a band-edge discontinuity in the inelastic neutron scattering.

References

[1] M. Udagawa: Phys. Rev. B **98** (2018) 220404(R)-1-5.

[2] M. Udagawa and R. Moessner: Phys. Rev. Lett. **122** (2019) 117201-1-6.

Quantized excitation spectra by confinement in quasi one-dimensional S=1 spin chains

Takafumi SUZUKI
Institute for Solid State Physics,
University of Hyogo, Shosha, Himeji, Hyogo 670-0083

In a pioneering study for the S=1/2 ferromagnetic (FM) Ising spin chain in weak transverse and longitudinal magnetic fields, it has been clarified that the excitation continuum shows the quantization by confinement of spinons [1]. The low energy excitation of the S=1/2 FM Ising spin chain is described by domain wall excitation that is achieved by flipping the spins of arbitrary length. The end of each domain wall carries ΔS=1/2 spinons and these spinons travel in the chain by the transverse field, which composes the excitation continuum. When the longitudinal field is further applied, it works as the linear potential for the flipped spins. Thus, the longitudinal field works as the confinement potential between the two spinons. This confinement potential causes the quantized excitation spectra whose excitation energies are well explained by the negative zeros of the Airy function (NZAF) [1]. The quasi-one-dimensional (Q1D) antiferromagnetic (AF) S=1/2 spin chains also have a chance to show the similar quantization. Shiba has argued [2] that the quantized spectra also appear in the Q1D AF Ising-like XXZ spin chains when the interchain interaction is very weak. In the Q1D Ising-like XXZ spin chains, the weak interchain interaction induces the staggered field in the spin chain at a low temperature. When the spinon-excitation continuum exists in the low-lying excitation, the staggered field works as the confinement potential between the spinons and causes the quantized spectra. In recent inelastic neutron scattering measurements on the Q1D S=1/2 spin chain compounds, $CoNb_2O_6$[3] and $(Ba/Sr)Co_2V_2O_8$[4,5], the quantized spectra explained by NZAF have been observed. The former and latter compounds are described by the FM Ising spin-chain model and the AF Ising-like XXZ spin-chain model, respectively.

In this project, we have investigated the possibility of the quantized spectra in the Q1D AF S=1 spin chains with the single-ion anisotropy by using infinite-time-evolving-block-decimation method. The Hamiltonian is written as

$$H = \sum_i [J\boldsymbol{S}_i \cdot \boldsymbol{S}_{i+1} + DS_i^{z2} + (-1)^i hS_i^z], \quad (1)$$

where $J > 0$. The last term of the Hamiltonian (1) denotes the staggered field originating from the weak interchain interaction. We have applied the real-time evolutions for the obtained ground-state wave function of the Hamiltonian (1) and calculated the dynamical spin-structure factor (DSF) via Fourier transformation of the dynamical spin-spin correlation function.

In the low-energy excitation of the AF S=1 spin chain, the multi magnon excitation appears. We have found that the magnon excitation continuum is quantized when the single-ion anisotropy is negatively large [6]. We discuss the origin of the quantization of the magnon excitation continuum below. In the following discussions, we suppose the bipartite system. In the bipartite system, all sites are classified into the two sublattice. First, we rotate the spin axis 180 degrees around the S^x axis for all spins in the sublattice B. The Hamiltonian is mapped onto $H=H_0+H_1$, where $H_0=\Sigma[-JS_i^zS_{i+1}^z+DS_i^{z2}-hS_i^z]$ and $H_1=\Sigma[S_i^+S_{i+1}^+-S_i^-S_{i+1}^-]$. Note that the staggered field is mapped onto the uniform longitudinal field. When the single-ion anisotropy is negatively large, the ground state of H_0 is given by the fully polarized state, ψ_0=|...+++++...> (or |...-----...>), where "+", "-" and "0" denote the site carrying S^z=1, -1, and 0, respectively. The low-lying excitation in the transverse component of the DSF is described by the dynamics of the excited state whose initial state is $\psi'=S^y\psi_0 \propto S^-\psi_0$ =|...++0++...>. Thus, this initial state is interpreted as an one magnon state. Next, we apply H_1 to the S^z=0 site in ψ'. The S^z =0 site shifts to the nearest-neighbor site with creating the S^z=-1 site,

namely ψ’ ~ |...++-0+...>. By applying H_1 to the S^z=0 site repeatedly, the domain comprising the S^z=-1 sites develops and it results in the excitation continuum. We further apply the staggered field *h*, it works as the linear potential for ψ’ ~ |...+-----0+...>. Therefore, the excitation continuum shows the quantized by the staggered field. For the longitudinal component, the similar discussion can be applied. In the longitudinal component of the DSF, the low-lying excitation is described by the two-magnon excitation, ψ’’=|...++00++...>. When we apply H_1 to the S^z=0 site, the S^z=0 site moves to the nearest-neighbor site creating the Sz=-1 site. By applying H_1 to the S^z=0 site repeatedly, the domain-wall excitation ψ’’=|...+0-----0+...> emerges. This domain-wall excitation constructs the excitation continuum. When the staggered field *h* is applied, it also works as the linear potential for ψ’’ and the excitation continuum is quantized. From the numerical results, we have confirmed that the excitation continuum is quantized by the weak staggered field, and the quantized excitation energies are well explained by NZAF for $D << 0$[6].

We have also investigated the DSF of the FM S=1 Ising spin chain and argued whether the ΔS=2 excitation continuum in the system shows the quantization or not [7]. We have found that in the DSF the domain-wall excitation carrying ΔS=2, which is expressed as the superposition of ψ ~ |...++----++...>, can appear below the isolated mode by single magnon excitation. This excitation continuum is also quantized by the weak longitudinal fields [7]. The obtained results indicate that several S=1 compounds have a potential to show the quantized spectra below the Neel temperature.

References

[1] B. M. McCoy and T. –T. Wu, Phys. Rev. B 18, 1259 (1978).
[2] H. Shiba, Prog. Theor. Phys. 64, 466 (1980).
[3] R. Coldea, et al., Science 327, 177 (2010).
[4] B. Grenier, et al., Phys. Rev. Lett. 114, 017201 (2015) .
[5] Q. Faure, et al., Nat. Phys. 14, 716 (2018).
[6] T. Suzuki and S. Suga, Phys. Rev. B
[7] T. Suzuki and S. Suga, accepted in J. Phys. Soc. Jpn.

Numerical Study on Quantum Phase Transitions of the Spin Tubes

Tôru SAKAI[1,2,3], Hiroki NAKANO[1,2], and Tokuro SHIMOKAWA[4],
[1]*Graduate School of Material Science, University of Hyogo, Kouto, Kamigori, Hyogo 678-1297, Japan*
[2]*Research Center for New Functional Materials, University of Hyogo, Kouto, Kamigori, Hyogo 678-1297, Japan*
[3]*Synchrotron Radiation Research Center, Kansai Photon Science Institute, Quantum Beam Science Research Directorate, National Institute for Quantum and Radiological Science and Technology (QST) SPring-8, Kouto, Sayo, Hyogo 679-5148, Japan*
[4]*Okinawa Institute of Science and Technology Graduate University, Onna, Okinawa 904-0945, Japan*

Frustrated quantum spin systems have attracted a lot of interest in the field of strongly correlated electron systems. The $S = 1/2$ threeleg spin tube [1] has the spin gap because of the frustration, while the three-leg spin ladder is gapless. In the previous work using the numerical exact diagonalization of finite clusters and the finite-size scaling analysis indicated that the lattice distortion of the three-spin unit from the equilateral triangle to the isosceles one gives rise to the quantum phase transition from the spin gap phase to the gapless one [2]. One of the candidate materials of the $S = 1/2$ three-leg spin tube is the compound $[(CuCl_2tachH)_3Cl]Cl_2$ [3, 4]. However, this material has a twisted three-leg structure. Thus it would be useful to investigate the effect of the same lattice distortion on the twisted three-leg spin tube. In this paper, the lattice distortion to the isosceles triangle of the $S = 1/2$ twisted three-leg spin tube is investigated by the numerical exact diagonalization of finite clusters and the finite-size scaling analysis. As a result it is found that a quantum phase transition from the spin gap phase to the gapless Tomonaga-Luttinger liquid phase with respect to the lattice distortion. The ground state phase diagram is also presented [5].

References

[1] T. Sakai, M. Sato, K. Okamoto, K. Okunishi, and C. Itoi, J. Phys.: Condens. Matter, 22, 403201 (2010).

[2] T. Sakai, M. Sato, K. Okunishi, Y. Otsuka, K.Okamoto, and C. Itoi, Phys.Rev. B, 78, 184415 (2008).

[3] J. Schnack, H. Nojiri, P. Koegerler, G. J. T. Cooper, and L. Cronin, Phys. Rev. B 70, 174429 (2004).

[4] J. -B. Fouet, A. Laeuchli, S. Pilgram, R. M. Noack, and F. Mila, Phys. Rev. B, 73, 014409 (2006).

[5] Y. Tachibana, Y. Ueno, T. Zenda, K. Okamoto and T. Sakai, in preparation.

Numerical Diagonalization Study on the Quantum Spin Liquid in Frustrated Spin Systems

Tôru SAKAI[1,2,3], Hiroki NAKANO[1,2], and Tokuro SHIMOKAWA[4],
[1]*Graduate School of Material Science, University of Hyogo, Kouto, Kamigori, Hyogo 678-1297, Japan*
[2]*Research Center for New Functional Materials, University of Hyogo, Kouto, Kamigori, Hyogo 678-1297, Japan*
[3]*Synchrotron Radiation Research Center, Kansai Photon Science Institute, Quantum Beam Science Research Directorate, National Institute for Quantum and Radiological Science and Technology (QST) SPring-8, Kouto, Sayo, Hyogo 679-5148, Japan*
[4]*Okinawa Institute of Science and Technology Graduate University, Onna, Okinawa 904-0945, Japan*

The spin nematic phase, which is a kind of multipole phases, has attracted a lot of interest in the field of the strongly correlated electron systems, as well as the quantum spin liquid phase. Using the numerical exact diagonalization, the density matrix renormalization group (DMRG) calculation, and the finite-size scaling analysis, it is found that some spin nematic and spin liquid phases are induced by external magnetic field in the anisotropic and/or frustrated quantum spin systems. In our previous work [1], it was found that a field-induced nematic phase appears at some critical field in the anisotropic spin ladder and the mixed spin chain. The nematic phase is characterized by the power-law decay in the correlation function of the second-order spin moment. In addition at some higher critical field a quantum phase transition can occur to the conventional field-induced Tomonaga-Luttinger liquid. Several typical magnetization curves calculated by DMRG are presented. Recently the field-induced nematic phase was observed on the frustrated spin ladder system [2]. So we study on a frustrated spin ladder system [3], using the numerical diagonalization and DMRG. As a result, it is found that several exotic quantum phases, including the spin-nematic liquid phase. We also report some exact eigenstates of the present model and present several interesting phase diagrams [4]. Our recent numerical diagonalization study [5] on the $S = 1$ spin ladder system with the easyaxis single-ion anisotropy suggested that the field-induced nematic Tomonag-Luttinger liquid (TLL) phase appears. In addition another spin nematic liquid phases were predicted in the three-leg ladder system with the ring exchange interaction [6].

References

[1] T. Sakai, T. Tonegawa and K. Okamoto, Physica Status Solidi B 247, 583 (2010) .

[2] N. Buttgen, K. Nawa, T. Fujita, M. Hagiwara, P. Kuhns, A. Prokofiev, A. P. Reyes, L. E. Svistov, K. Yoshimura, and M. Takigawa, Phys. Rev B 90, 134401 (2014) .

[3] T. Hikihara, T. Tonegawa, K. Okamoto and T. Sakai, J. Phys. Soc. Jpn. 86, 054709 (2017).

[4] T. Tonegawa, T. Hikihara, K. Okamoto, S. C. Furuya, and T. Sakai, J. Phys. So. Jpn. 87, 104002 (2018).

[5] R. Yamanokuchi, K. Okamoto and T. Sakai, to appear in Proceedings of Inter-

national Conference on Megagauss Magnetic Field Generation and Related Topics (2018).

[6] Y. Tachibana, K. Okamoto and T. Sakai, in preparation.

Nonequilibrium relaxation analysis for the antiferromagnetic triangular Heisenberg model in a uniform field

Y. Ozeki and K. Murayama

Graduate School of Informatics and Engineering, The University of Electro-Communications

The antiferromagnetic (AF) triangular Heisenberg model in a uniform field is investigated by means of the nonequilibrium relaxation (NER) method [1]. The magnetic field h is applied along the z-axis. When the magnetic field is absent, it has been pointed out that a topological phase called the Z_2 vortex phase, which is a Kosterlitz-Thouless (KT) phase of vector chirality, appears [2]. In the case of non-zero field, the system shows two different symmetries, the Z_3 symmetry associated with the three sub-lattice on triangular lattice and the $O(2)$ symmetry around the direction of the applied field. The phase diagram has been obtained previously by the equilibrium Monte Carlo simulation [3], in which a coplanar phase called the Y phase, a colinear phase along the z-axis called the up-up-down phase and a non-colinear phase called the cant phase appear from low field to high field in low temperature regime. The slow dynamics due to the low dimensionality and the frustrations make it difficult to equilibrate the system around the transition point, and some problems have remained unsolved.

We study the system by the use of the NER method, and clarify the order parameters and an appropriate initial states for each phase and each boundary of phases. Preliminary calculations show the validity for these choice. Here, we report the result for high field regime where the (non-colinear) cant phase appears in low temperatures. In the previous work [3], it was concluded that the Z_3 symmetry breaks with a second order transition and a topological transition occurs due to the $O(2)$ symmetry, where the transition points are coincide with each other. In contrast to this result, we obtain a different picture on the phase transition; we observe that the $O(2)$ symmetry also breaks with a second order transition, and the finite order for this symmetry exists in the cant phase. While it has been well-known by so-called the Mermin-Wagner theorem that there is no long-range order with continuous symmetry-breaking in 2D continuous spin systems, rigorously speaking, a strict condition is necessary for the order parameter on the contribution to the Hamiltonian, which is not satisfied in the present case. Thus, the theorem can not be applied.

The Hamiltonian we consider is

$$\mathcal{H} = |J| \sum_{\langle ij \rangle} \mathbf{S}_i \cdot \mathbf{S}_j - h \sum_i S_i^z,$$

where summation for $\langle ij \rangle$ is taken over all nearest-neighboring sites on a triangular lattice. In the present study, we investigate for $h/|J| = 5$ case. The initial state of relaxation is prepared as the ground state for $h/|J| = 5$ which can be obtained exactly. We estimate the relaxation of order parameters ψ_{ABC} for the Z_3 symmetry and m_y for the $O(2)$ symmetry; m_y is the projection of the xy component on the the initial state and detects the symmetry-breaking for $O(2)$ along the z-axis.

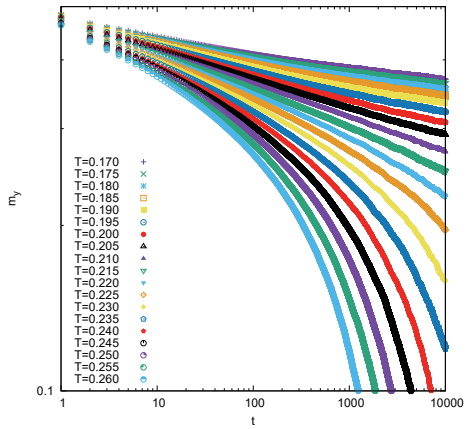

Figure 1: Relaxation of m_y for several temperatures.

Calculations are carried out on 1142×1143 triangular lattice with a skew boundary condition up to an observation time of 10^4 Monte Carlo steps (MCSs). About 40 samples are taken for statistical averaging. The estimations for m_y are plotted in Fig. 1. Using the improved dynamical scaling

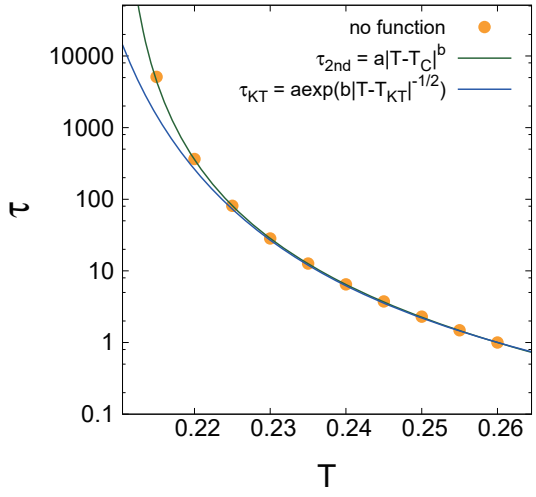

Figure 2: Comparison of estimated relaxation time.

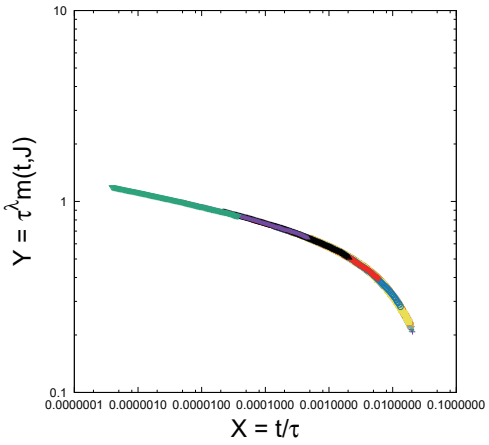

Figure 3: Scaling plot fore the high temperature regime $T \geq 0.215$.

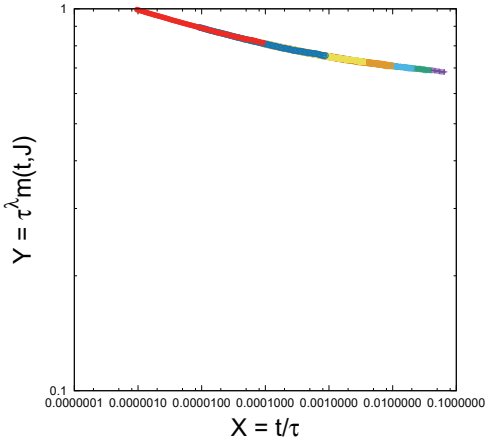

Figure 4: Scaling plot fore the low temperature regime $T \leq 0.200$.

analysis for the NER data [4], we analyze the dynamical scaling form,

$$m_y(t,T) = \tau(T)^{-\lambda} F[t/\tau(t)],$$

where T is the temperature measured in a unit of $|J|/k_{\rm B}$, $\tau(T)$ is the relaxation time, λ is a dynamical critical exponent, and t is the MCSs. We concentrate on the behavior of m_y. The result of $\psi_{\rm ABC}$ by dynamical scaling shows the second order transition consistent with the previous work [3].

Three types of scaling are performed for the data in higher temperature regime; assuming the second order transition with $\tau = a|T-T_{\rm c}|^{-b}$, assuming the KT transition with $\tau = a\exp\left[b/\sqrt{T-T_{\rm c}}\right]$, and no assumption for τ in which the estimated $\tau(T)$'s are more reliable than those obtained with an assumption. In Fig. 2, we plot the result for comparison of τ. It is shown that the second order transition is more favorable than the KT transition, which indicates that the $O(2)$ symmetry is broken and there might be a finite order for it. Thus, we analyze the data assuming the second order transition with $\tau = a|T-T_{\rm c}|^{b}$ for high temperature regime and low temperature one separately. The resulting scaling plots are shown in Figs. 3-4, with the estimated transition temperature $T_{\rm c} \sim 0.212$, which is consistent with the scaling analysis for $\psi_{\rm ABC}$ and that obtained in [3]. It is noted that, in Fig. 4, the upward trend of the scaling function reveals a finite ordering which indicates the break down of the $O(2)$ symmetry in two dimensional continuous system. While it has been well-known by so-called the Mermin-Wagner theorem that there is no long-range order with continuous symmetry-breaking in 2D continuous spin systems, rigorously speaking, a strict condition is necessary for the order parameter on the contribution to the Hamiltonian, which is not satisfied in the present case. Farther investigations are necessary to settle these problems.

References

[1] Y. Ozeki and N. Ito, J. Phys.: Math. Theor. **40** R149 (2007).

[2] H. Kawamura and S. Miyashita, J. Phys. Soc. Jpn. **53** 4138 (1984); H. Kawamura, et. al., J. Phys. Soc. Jpn. **79** 023701 (2010).

[3] L.Sebra, T. Momoi, P.Sindzingre, and N. Shannon, Phys. Rev. B**84** 214418 (2011)

[4] Y. Echinaka and Y. Ozeki, Phys. Rev. E**94** 043312 (2016); Y. Ozeki, A. Matsuda and Y. Echinaka, Phys. Rev. E**99** 012116 (2019).

Manipulation of quantum state by external fields

Seiji Miyashita
Department of Physics, University of Tokyo
Hongo, Bunkyo-ku, Tokyo, 113-0033

We studied the optical Bistability which is a discontinuous change of output light from a cavity as a function of strength of input. To investigate this phenomenon, we study the Tavis-Cummings model which represents a system of microcavity including atoms (or spins) with discrete energy levels contacting individual thermal bath. We have developed a highly parallelized code to study time evolution of the density matrix by a quantum master equation[1]. And we study the properties of bistability from a view point of an eigenvalue problem of time evolution operator. From the size dependence of photon density as a function of the strength of the driving force ξ, we determined the point of the first order phase transition point in the bistable region.

It is known that there are two types of regions of the steady state of such system[2]. In the low photon region, the photon and atoms strongly couple and the hybridization of both degree of freedom plays an important role, while in the high photon region, the photon plays as the classical electromagnetic field. So far, the optical bistability has been studied as a transition between the low and high photon region. In particular, in the present work, we studied the case where the photon-density in the cavity is low. We found that the transmission spectrum of detuning frequency behaves differently from the conventional case.

Moreover, we characterized the bistability by the size dependence of the relaxation time. The relaxation time is calculated from the second eigenvalue of the time evolution function. We found that the relaxation time increases exponentially with the size. We also find that it decrease inversely proportional to the sweeping rate of ξ (Fig. 1).

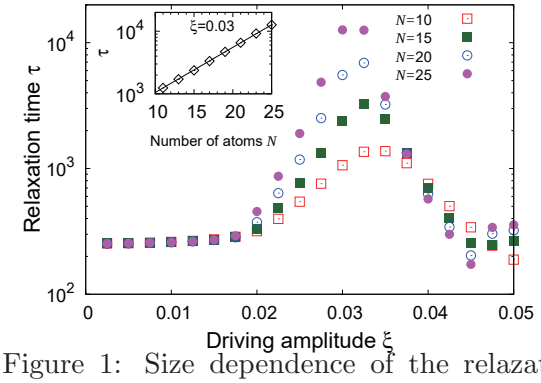

Figure 1: Size dependence of the relazation time in the bistable region of the optical bisatability

We also studied characterization of the effective spin ($S = 1/2$) induced by impurities in the so-called gapped spin chains by making use of the matrix product state (MPS). We first studied AKLT model as a prototype and found a characteristic response to the external field, and then we studied the bond-alternating Heisenberg antiferromagnetic chain (BAHAF) with MPS. We successfully constructed MPS and studied the precision of the MPS as a function of bond-dimension of the matrix [3].

References

[1] Tatsuhiko Shirai, Synge Todo, Hans de Raedt, and Seiji Miyashita, Phys. Rev. A **98**, 043802 (2018).

[2] S. Miyashita, et al.J. Phys. B Atomic Mol and Opt Phys 45, 124010 (2012).

[3] H. Nakano, Master thesis (University of Tokyo 2019)

Oligomerization process of full-length amyloid-beta peptides studied by molecular dynamics simulations

Satoru G. Itoh and Hisashi Okumura

Research Center for Computational Science,

Institute for Molecular Science, Okazaki, Aichi 444-8585

Many proteins aggregate at higher concentrations and form spherical substances called oligomers and acicular substances called amyloid fibrils. These protein aggregates cause more than 40 kinds of diseases. For example, aggregates of amyloid-β (Aβ) peptides cause Alzheimer's disease, and α-synuclein aggregates lead to Parkinson's disease. To overcome these diseases, it is essential to understand the formation mechanism of the protein oligomers and amyloid fibrils. For this purpose, we have been performing several molecular dynamics (MD) simulations of the oligomers and amyloid fibrils: We have so far revealed (a) the aggregation mechanism of Aβ fragments [1, 2], (b) conformations of full-length Aβ peptides at a hydrophilic/ hydrophobic interface [3], (c) structural difference between two ends of the Aβ amyloid fibril [4], and (d) disruption process of the Aβ amyloid fibril by a supersonic wave [5].

As for the aggregation of Aβ, we have so far mainly dealt with relatively simple systems such as Aβ fragments (i.e. not full length) in pure solvent. However, we are now trying more realistic systems with the full-length Aβ peptides. Aβ has two types, Aβ 40 (40 residues) and Aβ 42 (42 residues), which differ in the number of amino acids in the C-terminal region. It is known that the oligomerization and amyloid formation speed of Aβ42 are faster than those of Aβ40, but it is not clear why such a difference occurs. Initial formation of amyloid fibrils in the brains of Alzheimer's disease patients is thought to be caused by aggregation of Aβ42 rather than Aβ40. We performed a Hamiltonian replica-permutation MD simulation, the method of which was developed by our group, on each of the Aβ 40 dimer and Aβ 42 dimer systems. In this fiscal year, we extended the simulations to 1 μs per replica.

As a result, we observed the aggregation process as shown in Fig. 1. and found that Aβ42 forms intermolecular β-sheet more than Aβ40. We also found that this difference is caused by the fact that Aβ42 tends to form a β-hairpin more easily and a stable intermolecular β-sheet is formed between this β-hairpin and another Aβ42.

Fig. 1: Aggregation process of Aβ42 peptides.

References

[1] S. G. Itoh and H. Okumura: J. Phys. Chem. B **118** (2014) 11428.

[2] S. G. Itoh and H. Okumura: J. Comput. Chem. **120** (2016) 6555.

[3] S. G. Itoh, M. Yagi-Utsumi, K. Kato, and H. Okumura: J. Phys. Chem. B **123** (2019) 160.

[4] H. Okumura and S. G. Itoh: Sci. Rep. **6** (2016) 28422.

[5] H. Okumura and S. G. Itoh: J. Am. Chem. Soc. **136** (2014) 10549.

Doping effect on electronic structure and superconductivity in two-dimensional layered materials

Harald O. Jeschke
Research Institute for Interdisciplinary Science, Okayama University
Kita-ku, Okayama, Okayama 700-8530

Iron based superconductors are among the most intensively studied class of materials of the past decade. Significant insight into unconventional superconductivity was precipitated by the discovery of the first large family of high temperature superconductors since the discovery of the cuprates. At present, FeSe which belongs to the iron chalcogenide class of materials is at the forefront of theoretical and experimental efforts. In particular, the exceptionally large nematic region, the peculiar magnetism and the strong sensitivity to pressure are hot topics in this field. Among iron chalcogenide superconductors, lithium intercalated iron selenide, $Li_x(C_3N_2H_{10})_{0.37}FeSe$ is attracting interest [1]. In this material, it was reported experimentally [3] that the superconducting critical temperature T_c increases up to $T_c = 46$K ($x = 0.37$) and decreases when the doping level x is increased. This study suggests that increasing x changes the electronic structure dramatically, and the superconductivity changes.

We have investigated changes in electronic structure and superconductivity in lithium intercalated iron selenide, $Li_x(C_3N_2H_{10})_{0.37}FeSe$ under pressure and under doping. We perform density functional theory calculations using structural information from experiments, and we use spin fluctuation theory calculations to investigate superconductivity driven by spin fluctuation.

DFT calculations reveal that Lifshitz transitons occur as a function of x where a Fermi pocket disappears and appears around the Γ point in the unfolded Brillouin zone (Figure. 1). Furthermore, we construct five band tight binding models including the iron $3d$ orbitals, and clarified that these Lifshitz transitions leads to the enhancement of T_c as a function of x [4].

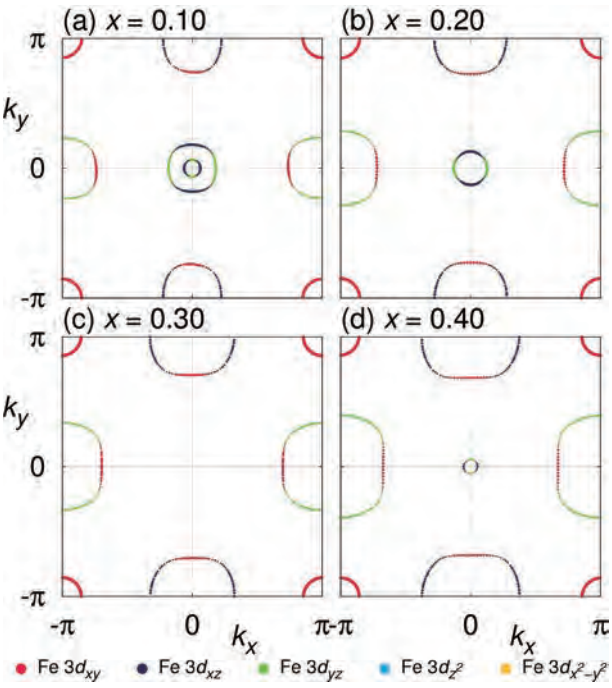

Figure 1: Change of Fermi surface in $Li_x(C_3N_2H_{10})_{0.37}FeSe$. The two hole pockets around Γ point disappears ((a), (b) and (c)). As increasing x more, one of them reappears (d).

References

[1] D. Guterding, *et al.*, Phys. Rev. **B** 91, 041112(R) (2015)

[2] M. Shimizu *et al.*, Phys. Rev. Lett. **121** (2018) 137001.

[3] R. J. Sun *et al.*, Phys. Rev. B **98** (2018) 214508.

[4] M. Shimizu *et al.*, in preparation.

Statistical-mechanical study for chiral magnets

Koji Hukushima
Department of Basic Science, University of Tokyo
3-8-1 Komaba, Meguro-ku, Tokyo 153-8902

In recent years, spin textures such as magnetic skyrmions or chiral solitons were observed in chiral magnets governed by antisymmetric Dzyaloshinskii-Moriya (DM) interactions. In magnetic systems, skyrmions were proposed theoretically as local spin vortices that are characterized by a topological charge. These fascinating topological excitations have since been extensively studied in experiments and through theoretical models.

In this project, we have numerically studied phase transitions of skyrmions in a two-dimensional chiral Heisenberg system using massively parallelized Monte Carlo simulations with a dedicated algorithm that avoids the difficulty of relaxation to equilibrium due to the long skyrmion lifetime. Our analysis relies on the analogy of the skyrmion system with interacting particle models in two dimensions. Two-dimensional particle systems, in the absence of a periodic substrate, cannot crystallize at finite temperature, that is, develop long-range positional order, but they can form a solid with algebraically decaying positional correlation functions and long-range orientational order.

At low temperature, two-dimensional chiral magnets in a magnetic field have many skyrmions as thermodynamically stable objects. In order to compute correlation functions of skyrmions at long distance, it is necessary to simulate very large systems of a two-dimensional chiral magnet. However, due to the low symmetry of chiral magnets, Monte Carlo simulation with local algorithms suffers from slow relaxation at low temperature. Our Monte Carlo method is based on modified heat-bath and over-relaxation algorithms. With the help of the local nature of both algorithms, their implementation on GPUs is rather easy to simulate the system with a checkerboard decomposition.

Each skyrmion is composed of Heisenberg spins on a discrete square lattice. Then, we assigned it a real-valued position using a local mask and compute high-quality spatial correlation functions at the fixed number of skyrmions[1]. This allows us to map the Heisenberg spin model to a model of interacting particles and to determine positional and orientational correlation functions, in analogy to what is done for two-dimensional particle systems.

At zero temperature we confirm that the ground state of the system is a triangular skyrmion crystal state with long-range positional order with locally triangular order minimally disturbed to accommodate the substrate potential. This state is incommensurate with the substrate at all densities. We find that commensurate square-shaped skyrmion crystals have higher energy than triangular crystals, even in the very dilute limit near the transition field at zero temperature.

At finite temperature, however, the ordered skyrmion state is a locally triangular "floating" solid, and it has long-range orientational correlations yet only quasi-long-range positional correlations. This solid nature of the low-temperature phase, characteristic of two-dimensional systems, is nontrivial in our system, which has discrete translational symmetry. The coupling potential affects the melting of the low-temperature skyrmion-solid state. As predicted by the KTHNY theory, we find that the skyrmion solid melts without an intermediate hexatic phase with a quasi-long-range orientational correlation.

[1] Y. Nishikawa, W. Krauth, K. Hukushima: Phys. Rev. B**99**, 064435 (2019).

Topological Order and Quantum Dynamics in Quantum Many-body Systems

Synge Todo
Department of Physics, University of Tokyo, Tokyo 113-0033, Japan
Institute for Solid State Physics, University of Tokyo, Kashiwa, 277-8581, Japan

We have developed various novel quantum Monte Carlo methods for quantum many-body systems with strong entanglement. For calculating the entanglement entropy of quantum spin systems, an efficient quantum Monte Carlo method has been developed. The entanglement entropy is one of the important indices that characterize quantum correlations and the topological order in quantum many-body systems. Our method works directly at absolutely zero temperature, and thus it is completely free from systematic errors coming from extrapolation to the zero temperature limit unlike the previous methods.

We have improved the path integral Monte Carlo method in continuous space. By using the event-chain Monte Carlo method and introducing special type of cuts in the world line configurations, we have achieved an efficient Monte Carlo update that breaks the detailed balance condition and can work in the canonical ensemble. We have applied this algorithm to a system of Bosons, and demonstrated that the convergence of distribution is much faster than the conventional method, and the time complexity with respect to the Trotter number is improved greatly.

We also have developed a nonlocal-update quantum Monte Carlo method for quantum dimer models on general lattices. Although there is no negative sign problem in the Hamiltonian of the quantum dimer models, Monte Carlo simulations had been very difficult due to the strong geometric restriction on the arrangement of dimers. By developing a method that can transition between different topological sectors, it becomes possible to discuss the phase diagram at finite temperatures in addition to absolute zero.

On the other hand, numerical methods based on the tensor network representation have been focused recently as they requires less computational cost than the exponentially expensive exact diagonalization. Representative methods include TRG and HOTRG. So far, the tensor network methods have been used mainly for uniform systems. We have extended HOTRG using projectors instead of isometries for non-uniform systems, and apply it to the Ising model with bond dilution. We have confirmed that the method using projectors converges much faster than the conventional one.

Spins coupled with photon degrees of freedom in the cavity exhibit a non-equilibrium phase transition with bistability in the number of photons. We have performed simulation based on the quantum master equations, and from the eigenvalues and eigenstates of the time evolution operator, we discussed the correspondence to the first order phase transition in the equilibrium system [1]. We also have calculated the hysteresis loop under the periodic modulation of laser intensity, from the viewpoint of the Floquet operator, and clarify that a dynamical phase transition phenomenon appears with respect to the period of modulation.

References

[1] T. Shirai, S. Todo, H. de Raedt, S. Miyashita, Phys. Rev. A **98**, 043802 (2018).

Novel phases in honeycomb lattice Kitaev materials

Tsuyoshi OKUBO
Department of Physics, The University of Tokyo
7-3-1 Hongo, Bunkyo-ku, Tokyo 133-0033

Recently, magnetic compounds with the strong spin-orbit interaction have attracted great interest. In several compounds, including Na_2IrO_3 and α-$RuCl_3$, the dominant magnetic interaction is induced by the strong spin-orbit coupling and it is considered to be the Kitaev interaction which is an Ising like anisotropic interaction with different spin component depending on the bonds. It is known that when there is only the Kitaev interaction (Kitaev model), the ground state of the $S = 1/2$ Kitaev model on the honeycomb lattice is a quantum spin liquid [1]. On the other hand, real compounds contain other interactions such as the Heisenberg interaction, further neighbor interactions, or the off-diagonal Γ interaction, which induce magnetic long range orders in these compounds at low temperature.

In order to clarify the nature of there Kitaev materials, we numerically calculate the ground states of the models with the Kitaev interaction and other interactions by means of a tensor network method. We represent the ground state wave function as a network of small tensors, and optimize each tensor element so that the energy expectation value becomes smaller. One of the most important aspect of such tensor network method is that by choosing proper tensor network structures, we can express the wave function of infinitely large systems by assuming a translational symmetry. We use the infinite tensor product states (iTPS), which is also called as the infinite projected entangled-pair states (iPEPS), as our tensor network states.

In this year, we mainly investigated the Kitaev-Gamma model where an off-diagonal interaction, the Γ term, exists in addition to the Kitaev interaction [2, 3]. The Hamiltonian of the model is given by

$$\mathcal{H} = \sum_{\gamma \in x,y,z} \mathcal{H}_\gamma, \tag{1}$$

and on z-bond,

$$\mathcal{H}_z = \sum_{\langle i,j \rangle_z} [K S_i^z S_j^z + \Gamma (S_i^x S_j^y + S_i^y S_j^x)]. \tag{2}$$

This model is considered to be an effective model for α-$RuCl_3$. In order to investigate the effect of the Γ term to the Kitaev spin liquid accurately, firstly we constructed a very accurate iTPS representation of the Kitaev spin liquid [4]. In the previous studies in the vicinity of Kitaev spin liquid, there was a serious difficulty for optimization of iTPS; it was not easy to obtain accurate Kitaev spin liquid wave function when we used random initial tensors. However, by using our iTPS representation of Kitaev spin liquid as the initial state, we obtained accurately optimized Kitaev spin liquid state even if away from the pure Kitaev model. Based on this technique we estimated that the Kitaev spin liquid state becomes unstable for $\Gamma/|K| \gtrsim 0.04$ for negative K, and, instead, a state which spontaneously breaks the lattice rotational symmetry is stabilized. This phase transition seems to be inconsistent with the previous numerical results by the exact diagonalization (ED) [2] or by the infinite density matrix renormalization group (iDMRG) [3]; they concluded that the Kitaev spin liquid state was stable for $\Gamma/|K| < \infty$.

In order to clarify this discrepancy, we might need further calculations with a larger tensor size and more sophisticated optimization techniques.

References

[1] A. Kitaev: Ann. Phys. **321** (2006) 2.

[2] A. Catuneanu, Y. Yamaji, G. Wachtel, H.-Y. Kee, and Y. B. Kim: npj Quantum Materials, **3**, (2018) 23.

[3] M. Gohlke, G. Wachtel, Y. Yamaji, F. Pollmann, and Y. B. Kim: Phys. Rev. B **97** (2018) 075126.

[4] H.-Y. Lee, R. Kaneko, T. Okubo, and N. Kawashima, arXiv:1901.05786.

Scaling theories of random topological and non topological systems

TOMI OHTSUKI[1]
TOHRU KAWARABAYASHI[2]
KEITH SLEVIN[3]
KOJI KOBAYASHI[4]
1) Dept. Phys., Sophia University, Chiyoda-ku, Tokyo 102-8554, Japan
2) Dept. Phys., Toho University, Miyama 2-2-1, Funabashi 274-8510, Japan
3) Dept. Phys., Osaka University, Toyonaka, Osaka 560-0043, Japan
4) IMR, Tohoku University, Sendai 980-8577, Japan

Recent discoveries of Weyl semimetal (WSM) have inspired extensive research of these novel topological materials. Here we have studied the effects of disorder on WSM. Based on the renormalization group analysis, we have proposed the scaling theory near the multicritical point of WSM-CI-Metal, and have verified the scaling behavior numerically [1]. We have shown that the Anderson localized phase appears between CI-Metal, while the transition is direct for WSM-Metal and CI-WSM. We have also discussed novel scaling behavior of CI-WSM transition [2].

We have also studied the Anderson transition using massively parallel supercomputing. The most precise estimations of the critical exponent for the Anderson transition have been made using the transfer matrix method. This method involves the simulation of extremely long quasi one-dimensional systems, and is inherently serial and is not well suited to modern massively parallel supercomputers. We show that this problem can be avoided by generating random sets of orthogonal initial vectors with an appropriate stationary probability distribution. We have applied this method to the Anderson transition in the three-dimensional orthogonal universality class and been able to increase the largest $L \times L$ cross section simulated from $L = 24$ (New J. Physics, **16**, 015012 (2014)) to $L = 64$ here. This permits an estimation of the critical exponent with improved precision and without the necessity of introducing an irrelevant scaling variable. In addition, this approach is better suited to simulations with correlated random potentials such as is needed in quantum Hall or cold atom systems [3]. In addition, we have calculated the distribution of Kondo temperature at the Anderson transition from the local density of states obtained by kernel polynomial method.

References

1. X. Luo, B. Xu, T. Ohtsuki, R. Shindou: Physical Reivew B **97**, 045129 (2018).
2. X. Luo, T. Ohtsuki, R. Shindou: Physical Review B **98**, 020201(R)(2018).
3. K. Slevin, T. Ohtsuki: Journal of the Physical Society of Japan **87**, 094703 (2018).

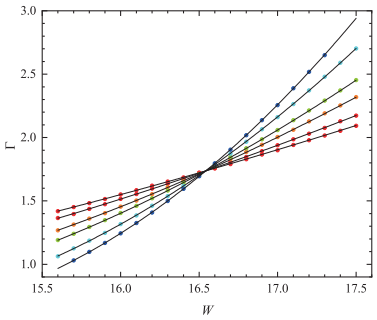

Figure 1: The estimates of normalized Lyapunov exponent $\Gamma = \langle \tilde{\gamma}_N \rangle L$ for width L =12, 16, 24, 32, 48 and 64 for various disorders W together with the finite size scaling fit (solid lines). The error bars of the numerical data are smaller than the symbol size. Taken from [3].

Data-integration approach to optimize a ferromagnet for rare-earth permanent magnets

Munehisa Matsumoto
Institute for Solid State Physics, University of Tokyo
Kashiwa-no-ha, Kashiwa, Chiba 277-8581

April 26, 2019

Permanent magnets are expected to make a significant part of the key materials in the upcoming decades in order to provide a sustainable solution to the energy problem. We are developing methods to propose a good candidate as a magnetic material for a given utility such as characterized by a typical temperature range for practical applications. Even though the champion rare-earth permanent magnet (REPM) made of Nd-Fe-B ternary alloys has been dominating the market in the past few decades, it is by no means straightforward to pin-point what would be the best material in a given situation for demands. Addition of Dy had been the solution for traction motors in hybrid cars where sufficiently strong magnetic properties at high-temperatures up to 450K are indispensable, but various instabilities in the supply of heavy rare earth elements including Dy pushed us to look for alternative chemical compositions in the past decade. Valence-fluctuating Ce can be of potential use in controlling the magnetic properties toward a desirable direction by fine-tuning the $4f$-electron states around or slightly below the Fermi level. Here we report about a recent case study [1] to demonstrate how a best candidate within the La-Ce-Fe-B quaternary alloy can be identified on the basis of *ab initio* data sets and a practical data integration approach, making an application-oriented optimization framework.

The description of REPM's involves multiple physics, starting with the microscopic electronic structure on the basis of quantum mechanics to the classical electrodynamics that govern the macroscopic magnetization dynamics. Bridging widely different scales is hardly doable at present, partly due to the lack of good numerical methodology to deal with too demanding computational costs that grow exponentially with respect to the length scale, and more fundamentally due to the lack of our understanding concerning how the microscopic electronic structure is coarse-grained through the particular microstructure of metallic materials to yield the macroscopic and off-equilibrium properties.

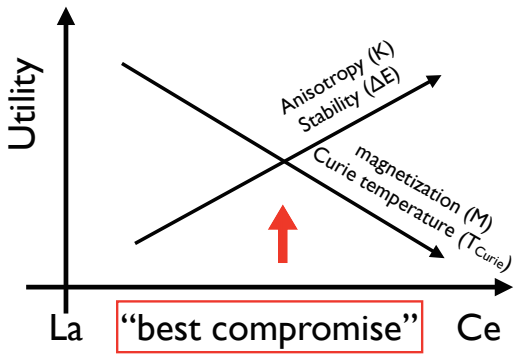

Figure 1: The overall optimization for $(La,Ce)_2Fe_{14}B$.

We calculated all of the relevant intrinsic properties of the ferromagnets $R_2Fe_{14}B$

(R=rare earth), that make the main phase of the champion REPM. Open-source package for *ab initio* electronic structure calculations, AkaiKKR [2] and OpenMX [3] are used. Magnetization M, uni-axial magnetic anisotropy energy K, Curie temperature T_{Curie}, and the formation energy ΔE as an indicator of the structure stability are calculated by appropriately combining AkaiKKR and OpenMX on the chemical composition space that is multi-dimensional in general. We focus on the cross section therein for $(La_{1-x}Ce_x)_2Fe_{14}B$ [4]. A utility function is defined for each of the observables referring to the intrinsic properties of the champion magnet compound, $Nd_2Fe_{14}B$, and integrated to assess the overall utility of the compound $(La_{1-x}Ce_x)_2Fe_{14}B$ as a function of x. The setup of the optimization problem is schematically shown in Fig. 1 While Ce-rich compounds come with better magnetic anisotropy and structure stability, La-rich compounds exceeds in Curie temperature and magnetization.

Depending on how the high-temperature edge of practical applications are given, the optimal point on the Ce-concentration axis is shifted. Interestingly, when the application temperature range spanning up to 450K is assumed, we identified that the optimal point falls on the range around 70% of Ce, in a semi-quantitative agreement with the recent technological achievement in the development of a La-Ce-based permanent magnet [5].

In this study, multiple-scale physics in REPM's and external demands on them have been incorporated in a simple-minded data model. While the fundamental developments to bridge over multiple scales are still in progress, thus constructed data models may help in providing a working phenomenology to which more fundamental theory is compared.

Construction of a more comprehensive data model will be presented elsewhere [6].

References

[1] M. Matsumoto. M. Ito, N. Sakuma, M. Yano, T. Shoji, H. Akai: preprint (arXiv:1901.10119).

[2] H. Akai: `ttp://kkr.issp.u-tokyo.ac.jp/jp/}.Seealso{\url`ttps://ma.issp.u-tokyo.ac.jp/app/113.

[3] T. Ozaki *et al*: `ttp://www.openmx-square.org/}.Seealso{\url`ttps://ma.issp.u-tokyo.ac.jp/app/594.

[4] C. V. Colin, M. Ito, M. Yano, N. M. Dempsey, E. Suard, and D. Givord: Appl. Phys. Lett. **108** (2016) 242415.

[5] T. Shoji *et al.*: Journal of Society of Automotive Engineers of Japan (2018) **72**, 102 (in Japanese); See also `https://newsroom.toyota.co.jp/en/corporate/21139684.html`

[6] Y. Harashima *et al*, in preparation.

Efficient Sampling Simulation of the Soft Modes Significantly Contribute to Protein Properties

Kazuhiro TAKEMURA, Duy TRAN, Hiroaki HATA, Kenichiro TAKABA, Ai SHINOBU, and Akio KITAO

School of Life Science and Technology, Tokyo Institute of Technology

Ookayama, Meguro, Tokyo 152-8550

Last year, we reported a simple but efficient and accurate method to generate protein-ligand complex structures, called Concentrated ligand Docking (ColDock)[1], which successfully predicted several protein-ligand complex structures. This year, we report that ColDock is also successful in observing the effects of amino acid mutations on protein-ligand complex bindings and reproducing binding pose of bulky ligands.

Proteins exert their function by interacting with other proteins or ligands. Accurate prediction of protein-protein/ligand complex structures is a key to understanding the protein function. We proposed ColDock as an efficient but accurate method to generate protein-ligand complex structures using molecular dynamics (MD) simulations at relatively high ligand concentrations. The procedure of ColDock for a given protein-ligand pair is as follows: (i) Multiple ligands are distributed randomly around the protein at relatively high concentration (~100 mM); (ii) Multiple short (100 ns) independent MD simulations are conducted. To prevent ligand aggregations which might be caused by high concentration, extra repulsive forces are applied between the ligands; (iii) The ligands in contact with the protein are selected; (iv) The selected ligands are clustered according to a root-mean-square-deviation of ligand (L-RMSD). The ligand poses are predicted as the representative poses of populated clusters.

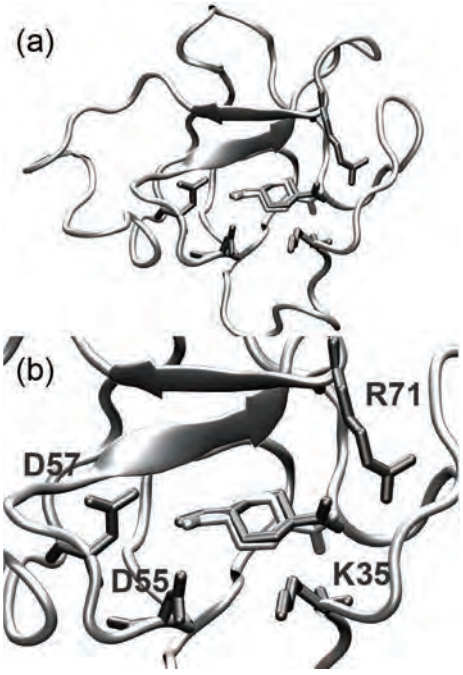

Fig. 1 Predicted (gray) and crystal (white) structures of human plasminogen kringle 4 with AMH. Effects of mutations on the labeled residues were examined.

We examined the effects of amino acid mutations on the complex of plasminogen kringle 4 with transaminomethyl-cyclohexanoic acid (AMH, Fig.1) using ColDock. An experimental study[2] showed that the D55N and R71Q mutations decrease the binding affinity, whereas K35I increases the binding affinity, and no binding was observed in D57N. We observed ligand bindings to all mutants including D57N, for which the binding was not detected experimentally. Consistent with this, only a single unbinding event among all the 50 MD simulations was observed in D57N. ColDock accurately predicted the ligand pose using the wild type (L-RMSD: 1.2 Å. Fig. 1). The populations of the first cluster were 32, 55, 25, 27, and 10 % for WT, K35I, D55N, D57N, and R71Q, respectively. The reported binding free energies of WT, K35I, D55N, and R71Q are −6.53, −6.96, −5.05, and −4.93 kcal/mol, respectively. Thus the simulated population anticorrelated very well with the reported binding free energies. Results indicated that ColDock can investigate the effects of mutations on ligand bindings.

We also examined FK506 binding to FKBP as a more difficult challenge of docking to a bulky ligand. Considering flexibility and size of the ligand, we introduced four interaction sites in each ligand molecule, and successfully prevented aggregation of FK506. In addition, we performed twenty independent 200-ns MD simulations for this target. FK506 molecules entered the binding site in 9 out of 20 simulations. We detected three largely populated clusters in the binding site. Three representative structures reproduced fraction of native contacts very well (> 0.87), and the second-ranked pose showed the lowest L-RMSD (1.2 Å, Fig. 2) among them. Although only one out of twenty trajectories reached to the pose very similar to the crystal structure, the population of the cluster was relatively high due to the stability of the pose. The results imply that ColDock can be also used for the docking of bulky ligands.

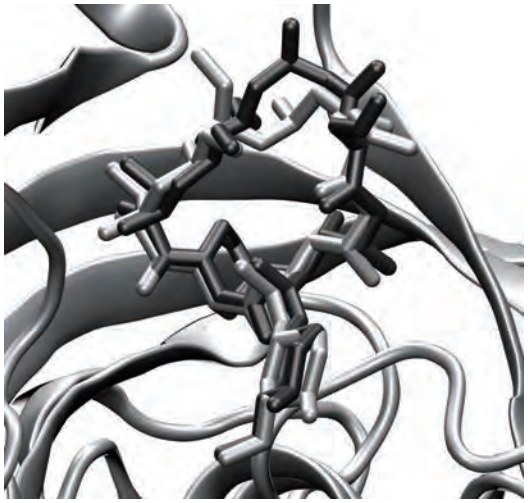

Fig. 2 Predicted (black) and crystal (white) structures of FK506 to FKBP

References

[1] K. Takemura, C. Sato & A. Kitao. J Phys Chem B 122, 7191-7200 (2018).

[2] J.H. Graversen, B.W. Sigurskjold, H.C. Thogersen, M. Etzerodt, Biochemistry, 39, 7414-9 (2000).

Multiple-Q states of the frustrated Heisenberg model on the honeycomb lattice

TOKURO SHIMOKAWA[1] and HIKARU KAWAMURA[2]
[1]*Okinawa Institute of Science and Technology Graduate University, Onna, Okinawa, 904-0495, Japan*
[2]*Department of Earth and Space Science, Graduate School of Science, Osaka University, Toyonaka, Osaka 560-0043, Japan*

Motivated by a theoretical study by Okubo *et al* [1] of the possible realization of the triple-q skyrmion-lattice state in the J_1-J_2 or J_1-J_3 triangular-lattice Heisenberg model, we here investigate the ordering properties in the J_1-J_2 classical honeycomb-lattice Heisenberg model under magnetic field.

The Hamiltonian of the honeycomb-lattice Heisenberg model is given by,

$$\begin{aligned}\mathcal{H} = &- J_1 \sum_{\langle i,j \rangle} \mathbf{S}_i \cdot \mathbf{S}_j - J_2 \sum_{\langle\langle i,j \rangle\rangle} \mathbf{S}_i \cdot \mathbf{S}_j \\ &- H \sum_i S_i^z, \end{aligned} \tag{1}$$

where $\mathbf{S}_i = (S_i^x, S_i^y, S_i^z)$ is the classical Heisenberg spin with the fixed length of $|\mathbf{S}_i| = 1$ located at the i-th site on the honeycomb lattice, $J_1 < 0$ and $J_2 < 0$ represent the antiferromagnetic NN and NNN interactions, while the $\sum_{\langle i,j \rangle}$ and $\sum_{\langle\langle i,j \rangle\rangle}$ are taken over the NN and NNN pairs J_1 and J_2, respectively.

This model has been known that the ground state of the model in zero field exhibits, for $J_2/J_1 > 1/6$, a single-q helical order with an incommensurate wavevector with an infinite ring-like degeneracy in the q-space, while, for $J_2/J_1 \leq 1/6$, the standard two-sublattice antiferromagnetic order [2]. Finite-temperature ordering properties in zero field have also been investigated by Okumura *et al* [3], and then only a single-q helical ordered state has been found as an quasi-long ranged ordered state. The in-field ordering process of the present honeycomb-lattice model is a remaining big issue since the interplay between macroscopic degeneracy in the ground state and fluctuations might lead to a intriguing behavior.

We investigate the in-field ordering properties of the model paying attention to the possible appearance of exotic multiple-q states with focusing on the parameter region, $1/6 < J_2/J_1 < 0.5$. We are successful in finding various exotic multiple-q states by means of extensive monte carlo (MC) methods after careful treatment of large finite-size dependences owing to the strong incommensurability. We have summarized our results in two papers.[4, 5]

Our results are obtained by using CPU node of system B. Our MC code is executed in parallel by using both OpenMP and MPI techniques.

References

[1] T. Okubo, S. Chung, and H. Kawamura, Phys. Rev. Lett. **108**, 017206 (2012).

[2] S. Katsura, T. Ide, and T. Morita: J. Stat. Phys. **42**, 381 (1986).

[3] S. Okumura, H. Kawamura, T. Okubo, and Y. Motome, J. Phys. Soc. Jpn. **79**, 114705 (2010).

[4] T. Shimokawa, and H. Kawamura, arXiv:1810.02951.

[5] T. Shimokawa, T. Okubo, and H. Kawamura, arXiv:1902.01582.

Bold Diagrammatic Monte Carlo Studies on the Unitary Fermi Gas

Takahiro OHGOE

Department of Applied Physics,

The University of Tokyo, Hongo, Bunkyo-ku, Tokyo 113-8656

Feynman diagrams are powerful tools for studying various fields of physics. Still, the analysis usually involves approximations, because only some types of diagrams or low-order diagrams are considered there. However, the Monte Carlo method for unbiased sampling of Feynman diagrams has been recently developed [1]. On the other hand, the diagrammatic series sometimes have zero radius of convergence. The question is whether it is still possible to make accurate predictions by summing up Feynman diagrams.

Here we report high-precision results obtained by the bold-line diagrammatic Monte Carlo method for the unitary Fermi gas with zero convergence radius [2]. We derive the large-order asymptotic behavior of the diagrammatic series, and we give mathematical arguments and numerical evidence for the resummability of the series by a specifically designed conformal-Borel method that incorporates the large-order behavior. Combining this new resummation method with diagrammatic Monte Carlo evaluation up to order 9, we obtain new results for the equation of state, which agree with the ultracold-atom experimental data, except for the 4-th virial coefficient for which our data point to the theoretically conjectured value. Furthermore, We obtained our accurate results of Tan's contact [3].

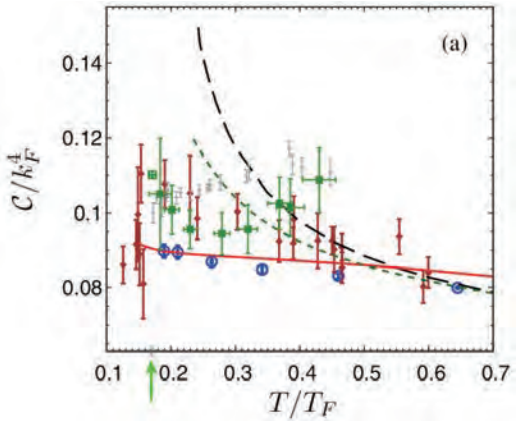

Figure 1: Tan's contact obtained by several methods. Open Circles represent our results.

References

[1] K. Van Houcke, F. Werner, T. Ohgoe, N.V. Prokof'ev and B. V. Svistunov: Phys. Rev. B **99** (2019) 035140

[2] R. Rossi, T. Ohgoe, K. Van Houcke, and F. Werner: Phys. Rev. Lett. **121** (2018) 130405

[3] R. Rossi, T. Ohgoe, E. Kozik, N. Prokof'ev and B. Svistunov, K. Van Houcke, and F. Werner: Phys. Rev. Lett. **121** (2018) 130406

Numerical study on low-energy states of quantum spin systems

Hiroki NAKANO
Graduate School of Material Science, University of Hyogo
3-2-1 Kouto, Kamigori-cho, Ako-gun, Hyogo 678-1297, Japan

It is well known that physical quantities for many-body problems are di cult to estimate precisely; in condensed matter physics, in particular, such many-body problems very often appear. Quantum spin systems are belonging to such many-body problems. To study the systems, therefore, numerical approaches have widely been employed as e ective ones. A lot of computational studies have been carried out and contributed much to our deeper understanding of the target systems.

For quantum spin systems, nowadays, three methods are often used; the numerical diagonalizations, the quantum Monte Carlo (QMC) simulations, and the density matrix renormalization group (DMRG) calculations. Each of them has merits and demerits at the same time. In the QMC simulations, large systems are handled irrespective of their spatial dimensions although the negative sign problem occurs and prevents us from obtaining precise evaluations when the systems include frustrations. The DMRG method is very powerful when a target system is one-dimensional irrespective of the presence of frustrations while this method is still under development for the cases when the spatial dimension of a target system is larger than one. The numerical diagonalization method is applicable irrespective of the presence of frustrations and the spatial dimension; however, this method also has a serious weak point. Namely, this method can treat only very small system sizes. To overcome this disadvantage as much as possible, we successfully developed a hybrid-type parallelized code of Lanczos diagonalization[1]. If we use this Lanczos-diagonalization code that we developed, we can treat various large systems that have not been previously treated yet within this method. So, we examine various quantum spin systems by this method as a primary approach.

In the project in 2018, we tackled three systems. The rst one is the $S = 1/2$ Heisenberg antiferromagnet on the kagome lattice[2]. We examine the magnetization process of this system from our result of a 45-site cluster. This study is the rst one reporting the magnetization process of a spin-1/2 Heisenberg antiferromagnet in the entire range of the magnetization for a 45-site system on an arbitrary lattice structure. From the analysis based on the 45-site result and the ones for systems smaller than the 45-site cluster, it is suggested that the magnetization plateau at the one-ninth height of the saturation does not open in the thermodynamic limit.

The second one is the $S = 2$ Heisenberg antiferromagnet in one dimension[3]. We attempt a precise estimation of the Haldane gap of this system. This system was studied in Ref. [1] where systems up to 16 sites were treated. Due to the situation that the maximum of the treated system sizes was small, a multistep convergence-acceleration procedure was not able to be carried out. Reference [3] successfully treat clusters of 18 and 20 sites additionally. Particularly, the result of the 20-site system has been obtained in a“ Large-scale HPC Challenge ” Project of the Joint Center for Advanced High Performance Computing. The obtained data sequence of the $S = 2$ nite-size spin excitation under the twisted boundary condition successfully give a more precise estimate for the $S = 2$ Haldane gap through the multistep convergence-acceleration proce-

dure.

The third one is the $S = 1/2$ Heisenberg antiferromagnet on the orthogonal-dimer lattice. This system is also called the Shastry-Sutherland model, which includes antiferromagnetic interaction forming the square lattice (J_2) and antiferromagnetic interaction at orthogonal-dimer pairs (J_1). It is well known that this system shows the mathematically exact dimer ground state when J_2/J_1 is small. This model shows, on the other hand, that the Néel-ordered ground state appears in the region of large J_2/J_1. It was pointed out that the plaquette-singlet phase exists in an intermediate region. Reference [4] reports numerical-diagonalization results for 36-site and 40-site clusters that have not been examined yet. Our calculations clearly capture the edge of the dimer phase and the edge of the Néel-ordered phase. Our calculations suggest at the same time that there appears a new boundary which is di erent from the two phase boundaries.

We also carried out calculations for other di erent systems with frustration and studied them in various viewpoints[5, 6, 7, 8, 9, 10]. Our studies contribute to our understandings of the various antiferromagnets and the nontrivial e ect of frustration in magnetic materials.

References

[1] H. Nakano and A. Terai: J. Phys. Soc. Jpn. **78** (2009) 014003.

[2] H. Nakano and T. Sakai: J. Phys. Soc. Jpn. **87** (2018) 063706(1-5)

[3] H. Nakano and T. Sakai: J. Phys. Soc. Jpn. **87** (2018) 105002(1-2)

[4] H. Nakano and T. Sakai: J. Phys. Soc. Jpn. **87** (2018) 123702(1-5)

[5] Y. Fukumoto, Y. Yokoyama, and H. Nakano: J. Phys. Soc. Jpn. **87** (2018) 124710(1-6)

[6] Y. Hasegawa, H. Nakano, and T. Sakai: Phys. Rev. B **98** (2018) 014404(1-9)

[7] T. Sakai and H. Nakano: AIP Adv. **8** (2018) 101408(1-5)

[8] T. Sakai and H. Nakano: Physica B **536** (2018) 85-88

[9] A. Shimada, T. Sakai, H. Nakano, and K. Yoshimura: J. Phys.: Conf. Series **969** (2018) 012126(1-6)

[10] T. Sakai and H. Nakano: J. Phys.: Conf. Series **969** (2018) 012127(1-6)

Microscopic calculation of the flux-flow Hall effect based on the augmented quasiclassical equations

Takafumi KITA
Department of Physics, Hokkaido University
Sapporo, 060-0810

Superconductors exhibit many interesting phenomena distinct from normal states, such as the sign change of the flux-flow Hall coefficient as a function of temperature or magnetic field. It has been pointed out that this sign change is closely related to the charge accumulated around the vortex core region. We have studied this vortex-core charging microscopically, including the mechanism of charge accumulation.

It has been elucidated that the vortex-core charging is caused by three forces: (i) the Lorentz force that acts on supercurrent, (ii) pair-potential-gradient (PPG) force, and (iii) the pressure difference arising from the slope in the density of states. London first included the Lorentz force in his phenomenological equations of superconductivity [1], and predicted emergence of net charge due to the Hall effect whenever supercurrent flows. The PPG force was first discussed by Kopnin [2]. In recent years, microscopic studies on flux-flow Hall effect has been carried out based on the augmented quasiclassical equations in the Keldysh formalism with the Lorentz and PPG forces [3]. The pressure difference arising from the slope in the density of states was first proposed by Khomskii and Freimuth [4]. Despite all these studies, the vortex-charging had not been fully understood microscopically. This is because all the force terms for describing charging are missing from the standard Eilenberger equations, which are also called quasiclassical equations of superconductivity and have been used extensively to study superconductors in a magnetic field microscopically. Very recently, we have derived augmented quasiclassical equations that incorporate all the terms responsible for charging. Using it, we have studied charging of a single vortex in three-dimensional s-wave superconductors. However, the magnetic field dependence of the vortex-charging in the Abrikosov lattice has not been fully calculated. Therefore, we calculated the magnetic field dependence of the vortex-core charging in two-dimensional s-wave superconductors due to the Lorentz and PPG forces by using the augmented quasiclassical equations in the Matsubara formalism. The force caused from the slope in the density of states is absent for this case with the cylindrical Fermi surface.

The charge caused by the Lorentz force has a strong field dependence with a peak and can be enhanced substantially from the value of an isolated vortex [6]. On the other hand, the charge caused by the PPG force decreases as the field is increased and may change its sign(Figure 1). The parameters of this system are the coherence length ξ_0, magnetic penetration depth λ_0, Thomas–Fermi screening length $\lambda_{\rm TF}$, and quasiclassical parameter δ. Figure 1 show the spatial variation of the charge density around vortex core at $\lambda_0 = 5\xi_0$, $\delta = 0.1\xi_0$, $\lambda_{\rm TF} = \delta$, temperature $T = 0.2T_{\rm c}$, and average flux density $\bar{B} = 0.88B_{\rm c2}$, where $T_{\rm c}$ is critical temperature and $B_{\rm c2}$ is upper critical field, respectively. We unveiled that the vortex charging due to the PPG force cancels the one due

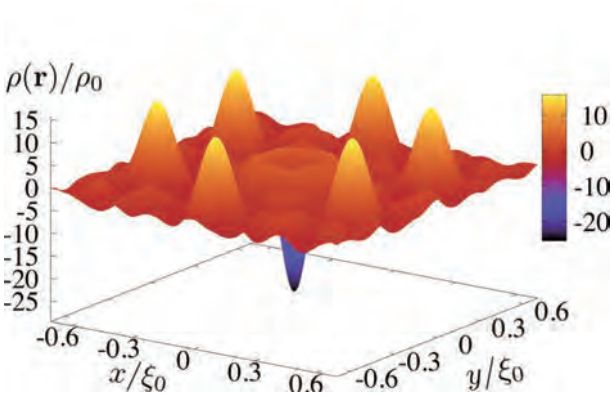

Figure 1: Vortex-charge density $\rho(\mathbf{r})/\rho_0$ in the region $-0.6\xi_0 \leq x/y \leq 0.6\xi_0$ for $\bar{B} = 0.88B_{c2}$ at $T = 0.2T_c$.

to the Lorentz force except at low magnetic field region.

In summary, we have numerically studied the magnetic field dependence of the vortex-core charging caused by the Lorentz and PPG forces in the Abrikosov lattice. The sign of the vortex-core charge due to the PPG force may change as a function of magnetic field. In the near future, we are planning to calculate transport phenomena such as the flux-flow Hall effect and non-reciprocal effect in type-II superconductors.

References

[1] F. London, *Superfluids* (Dover, New York, 1961), Vol. 1, p. 56.

[2] N. B. Kopnin, J. Low Temp. Phys. **97** (1994) 157.

[3] E. Arahata and Y. Kato, J. Low. Temp. Phys. **175** (2014) 364.

[4] D. I. Khomskii and F. V. Kusmartsev, Phys. Rev. B **46** (1992) 14245.

[5] H. Ueki, M. Ohuchi, and T. Kita, J. Phys. Soc. Jpn. **87** (2018) 044704.

[6] W. Kohno, H. Ueki, and T. Kita, J. Phys. Soc. Jpn. **85** (2016) 083705.

Analysis of Many-Body Effects in Bose–Einstein Condensate

Takafumi KITA
Department of Physics, Hokkaido University
Sapporo, Hokkaido, 060-0810

In the Bose–Einstein condensate (BEC), the 3/2-body correlations, which are the two-body processes of the exchanging one particle between condensate and non-condensate, are the sources of the many-body effects. However, it is difficult to incorporate these correlations since they are omitted in the mean-field approximation by Wick's decomposition. In recent years, we constructed the variational wave function for the ground state of the weakly interacting bosons and found that the 3/2-body correlations give a contribution comparable to the mean-field energy toward lowering the ground state energy.[1, 2, 3] Thus, it is expected that the many-body effects change the properties of the BEC system even in the weak-coupling region.

We have developed the variational approach at finite temperatures, which does not depend on the specific form of Hamiltonians, to investigate the contributions of the many-body effects in equilibrium states.[4] We apply this formalism to the weak-coupling Bose–Einstein condensed phase and incorporate the 3/2-body correlations. Unlike the zero temperature formalism, we have to introduce the Matsubara Green's function for Bogoliubov's quasiparticles to evaluate the basic expectations of them. Besides, the self-consistent equations contain some functions with multivariable functions, so that it is necessary to deal with multiple loops for numerical calculations. For those reasons, we need to use the supercomputer in ISSP to perform parallel computing.

Numerical calculations were performed for the contact interaction model $U_k = U = 4\pi a_U/m$, where m is a mass of bosons. We have to introduce a cutoff wavenumber $k_{\rm c}$ to remove the ultraviolet divergence inherent in the potential. We choose $k_{\rm c}$ so that $k_{\rm c}a_U \ll 1$ is satisfied. The units of energy and wavenumber of this system are defined by $\varepsilon_U \equiv U\bar{n}$, $k_U \equiv \sqrt{2m\varepsilon_U}$, where $\bar{n}$ is a particle number density. We take the coupling constant so that $a_U^3\bar{n} \ll 1$ is satisfied corresponding to the dilute ultracold atomic gases. We solved the self-consistent equations in the low temperature region $0 < T < T_{\rm c0}/2$ ($T_{\rm c0}$ is the critical temperature for an ideal system), and compared the results with those of the self-consistent mean-field theory, i.e., Hartree–Fock–Bogoliubov (HFB) approximation.

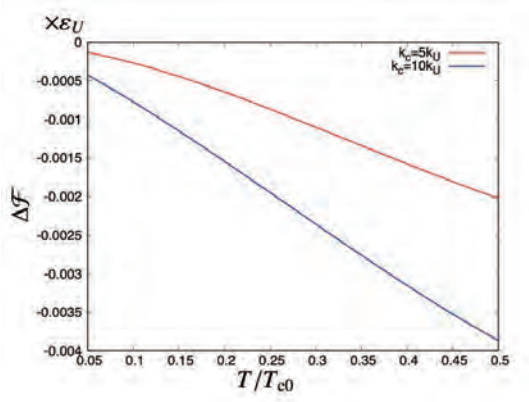

Figure 1: Free energy differences per a particle $\Delta\mathcal{F}$ as functions of T for $a_U^3\bar{n} = 10^{-6}$.

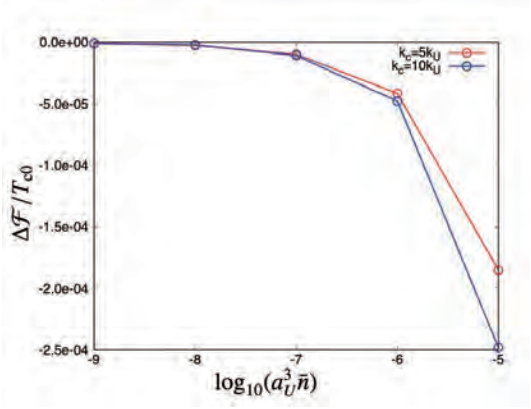

Figure 2: $\Delta\mathcal{F}$ as functions of $\log_{10}(a_U^3\bar{n})$ for $T = 0.3T_{c0}$.

Figure 1 shows the temperature dependence of the free energy. $\Delta\mathcal{F}$ is defined as the difference from the free energy of the HFB approximation. It turns out that the free energy of this system are lowered by the 3/2-body correlations as well as the zero temperature system. We also found that the contribution of the 3/2-body correlations increase with temperature and similar behavior also appears in the coupling constant dependence, as shown Figure 2. Therefore, the 3/2-body correlations should be incorporated self-consistently to investigate the thermodynamic properties even in collisionless regime.

Since the 3/2-body correlations give a finite contribution to the self-energy of the Bogoliubov's quasiparticles, it may be expected the qualitative changing the single-particle excitation as discussed in the zero temperature formalism.[1] Indeed, it turns out that the 3/2-body correlations are mainly contributed in the long wavelength region.

References

[1] T. Kita: J. Phys. Soc. Jpn. **86** (2017) 044003.

[2] W. Kohno, A. Kirikoshi, and T. Kita: J. Phys. Soc. Jpn. **87** (2018) 034002.

[3] W. Kohno, A. Kirikoshi, and T. Kita: J. Phys. Soc. Jpn. **87** (2018) 124004.

[4] A. Kirikoshi, W. Kohno, and T. Kita: J. Phys. Soc. Jpn., in press.

Dynamical DMRG study of spin dynamics in frustrated quantum spin systems

Takami TOHYAMA
Department of Applied Physics, Tokyo University of Science, Tokyo 125-8585

Two-dimensional frustrated quantum spin systems give rise to novel quantum states such as quantum spin liquids and valence bond crystal states owing to the influence of quantum fluctuation and frustration. One of possible systems will be those that have kagome-type structures. Very recently, a spin-1/2 quantum spin compound with square-kagome lattice (SKL), $Cu_6AlBiO_4(SO_4)_5$·KCl, was synthesized [1]. From the crystal structure of this compound, we naturally expect three nonequivalent exchange interactions as shown in Fig. 1. This model will provide a good starting point for studying this compound. The magnetic properties of SKL with the three nonequivalent exchange interactions have not been studied theoretically except for magnetization plateaus [2]. Therefore, it is necessary to investigate magnetic excitations on the SKL for the sake of forthcoming comparison with inelastic neutron scattering experiments.

In this project, we examine magnetic properties of the spin-1/2 Heisenberg model on SKL given by $H = \sum_{\langle i,j \rangle} J_{i,j} \mathbf{S}_i \cdot \mathbf{S}_j$, where $\mathbf{S}_i$ is the spin-$\frac{1}{2}$ operator at site i, $\langle i,j \rangle$ runs over the nearest-neighbor spin pairs, $J_{i,j}$ corresponds to one of J_1, J_2, and J_3 shown in Fig. 1.

Firstly, we theoretically calculate magnetic susceptibility and magnetization curve by finite-temperature Lanczos method and density-matrix renormalization group (DMRG), and compare them with experimental data in $Cu_6AlBiO_4(SO_4)_5$·KCl. We obtain a possible set of exchange interactions that can reproduce their experimental data:

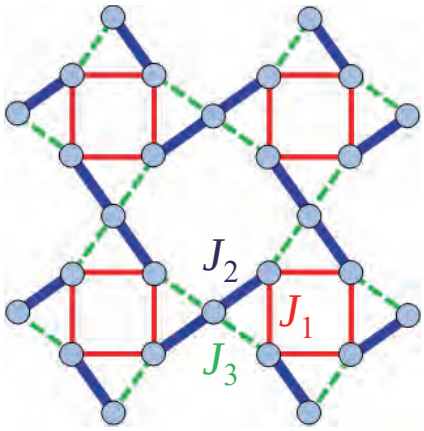

Figure 1: Square-kagome lattice with three nonequivalent exchange interactions.

$J_1 = 135$ K, $J_2 = 162$ K, and $J_3 = 115$ K.

Next we calculate dynamical spin structure factor defined by

$$S(\mathbf{q},\omega) = -\frac{1}{\pi N}\mathrm{Im}\,\langle 0|\, S^z_{-\mathbf{q}} \frac{1}{\omega - H + E_0 + i\eta} S^z_{\mathbf{q}}\,|0\rangle\,,$$

where $\mathbf{q}$ is the momentum in the extended Brillouin zone, $|0\rangle$ is the ground state with energy E_0, η is a broadening factor, and $S^z_{\mathbf{q}} = N^{-1/2}\sum_i e^{i\mathbf{q}\cdot\mathbf{R}_i} S^z_i$ with $\mathbf{R}_i$ being the position of spin i and S^z_i being the z component of $\mathbf{S}_i$. We use dynamical DMRG method for the SKL with system size $N = 48$ in the periodic boundary condition [3]. In our dynamical DMRG, the correction vector is expanded by the Legendre polynomial with a Gaussian averaging [4] and the broadening factor η is replaced by the width of the Gaussian, for which we set 0.1 in units of J_1. The number of states kept in

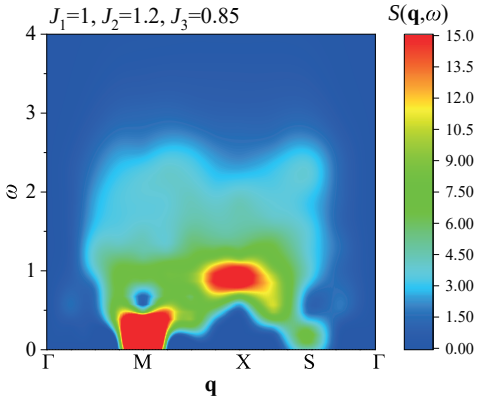

Figure 2: $S(\mathbf{q}, \omega)$ of spin-1/2 SKL Heisenberg model. J_1 is taken to be the unit of energy. The intensity in the contour map is truncated by 15.00 as shown in the intensity bar. The maximum value of intensity is 102 at the M point with $\omega = 0.15$.

the dynamical DMRG is $m = 6000$, leading to truncation error less than 1×10^{-3}.

Figure 2 shows $S(\mathbf{q}, \omega)$ along the symmetric momentum lines. The low-energy excitations less than $\omega = 0.5$ are mainly located at the M point, which indicates the presence of antiferromagnetic order in the present parameter set. However, the high-energy excitations above $\omega = 0.5$ are not given by a simple spin-wave form, but exhibit strong intensity at the X point followed by broad structure extending up to $\omega = 2$. These high-energy features may come from competing interactions giving rise to magnetic frustration. The change of intensity distribution in the momentum space between $\omega = 0.4$ and $\omega = 1$ is clearly seen in Fig. 3.

A recent preliminary result of inelastic neutron scattering experiment on polycrystalline sample of $Cu_6AlBiO_4(SO_4)_5 \cdot KCl$ reported low-energy excitations whose position does not correspond to the M point [1]. This inconsistent behavior between theory and experiment may require another parameter set of exchange interactions. This will be solved

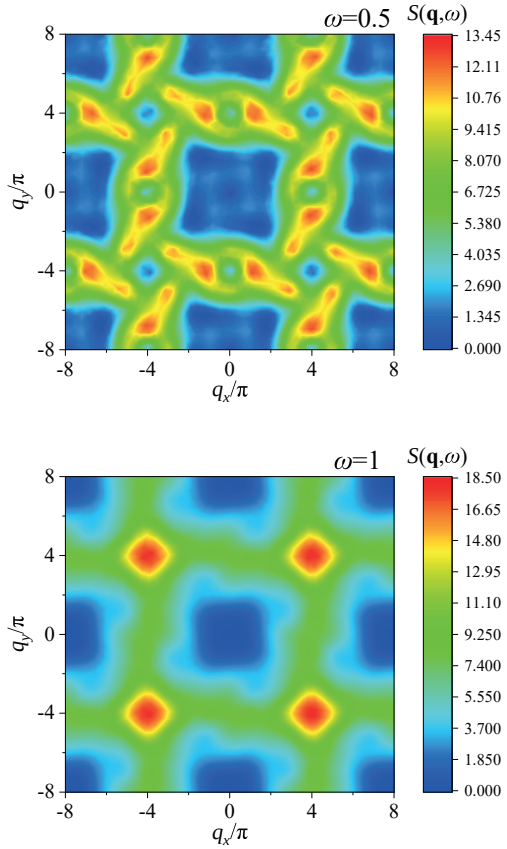

Figure 3: Intensity map of $S(\mathbf{q}, \omega)$ in the extended Brillouin zone at $\omega = 0.5$ (upper panel) and $\omega = 1$ (lower panel).

in the near future.

References

[1] M. Fujihala, K. Morita, S. Mitsuda, T. Tohyama *et al.*: unpublished.

[2] K. Morita and T. Tohyama: J. Phys. Soc. Jpn. **87** (2018) 043704.

[3] K. Morita and T. Tohyama: unpublished.

[4] S. Sota and T. Tohyama: Phys. Rev. B **82** (2010) 195130.

Numerical study of phase transition in non-equilibrium systems

Kenji HARADA
Graduate School of Informatics, Kyoto University, Kyoto 606-8501, Japan

We can define the phase of a macroscopic system out of equilibrium based on physical order parameters on a non-equilibrium steady-state distribution. The phase transition is confirmed theoretically and experimentally in many studies. However, we have little understanding of the informational aspect of a macroscopic non-equilibrium system. Recently, Wood *et al.* [1] analytically calculate the statistical Rényi entropy of the asymmetric exclusion process (ASEP). The phase boundary defined by the behavior of the Rényi entropy agrees with the conventional phase boundary of ASEP for three non-equilibrium phases. It shows the potential power of informational quantities. However, computation of the entropy is technically difficult; no method is known for the Monte Carlo simulation of a non-equilibrium system. Therefore, the knowledge about the informational aspect of a non-equilibrium system is limited than that of an equilibrium system.

In this study, overcoming the technical difficulty by the tensor network method, we will focus on the informational aspect of a $(1+1)$-dimensional directed percolation (DP) through the Rényi entropy and the entanglement entropy. If we regard a percolating direction of objects as a time direction, the $(d+1)$-dimensional DP corresponds to the d-dimensional reaction-diffusion process. There are generally two phases in a reaction-diffusion process; the active phase with finite density of objects and the inactive phase with zero density in the long-time limit, called the "absorbing" state. As shown in many numerical studies for DP[2], the transition between the active phase and the inactive phase is critical, and the concept of the universality is also extended as the DP universality class. Because of the extreme simplicity, the universality class is expected to be ubiquitous[3].

Using a tensor network scheme, we numerically calculate the time evolution of state probability distribution of DP. We find a universal relaxation of Rényi entropy at the absorbing phase transition point and a new singularity in the active phase where the second-order Rényi entropy has a cusp and the dynamical behavior of entanglement entropy changes from asymptotically-complete disentanglement to finite entanglement. We confirm that the absorbing state, though its occurrence is exponentially rare in the active phase, is responsible for these phenomena. This interpretation provides us with a unified understanding of time-evolution of the Rényi entropy at the critical point as well as in the active phase.

[1] A. J. Wood, R. A. Blythe, and M. R. Evans, *Journal of Physics A: Mathematical and Theoretical*, **50**, 475005(2017).

[2] M. Henkel, H. Hinrichsen, and S. Lübeck, *Non-Equilibrium Phase Transitions. Volume 1: Absorbing Phase Transitions*, volume 1. Springer, 2008.

[3] K.A. Takeuchi, M. Kuroda, H. Chaté, and M. Sano, *Physical Review Letters*, **99**, 234503 (2007).

Numerical studies of topological phases and bulk-edge correspondence

Y. Hatsugai
Department of Physics, University of Tsukuba
1-1-1 Tennodai, Tsukuba 305-8571, Ibaraki, Japan

As for the topological phases, the bulk is usually hidden in a sense that the system without boundaries is characterized by the absence of low energy excitation. Still the phase is topologically non trivial implies that there is some toplogical quantity that is associated with the bulk. The Chern number of the bulk and the Berry phases are typical examples. They are, however, mostly invisible experimentally except the case of the quantum Hall effects. Experimentally observables of the topological phases are boundary states and/or impurities states, as generic edge states, reflecting special feature of the bulk. This is the bulk-edge correspondence[1]. It universal validity is established in various systems from the quantum Hall effects to toplogical mechanics.

In relation to the bulk-edge correspondence, we have performed several numerical studies.

As for a typical example of the classical mechanics in 3D, we have considered "mechanical diamond" as a spring mass model in 3D. The Weyl points in the mechanical dispersion are discussed in relation to the breakdown of the chiral symmetry and the mechanical Fermi-arc as mechanical edge states are demonstrated[2]. Fractionally quantized Berry phases are defined and numerically calculated for 1 D quantum spins with Z_N symmetry. Numerical advantages to determine the phase boundary is clearly demonstrated[3]. (See Fig.1)). To reduce numerical resources, the pseudopotential is deduced from a lattice model and the manybody Chern numbers are calculated when there exists an internal degree of freedom. Then the Chern number matrices are evaluated and discussed in relation to the effective theory[4]. When the system is sufficiently large, the system should be insensible to the boundary condition. It implies the integration to define a manybody Chern number is not necessary. We have numerically demonstrated it using a large scale manybody diagonalization[5]. (See Fig.2)). One of the recent hot topics in topological phases is a higher order topological phases. In relation to it, we have performed a machine learning studies[6]. Here characteristic edge states are essential in image recognition. Another new area of topological phases is non-hermitian extension of the system. It raises interesting problem. We have demonstrated a crucial role of the symmetry using numerical calculations.[7]

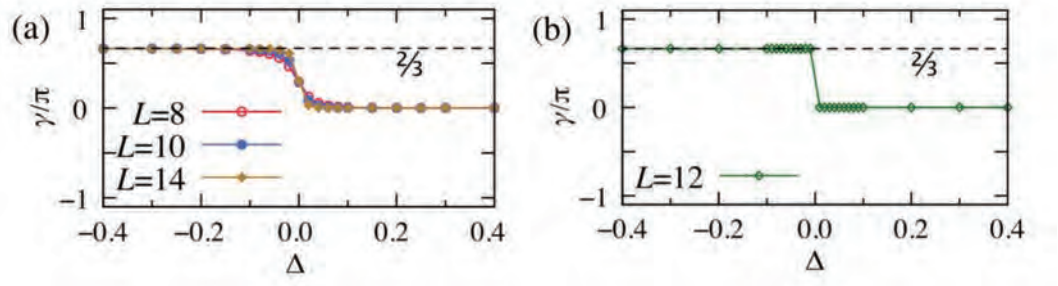

Figure 1: (a):The Berry phase for several system sizes by a usual integration path for Z_3 quantum spins. (b):The quantized Berry phase by an integration path along the high symmetric lines in the synthetic Brillouin zone. [3].

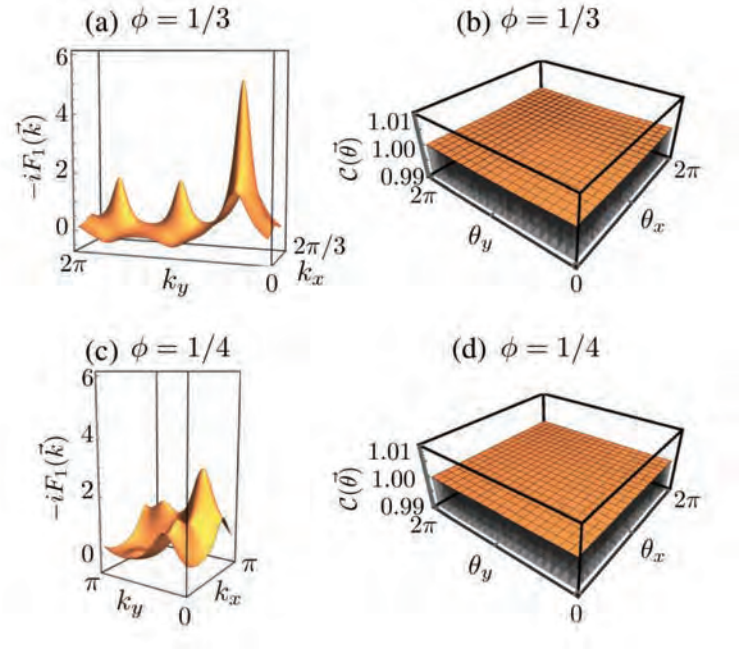

Figure 2: Single-particle Berry curvature (a), (c) and the one-plaquette Chern number (b)(d). The magnetic unit cell is (a): 3×1 and (c): 2×2. The system size is 24×24 for (b) and (d). The flux per plaquette is $\phi = 1/3$ for (a),(b) and $1/4$ for (c), (d). [5].

References

[1] Y. Hatsugai, "Chern Number and Edge States in the Integer Quantum Hall effect", Phys. Rev. Lett. 71, 3697 (1993).

[2] Y. Takahashi, T. Kariyado and Y. Hatsugai, "Weyl points of mechanical diamond", Phys. Rev. B 99, 024102 (2019).

[3] Toshikaze Kariyado, Takahiro Morimoto, and Yasuhiro Hatsugai, "Z_N Berry Phases in Symmetry Protected Topological Phases", Phys. Rev. Lett. 120, 247203 (1-5) (2018).

[4] K. Kudo and Y. Hatsugai, "Fractional Quantum Hall Effect in n = 0 Landau Band of Graphene with Chern Number Matrix", J. Phys. Soc. Jpn. 87, 063701 (1-5) (2018).

[5] Koji Kudo, Haruki Watanabe, Toshikaze Kariyado, and Yasuhiro Hatsugai, "Many-Body Chern Number without Integration", Phys. Rev. Lett. 122, 146601 (1-5) (2019), (Editors' Suggestion).

[6] H. Araki, T. Mizoguchi and Y. Hatsugai, "Phase diagram of a disordered higher-order topological insulator: A machine learning study", Phys. Rev. B 99, 085406 (1-8) (2018).

[7] Tsuneya Yoshida, Robert Peters, Norio Kawakami, and Yasuhiro Hatsugai, "Symmetry-protected exceptional rings in two-dimensional correlated systems with chiral symmetry", Phys. Rev. B 99, 121101(R)(1-5) (2019). a

Assembly process and mechanical properties of crystalline polymers by largescale coarse-grained molecular dynamics simulation

Yuji HIGUCHI
Institute for Solid State Physics, University of Tokyo
Kashiwa-no-ha, Kashiwa, Chiba 277-8581

We have studied deformation and fracture processes of polyethylene [1, 2] and double-network gels [3] using coarse-grained molecular dynamics simulations. This year, assembly process and mechanical properties of crystalline polymers were studied. For the improvement of the mechanical properties, to reveal the role of molecular structures on the stress transmitting processes during the stretching is essential. Thus, two different models of the lamellar structure consisting of amorphous and crystalline layers are stretched by large-scale coarse-grained molecular dynamics simulations on System B.

First, the lamellar structure consisting of 4×10^6 monomers is prepared. To reveal the role of molecular structures, tie chain rich and entanglement rich models are successfully constructed, where tie chains and entanglements connect solid crystalline layers in amorphous layers. Figure 1(a) shows the deformation and fracture processes in entanglement rich model. During the stretching simulations, tie chains and entanglements indeed transmit the stress. At low strain, the roles of these molecular structures are similar. At void generation, the tie chains are more important because of the rapid relaxation of the entanglements. On the other hand, entanglements delay void generation and its growth (Fig. 1(b)). Thus, the stress transmitting processes in the lamellar structure of crystalline polymers at the molecular level are successfully revealed.

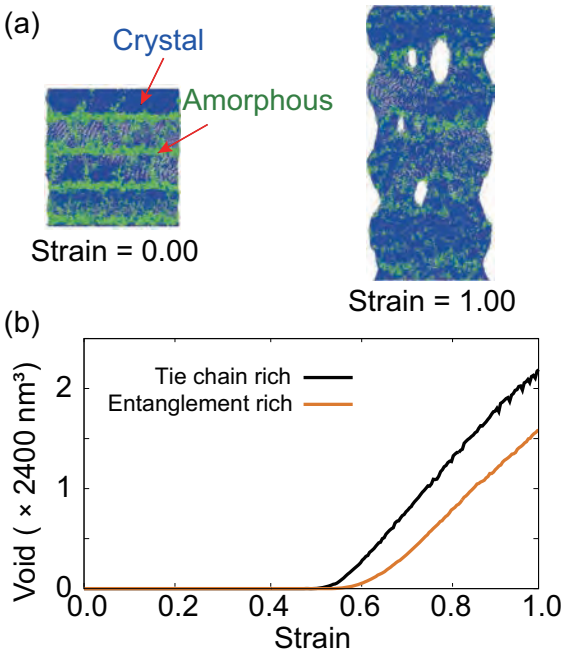

Figure 1: The deformation and fracture processes of the lamellar structure. (a) Cross-sectional snapshots in entanglement rich model. (b) Void generation and growth processes for two different models.

References

[1] Y. Higuchi and M. Kubo: Macromolecules **50** (2017) 3690.

[2] Y. Higuchi: Polym. J. **50** (2018) 579.

[3] Y. Higuchi, K. Saito, T. Sakai, J. P. Gong, and M. Kubo: Macromolecules **51** (2018) 3075.

Probable microscopic pathway of GeI_4's liquid–liquid transition

Kazuhiro Fuchizaki and Hiroki Naruta
Department of Physics, Ehime University, Matsuyama 790-8577
Takahiro Sakagami
Material Group Technology Center, AGC Techno Glass Co., Ltd., Shizuoka 421-0302

Stanley and Teixeira pioneered in 1980 that the thermodynamic anomalies in water are ascribable to the phenomena associated with a percolation transition of hydrogen bonds [1]. The nature of liquid–liquid transitions (LLTs) has been elucidated on thermodynamic basis [2]. However, to our knowledge, there has been no quantitative discussion on a microscopic basis. In particular, a relation between a liquid-liquid transition and a percolation transition has remained unanswered after the Stanley–Teixeira work.

Recently, we have shown that liquid GeI_4 undergoes a pressure-induced crossover from the low-pressure to high-pressure liquid state [3]. Here, we examine a possible microscopic pathway of the crossover by conducting an isothermal–isobaric molecular dynamics simulation. We prepared three sizes of a system consisting of 216, 1000, and 2744 molecules to allow a finite-size scaling analysis. The model employed was composed of rigid tetrahedral molecules interacting via iodine centers connected by Lennard-Jones (LJ) interaction. The LJ parameters were adjusted to reproduce the density at ambient conditions and the melting curve [4]. The deviation of the model's melting curve from the real one amounts to 40% at 1 GPa [4]. The molecular configurations generated for a 2744-system by the simulation were also used as initial inputs to a reverse Monte Carlo (RMC) analysis [5] of the experimental structure factor.

A polymerization scenario of the LLT of GeI_4 [6]

We define a physical bond between the nearest intermolecular iodine sites satisfying the conditions of forming the metallic I_2 bond. We then focus on the formation of molecular clusters in dynamic networks of the bonds. The clusters, which are mainly formed by molecules whose nearest pairs are in edge-to-edge, face-to-edge, and vertex-to-edge orientations, grow as pressure increases.

We could quantify the growth of clusters in an N-molecule system in terms of the percolation probability P and the mean cluster size S as functions of pressure p. We then evaluated the onset of percolation $\bar{p}$, which was observed below 1 GPa, and the width Δ of the transition region. We assumed the following system-size dependences for $\bar{p}$ and Δ: $\bar{p} - p_c \sim \Delta \sim N^{-1/\nu'}$, which allowed us to estimate the threshold pressure p_c in an infinite system. The scaling hypothesis indeed worked to give $p_c = 0.85(1)$ GPa and the exponent $\nu' = 4.2$. When the finite-size effects are taken into consideration, i.e., the correlation length $\xi \sim |p - p_c|^{-\nu'}$ is replaced by N, both P and $SN^{-\gamma'/\nu'}$ (with $\gamma'/\nu' \simeq 0.57$) could be consistently expressed by the universal functions of $z = (p - p_c)N^{1/\nu'}$.

We do not consider that the threshold pressure is located near the extension of the boundary between the two liquid phases is not a coincidence. We thus speculate that the liquid–

liquid crossover of GeI_4 is brought about by percolation of molecular networks.

The same microscopic scenario may apply to the LLT of liquid SnI_4, which offers similar polyamorphism. However, possible heterogeneity induced in the system before the transition would make the environment around molecules less random. A kind of bootstrap mechanism thus introduced could be reflected in the discontinuous nature of the LLT of SnI_4 if the percolation transition occurs below the liquid–liquid critical-point temperature.

Pressure-induced local symmetry breaking upon LLT of GeI_4 and SnI_4 [7]

Pressure-induced structural change in liquid SnI_4 and GeI_4 was known to be reflected in a shift of the broad peak at $\sim$ 7.5 $Å^{-1}$ of the structure factor (SF) toward lower wavenumbers [8, 3]. That is, the intramolecular Sn–I or Ge–I bond length seemed to be elongated upon compression as has been confirmed by the peak shift in the radial distribution functions [8, 3], Fourier inverted from the SFs. This curious "elongation" of the bond length has remained unresolved although we have used this aspect to judge whether the LLT occurs.

Applying the RMC method to infer the microscopic structure of liquid SnI_4 and GeI_4 offered an opportunity to address this issue. The RMC result suggested that both SnI_4 and GeI_4 molecules seem to be squashed in one direction upon compression. This speculation was confirmed by comparing the symmetry-adapted intramolecular SF, whose mathematically exact expression is obtainable, with the experimental SF.

The reduction of molecular symmetry from T_d to C_{3v} of GeI_4 molecules starts at such a low pressure as 1.5 GPa in the crossover region upon compression. We speculate that the symmetry lowering might be a precursor to the LLT because the interaction between molecules with lower symmetry can give rise to a potential function characterized by *two-length* scales [9]. The pressure-induced symmetry lowering of SnI_4 may occur in a narrow pressure range just below the LLT pressure of 1.5 GPa. The range is so narrow that the lowering could not be detected in our measurements carried out at rough pressure intervals [8]. However, the prior lowering of local symmetry is strongly expected considering a remarkable similarity in polyamorphic nature between SnI_4 and GeI_4. A local structural probe such as XAFS will be effective to confirm this prediction.

We have thus far used the model consisting of rigid molecules to discuss not only thermodynamic but also structural properties of liquid SnI_4 and GeI_4. The latter study made us realize the significance of molecular deformation on an LLT. We are now developing a new model in which molecules are deformable.

References

[1] H. E. Stanley and J. Teixeira, J. Chem. Phys. **73**, 3404 (1980).

[2] M. A. Anisimov *et al.*, Phys. Rev. X **8**, 011004 (2018).

[3] K. Fuchizaki *et al.*, J. Phys.: Condens. Matter **30**, 045401 (2018).

[4] K. Fuchizaki and Y. Asano, J. Phys. Soc. Jpn. **84**, 064601 (2015).

[5] R. L. McGreevy, J. Phys.: Condens. Matter **13**, R877 (2001).

[6] K. Fuchizaki *et al.*, J. Phys.: Condens. Matter **31**, 225101 (2019).

[7] K. Fuchizaki *et al.*, J. Chem. Phys. **150**, 114501 (2019).

[8] K. Fuchizaki *et al.*, J. Chem. Phys. **130**, 121101 (2009).

[9] E. A. Jagla, J. Chem. Phys. **111**, 8980 (1999).

Coarse grained MD simulation for fracture and reinforcement of polymer materials

Katsumi HAGITA

Department of Applied Physics,

National Defense Academy, Hashirimizu, Yokosuka, Kanagawa 239-8686

We have studied polymer materials through coarse grained MD simulations for their fracture and reinforcement. We focused on the following three subjects.

1) Fractures of polymer materials such as polyethylene including scission of main chains. Understanding of molecular mechanism and model development using various simulations.

2) Relationships between reinforcement and structure, and fracture and structure through coarse grained (CG) MD simulations.

3) Reinforcements and fractures of filler-filled rubber materials through CGMD simulations.

Especially, this year, we focused on the following research topics.

a) Crystallizations of polyethylene (PE) [1,2]. Comparison between ring and linear melts [1]. Structure formation of a quenched single polyethylene chain [2] to compare force fields.

b) Nanovoids (early fractures) in elongated polymer networks with crosslink [3] and with crosslink and nanoparticles [4].

c) Two-dimensional scattering patterns (2DSPs) in CGMD simulations. [3-9]

d) Reinforcements of filler-filled polymer materials. [3-6, 10]

e) Developments of simulation methods of coarse-grained models [11-13]

f) Visualization methods of material systems [14,15]

Regarding the subject 1), crystallization-behaviors of PE chains were studied through the topic a) in order to obtain a crystallized structure quickly. For PE, we found that united atom (UA) model with Deriding force fields provided acceleration of the crystallization process due to distribution of torsional angles [1,2]. Here, UA model can be regarded as a coarse-grained model of all-atomic simulations. LAMMPS was used for massive parallel simulations. We also investigated ReaxFF simulations using LAMMPS for continuing works from initial structure created by UAMD. Here, ReaxFF can be regarded as a coarse-grained model of DFT calculations.

Concerning the subject 2), 2DSPs originated from structure were investigated for the cases of phase-separation of ABA block copolymer [7] and nanovoids of crosslinked polymers [3] under stretching. For these topics, LAMMPS was used for massive parallel simulations. The analysis code to compute 2DSPs was developed

from scratch. As forthcoming works, studies of machine/deep learning for relationship between 2DPSs and stress-strain curves are in progress.

On the subject 3), CGMD simulations of polymer materials filled with nanoparticles [4, 6, 8] and clay (disc) [5]. Behaviors of 2DSPS were examined. For these topics, LAMMPS was used for massive parallel simulations. In addition, SMP parallelized version of OCTA/cognac was used for continuing researches. The analysis code to compute 2DSPs was developed from scratch. Moreover, particle-mesh version of two-dimensional pattern reverse Monte Carlo modeling was developed, modelling from 2DSPs of NPs in gels by CGMD simulations [8] were compared with reference NP-structure, and several verifications of actual experimental were carried.

Acknowledgement

These works were partially supported by JSPS KAKENHI, Japan, grant no.: JP18H04494. For these works, computing resources by the “Joint Usage/Research Center for Interdisciplinary Large-scale Information Infrastructures” and “High Performance Computing Infrastructure” were also contributed.

References

[1] K. Hagita, S. Fujiwara and N. Iwaoka: J. Chem. Phys. **4** (2019) 3990-3999.

[2] K. Hagita, S. Fujiwara and N. Iwaoka: AIP Advances **8** (2018) 115108.

[3] K. Hagita: Polymer **147** (2018) 247-259.

[4] K. Hagita Polymer (2019) in press.

[5] K. Hagita, Y. Shudo and M. Shibayama: Polymer **154** (2018) 62-79.

[6] K. Hagita Polymer **160** (2019) 65-72.

[7] K. Hagita, T. Tominaga, K. Akutagawa and H. Jinnai: Soft Matter **15** (2019) 926-936.

[8] K. Hagita: Polymer **166** (2019) 155-168.

[9] K. Hagita, T. Murashima and N. Iwaoka: Polymers **10** (2018) 1224.

[10] K. Hagita, T. Higuchi and H. Jinnai: Scientific reports **8** (2018) 5877.

[11] N. Iwaoka, K. Hagita and H. Takano: J. Chem. Phys. **149** (2018) 114901.

[12] K. Hagita and Y. Senda: J. Phys. Soc. Jpn., **87** (2018) 114803.

[13] T. Murashima, K. Hagita and T. Kawakatsu: J. Soc. Rheol. Jpn. (Nihon Reoroji Gakkaishi) **46** (2018) 207-220.

[14] K. Hagita, S. Matsumoto and K. Ohta: ACS Omega **4** (2019) 3990-3999.

[15] K. Hagita, Y. Kawazoe and M. Ogino: AIP Advances **9** (2019) 035001.

Large-Scale Molecular Dynamics Simulation Study on the Crystallization Mechanism of Water Including Air Molecules

Hiroki NADA

National Institute of Advanced Industrial Science and Technology (AIST),

16-1 Onogawa, Tsukuba, Ibaraki 305-8569

Studies on the crystallization mechanism of water including air molecules are important in connection with such issues as the formation of snow and ice crystals in nature. Molecular dynamics (MD) simulations are helpful tools to analyze the crystallization mechanism for real materials at the molecular level.

This study focused on the crystallization of water including air molecules in the upper region of troposphere, where metastable cubic ice (Ic) crystals are formed [1]. Since growth shapes of real Ic crystals are covered with {111} planes, an MD simulation was performed for an interface between an {111} plane of cubic ice and water including N_2 molecules. A modified six-site model was used to estimate the interaction between a pair of water molecules [2]. The potential of N_2 molecules was estimated using a model proposed by Murthy et al. [3].

The simulation indicated the growth of ice at the interface. Interestingly, the grown ice contained partly the structure of hexagonal ice (see arrows in Fig. 1). To infer whether the grown ice structure was affected by N_2 molecules, an MD simulation was also performed for the interface between an Ic {111} plane and pure water. This additional simulation did not show the hexagonal ice structure in the grown ice at the interface.

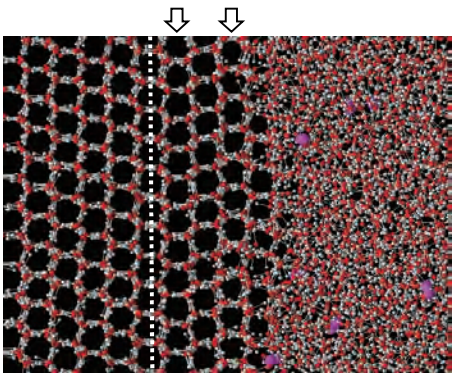

Fig. 1: Snapshots of water and N_2 molecules near the interface during growth. N atoms are represented by large pink spheres. The dashed line shows the initial position of the interface. Parts of the grown ice marked by arrows indicate the formation of hexagonal ice structure.

References

[1] T. Takahashi and T. Kobayashi: J. Cryst. Growth **64** (1983) 593.

[2] H. Nada, J. Chem. Phys. **145** (2016) 244706.

[3] C. S. Murthy, K. Singer, M. L. Klein, and I. R. McDonald, Mol. Phys. **41** (1980) 1387.

Analysis of Formation Mechanism of Calcium Phosphate Crystal by Large-Scale Molecular Dynamics Simulation Combined with Metadynamics Method

Hiroki NADA

National Institute of Advanced Industrial Science and Technology (AIST),

16-1 Onogawa, Tsukuba, Ibaraki 305-8569

Predicting crystal structures and their atomic-scale crystallization mechanisms for a multicomponent system, which has not yet been examined experimentally, using computer simulations largely contributes to the development of functional materials. Molecular dynamics (MD) simulations are helpful tools to analyze crystallization mechanisms at the atomic level. However, it is quite difficult to search for crystal structures that can be formed in a complicated multicomponent system using MD simulations, because the timescale of MD simulations is much shorter than that of crystallization in real systems.

Metadynamics (MTD [1]) is an enhanced sampling simulation method in which the transition of a system between different states is accelerated by increasing the probability of reaching high-energy states. The MTD method affords a free energy landscape that represents the thermodynamic stabilities of all possible structures of a system. Thus, if the MTD method is combined with an MD simulation, the thermodynamic stabilities of all possible crystal structures can be determined definitively, even if the simulation run is not very long.

In this study, an MD simulation combined with the MTD method was used to investigate the crystallization mechanism of calcium phosphates, which have been used for biomaterials. The simulation was performed for amorphous calcium phosphate (ACP), because the crystallization of calcium phosphates frequently occurs from ACP. Simulation results implied that the formation of metastable octa calcium phosphates (OCP) is kinetically preferable rather than the formation of hydroxy apatite (HAP). The results are qualitatively consistent with experimental observations reported so far.

References

[1] A. Laio and M. Parrinello: Proc. Natl. Acad. Sci. USA **99** (2002) 12562.

Construction of coarse-graining spin model and analysis of the coercivity

Taichi Hinokihara

Institute for Solid State Physics,

The University of Tokyo, Kashiwa-no-ha, Kashiwa, Chiba 277-8581

We have studied an atomistic scale classical spin model to analyze the coercivity of magnet. The coercivity depends on various features from microscopic properties, such as exchange couplings, to macroscopic properties, such as demagnetization field induced from the dipole-dipole interactions. Thus, it is one of the challenging problems to evaluate coercivity [1].

This year, we first focused on the construction of a new coarse-graining method that can treat temperature fluctuations. The micromagnetic model, which is frequently used to evaluate the coercivity, is only valid for the zero-temperature simulation. However, since the coercivity relates to the magnetization reversal process, which occurs stochastically, the new coarse-graining method that can take into account the thermal fluctuations are essential. We constructed the coarse-graining model by using the concept of the block spin transformation. As a result, we confirmed that our model well reproduces the domain-wall width and magnetizations.

Second, we constructed a new efficient method that can simulate spin dynamics with long-range interactions [2]. We implemented the stochastic cut-off (SCO) method into the time quantified Monte Carlo (TQMC) method. The new method, which we call TQMC+SCO method, can simulate the spin dynamics efficiently even in the case of the amorphous-like systems. In the case of three-dimensional systems, the computational time for the time step is proportional to $O(\beta N \ln N)$.

References

[1] S. Miyashita, et. al.: Scripta Materialia **154** (2018) 259.

[2] T. Hinokihara, Y. Okuyama, M. Sasaki, and S. Miyashita: arXiv: 1811.00237

Study on Complex Systems by Generalized-Ensemble Algorithms

Takuya HAYASHI, Daiki MATSUBARA, and Yuko OKAMOTO

Department of Physics, Graduate School of Science, Nagoya University

Furo-Cho, Chikusa-ku, Nagoya, Aichi 464-8602

Despite the experimental discovery of the residual entropy of ice Ih in the 1930's [1], highly accurate measurements have yet to be made in experiments. The calculation started from Pauling in the 1930's [2]. As a recent calculation, there are results [3,4] by multicanonical simulations [5]. In this work, we aim to drastically improve the accuracy in large scale and complex systems.

The entropy is proportional to a logarithm of the density of states. In order to obtain accurate density of states, we proposed a new method [6] to combine the multicanonical replica-exchange method [7] and replica-exchange Wang-Landau method [8]. The residual entropy is defined by

$$S_0 = k_{\mathrm{B}} \log W \ ,$$

and our latest result is: [9]

$$W = 1.507480 \ \pm 0.000036.$$

We have also developed a two-dimensional replica-exchange method in grand canonical ensemble and studied a Lennard-Jones system [10]. In this simulation, a two-dimensional random walk in temperature and chemical potential is realized. The gas-liquid phase transition was studied where a first-order phase transition curve ends at a second-order phase transition point. After a single simulation run, we could obtain free energy surface and number density as functions of temperature and chemical potential. The latter is shown in Fig. 1.

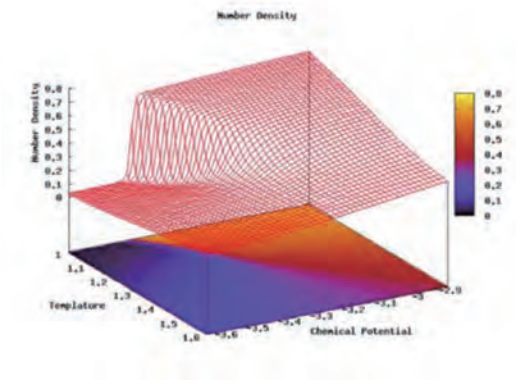

Fig. 1. Number density of a Lennard-Jones system as a function of temperature and chemical potential.

We are now studying the details of the phase transitions in this system using the two-dimensional replica-exchange method that we developed.

References

[1] J. D. Bernal and R. H. Fowler: J. Chem. Phys. **1** (1933) 515.

[2] L. Pauling, J. Am. Chem. Soc. **57** (1935) 2680.

[3] B. A. Berg, C. Muguruma, and Y. Okamoto, Phys. Rev. B **75** (2007) 092202.

[4] B. A. Berg, C. Muguruma, and Y. Okamoto, Mol. Sim. **38** (2012) 856.

[5] B. A. Berg and T. Neuhaus, Phys. Rev. Lett. **68** (1992) 9.

[6] T. Hayashi and Y. Okamoto, arXiv:1901.01430v1 (2019).

[7] Y. Sugita and Y. Okamoto, Chem. Phys. Lett. **329** (2000) 261.

[8] T. Vogel, Y. W. Li, T. Wüst and D. P. Landau, Phys. Rev. Lett. **110** (2013) 210603.

[9] T. Hayashi, C. Muguruma, and Y. Okaoto, in preparation.

[10] D. Matsubara and Y. Okamoto, in preparation.

Semiclassical dynamics of quantum spin systems

Takashi MORI
Riken CEMS, Wako 351-0198, Japan

I have studied the semiclassical dynamics of quantum spin systems with long-range interactions [1] using massive parallel computer simulations. In recent years, nonequilibrium dynamics of isolated quantum systems have extensively been studied. It has been observed that some isolated systems exhibit the phenomenon of *prethermalization*, that is the relaxation toward a quasi-stationary state before reaching true thermal equilibrium.

Prethermalization occurs due to several reasons. If the system is close to integrability, prethermalization occurs because of the presence of many quasi-conserved quantities. Here, quasi-conserved quantities are referred to as quantities that look conserved in short-time scales but relax in a longer timescale. It is known that prethermalization occurs in some quantum spin systems with long-range interactions. The mechanism of prethermalization in long-range interacting systems has not been understood.

I have clarified the mechanism of prethermalization in long-range interacting systems. I have proved that long-range interacting systems possess a family of quasi-conserved quantities, which explains prethermalization phenomena.

When long-range interaction potential decays as $1/r^\alpha$, where r is the distance between two spins and α satisfies $0 \leq \alpha < d$ with the spatial dimension d, the previous study reported that prethermalization occurs for $\alpha \leq d/2$ but not for $d/2 < \alpha < d$ [2]. However, I theoretically argued that prethermalization in general occurs for any $\alpha \in [0, d)$. The reason why prethermalization does not occur for $d/2 < \alpha < d$ in the previous work [2] is due to the speciality of the model considered. The model in Ref. [2] becomes completely integrable in the classical limit, while I argued that prethermalization should occur for any $\alpha \in [0, d)$ when the model becomes chaotic in the classical limit, which is more generic situation.

In order to support this theoretical prediction, I computed nonequilibrium dynamics of quantum spin systems with long-range interactions by using the method of truncated Wigner approximation, which is a kind of semiclassical approximations of the quantum dynamics. I consider the transverse-field Ising model with long-range interactions, which becomes chaotic in the classical limit. When there is no transverse field, the model becomes identical to the one studied in Ref. [2], and its classical limit leads to a completely integrable system.

As a result, I have found that numerical calculations support the theoretical prediction. Prethermalization occurs for any $\alpha \in [0, d)$ when a non-zero transverse field is applied.

References

[1] T. Mori, J. Phys. A **52**, 054001 (2019)

[2] M. Kastner, Phys. Rev. Lett. **106**, 130601 (2011)

Molecular Dynamics Simulation of Ferroelectrics Using a Shell Model IV

T. Hashimoto
Research Center for Computational Design of Advanced Functional Materials (CD-FMat), National Institute of Advanced Industrial Science and Technology (AIST), Tsukuba Central 2, 1-1-1 Umezono, Tsukuba, Ibaraki 305-8568, Japan

We have studied the structure of amorphous $BaTiO_3$. Amorphous $BaTiO_3$ can be formed by sputtering or molecular beam epitaxy (MBE) onto a substrate. The amorphous perovskites are assumed to have random networks of local bonding units (LBUs). By X-ray absorption fine-structure (XAFS) spectroscopy, the LBU in the amorphous phase was shown to be TiO_6[1]. The extended X-ray absorption fine structure (EXAFS) experiments show the evidence for the edge or face-sharing LBU linkages for amorphous $SrTiO_3$[2]. However, the LBU linkage is not well understood for amorphous $BaTiO_3$ because of the proximity of the Ba L_3 edge to the Ti K edge[1, 2], and it is only expected to be similar to that for amorphous $SrTiO_3$. To the author's knowledge, theoretical studies on the structure of amorphous $BaTiO_3$ are not done except for a classical MD simulations, but the LBU for amorphous $BaTiO_3$ is predicted to be TiO_4[3].

We used the isotropic shell model developed by Tinte *et al*[4]. In the shell model, each atom is composed of a core and a shell. The intra-atomic core-shell interaction is expressed by $V(r) = c_2r^2/2 + c_4r^4/24$, where r is the core-shell distance and c_2 and c_4 are parameters. The inter-atomic interaction is through the Coulomb interaction and the Buckingham type shell-shell interaction $V(r) = A\exp(-r/\rho) - C/r^6$, where r is the inter-atomic shell-shell distance and A, ρ, and C are parameters. The cutoff length for the non-bonded interactions were 10.0 Å. The computations were carried out in constant temperature and constant pressure (NPT) ensembles using the code developed by us. The pressure and the temperature were controlled by the Parrinello-Rahman method and the massive Nose-Hoover chain method, respectively. The externally applied pressure was set to 0 Pa.

In this study, the LBU in amorphous $BaTiO_3$ was mainly TiO_6, whitch is in agreement with the XAFS study[1]. The nearest Ti-Ti distance in the amorphous phase was about 1 Å shorter than that in the crystalline phase, and it had a trimodal distribution. It was shown that the trimodal distribution corresponds to apex, edge, and face-sharing LBUs, as expected experimentally for amorphous $SrTiO_3$[2].

References

[1] A. I. Frenkel, Y. Feldman, V. Lyahovitskaya, E. Wachtel, and I. Lubomirsky: Phys. Rev. B **71** (2005) 024116.

[2] A. I. Frenkel, D. Ehre, V. Lyahovitskaya, L. Kanner, E. Wachtel, and I. Lubomirsky: Phys. Rev. Lett. **99** (2007) 215502.

[3] P. P. Phule, P. A. Deymier, and S. H. Risbud: J. Mater. Res. **5** (1990) 1104.

[4] S. Tinte *et al.*: J. Phys.: Condens. Matter **16** (2004) 3495.

Randomness Effects on Spin-Peierls System

Chitoshi YASUDA and Shouta MIYARA
Department of Physics and Earth Sciences, Faculty of Science, University of the Ryukyus, Okinawa 903-0213, Japan

Since the quasi-one-dimensional (quasi-1D) inorganic compound $CuGeO_3$ was synthesized, randomness effects of the spin-Peierls (SP) system have attracted considerable attention. When nonmagnetic impurities are doped in the SP compound, an antiferromagnetic long-range order (AFLRO) is induced. The mechanism is understood by a cluster of magnetic moments induced near an impurity, which is called an 'effective spin'. By substituting nonmagnetic atoms for magnetic atoms, effective spins are induced near the nonmagnetic atoms. Since the effective spins interact through a sea of spin-singlet pairs, the AFLRO is induced. However, Cu nuclear quadrupole resonance (NQR) data contradictory to this interpretation was reported for $CuGe_{1-x}Si_xO_3$: the effective spins are not induced near diluted sites [1]. We need to take the lattice degrees of freedom into account in order to investigate positions of the effective spins.

In preceding projects, we investigated an $S = 1/2$ two-dimensional (2D) antiferromagnetic Heisenberg model composed by the intrachain interaction J coupled to the lattice distortion $\Delta_{i,j}$ and the interchain interaction J' using the quantum Monte Carlo (QMC) simulation with the continuous-imaginary-time loop algorithm [2]. Since this QMC simulation is suitable to parallel computing, we mainly performed parallel computing with the Message Passing Interface. As the result, we found that it is difficult to induce effective spins near diluted sites for large elastic constants, small interchain interactions, and large concentrations of dilution [3]. Furthermore, we estimated the dependence of the staggered magnetization on the concentration of site dilution at zero temperature assuming the situation obtained by the NQR measurements, and found that the AFLRO is induced at low concentrations of dilution [4]. We needed huge-scale numerical simulations for large size $N = 64 \times 64$ and extreme-low temperature $T = 0.0001J$.

In the previous works, we assume that the lattice distortions of the nondiluted chain are not affected by dilution and that they are expressed by those of the nondiluted system. For the quasi-1D magnet $CuGeO_3$, where the strength of the interchain interaction has been suggested to be $J' \sim 0.1$, this assumption seems to be reasonable. In the system with the large interchain interaction, however, the effect would be non-negligible.

In this project, we examine numerical methods to search self-consistently the lattice distortions of the nondiluted chains in the 2D system. In this method, the lattice distortions are optimized with the Lagrange multiplier method under the constraint $\sum_i \Delta_{i,j} = 0$ for all chains. Although the numerical convergence could be confirmed by repeating the calculations for several tens of times in the 1D system, we need large-scale time up to convergence in the 2D system. Therefore, the application of the Wolff algorithm for a calculation of the lattice distortion is under consideration.

References

[1] J. Kikuchi, *et al.*: Phys. Rev. Lett. **88**, 037603 (2002).

[2] S. Todo and K. Kato, Phys. Rev. Lett. **87**, 047203 (2001).

[3] C. Yasuda and S. Miyara: J. Phys. Soc. Jpn. **87**, 014704 (2018).

[4] S. Miyara and C. Yasuda: J. Phys. Soc. Jpn. **87**, 104702 (2018).

Quantitative computation of the dissociation rate of a protein-ligand complex using a manifold-learning technique

Takashi YOSHIDOME

Department of Applied Physics,

Tohoku University, 6-6-05, Aoba, Aramaki, Aoba-ku, Sendai 980-8579

The dissociation rate of a protein-ligand complex can be computed with a Markov state model (MSM) [1]. The model is constructed through the following steps: (i) Classify conformations into states; (ii) Calculate the transition probabilities between the states, and; (iii) Compute observables. We have previously demonstrated that an accurate computation of an observable is possible when a manifold-learning technique is employed for classification [2].

Toward applications of our MSM construction protocol to the computation of the dissociation rate, we first investigated a protocol for automatic determination of the number of states from the results of manifold-learning technique [3]. Trajectory of protein folding/unfolding of a coarse-grained molecular dynamics (MD) simulation was used. We found that automatic determination of the number of states is possible with the silhouette score.

Next, we moved on to construction of the MSMs of the processes of protein unfolding and ligand binding with all-atom MD simulations. After sampling trajectories of the processes, classification into states was performed. We have successfully found the transition state from the trajectories. However, more trajectories were required for quantitative computation of the transition probabilities toward the calculation of the dissociation rate.

The calculations were performed using the L4cpu, L2fat, and F18acc in the system B, and L4cpu in the system C. The programs AMBER16 [4] and CafeMol3.0 [5] were used for the MDs. We used our custom-made programs for constructing the MSMs.

References

[1] B.E. Husic and V.S. Pande, J. Am. Chem. Soc., **140**, 2386 (2018).

[2] R. Ito and T. Yoshidome, Chem. Phys. Lett., **691**, 22 (2018).

[3] R. Ito and T. Yoshidome, J. Phys. Soc. Jpn., **87**, 114802 (2018).

[4] D.A. Case, *et al.*, AMBER 2016, University of California, San Francisco (2016).

[5] H. Kenzaki, *et al.*, J. Chem. Theory and Comput., **7**, 1979 (2011).

Effect of interface on the dynamics of water confined in mesoporous silica

Tomoko MIZUGUCHI[1], Katsumi HAGITA[2], and Susumu FUJIWARA[1]

[1]*Faculty of Materials Science and Engineering, Kyoto Institute of Technology, Matsugasaki, Sakyo-ku, Kyoto 606-8585*
[2]*Department of Applied Physics, National Defense Academy, 1-10-20, Hashirimizu, Yokosuka, Kanagawa 239-8686*

Many studies have been done on water in confinement by both theoretical and experimental techniques and revealed that the properties of confined water may strongly differ from that of bulk water. It is clearly important to properly evaluate the influence of confinement on water, however, water behavior on amorphous surface is much more difficult to predict than that on crystalline surface because the topology of amorphous surface is ill-defined at the atomic level. We thus performed molecular dynamics (MD) simulations of confined water in nanoporous silica using the reactive force field (ReaxFF) [1] and examined the influence of amorphous surface on the physical properties of water. Specifically, the hydrogen bond (H-bond) dynamics was analyzed.

ReaxFF allows us to incorporate bond breakage and formation, which are particularly important on interface, in MD simulations with a lower computational cost than quantum-mechanics-level calculations. We used the ReaxFF parameter sets developed by Yeon and van Duin in 2015 to simulate hydrolysis reaxtions at silica/water interface [2]. All simulations were conducted in the NPT ensemble (T = 300 K and P = 1 atm) using the Nosé-Hoover thermostat and barostat with LAMMPS pre-installed in the supercomputer of ISSP. The ReaxFF MD simulations were carried out with a time step of 0.25 fs through the USER-REAXC package of LAMMPS. It is found that, in ReaxFF calculations using LAMMPS, FlatMPI parallelization is about twice as fast as than MPI/OpenMP Hybrid parallelization.

To investigate the structure and dynamics of water in the inhomogeneous system, we divided the cylindrical pore into hollow coaxial cylinders and calculated the physical quantities in each thin layer as a function of the radial distance from the pore central axis R. Figure 1 shows the average number of H-bonds per oxygen atom $\langle n_{\mathrm{HB}} \rangle$ and the first breakage time of H-bond τ_{on} as a function of R. The approximate location of the pore wall is also displayed, which is defined as the average location of the innermost Si atoms. τ_{on} is calculated using the following equation,

$$\tau_{\mathrm{on}} = \int_0^\infty t P_{\mathrm{on}}(t) dt, \qquad (1)$$

where $P_{\mathrm{on}}(t)$ is defined as the distribution of time from the formation of a H-bond to its destruction [3]. The H-bonds at 8 Å $< R <$ 11 Å have a longer lifetime, although $\langle n_{\mathrm{HB}} \rangle$ does not change from that in the pore center. It is because the H-bonds at 8 Å $< R <$ 11 Å include silanol (Si-OH) on the silica surface. Namely, the H-bonds including silanols are long-lived and lead to slower diffusion of water (not shown) near the surface.

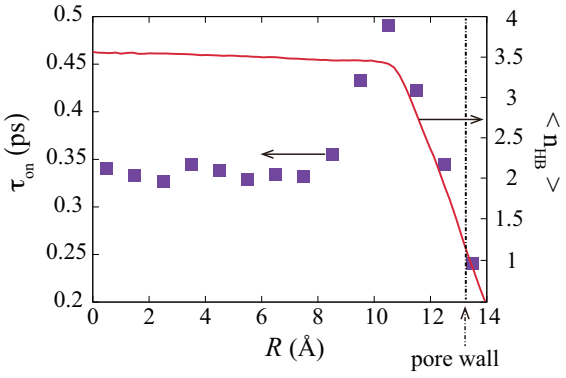

Figure 1: Average number of H-bonds per oxygen atom $\langle n_{\mathrm{HB}} \rangle$ (red solid line, right axis) and first breakage time of H-bond τ_{on} (filled square, left axis) as a function of the radial distance from the pore central axis R. $\langle n_{\mathrm{HB}} \rangle$ The approximate location of the pore wall is also displayed as a dash-dotted line.

References

[1] A. C. T. van Duin, S. Dasgupta, F. Lorant, and W. A. Goddard III: J. Phys. Chem. A **105** (2001) 9396.

[2] J. Yeon and A. C. T. van Duin: J. Phys. Chem. C **120** (2016) 305.

[3] Y. Tamai, H. Tanaka, K. Nakanishi. Macromolecules **29** (1996) 6761.

Numerical study of the off-diagonal ETH in disordered quantum spin chain.

Eiki Iyoda
Department of Physics, Tokai University
Kitakaname, Hiratsuka-shi, Kanagawa 259-1292

Thermalization in isolated quantum many-body systems recently attracts attention, and a plausible mechanism of thermalization is the eigenstate thermalization hypothesis (ETH) [1]. The ETH states that all the energy eigenstates in the microcanonical (MC) energy shell have thermal properties, i.e., the expectation value of an observable $\hat{O}$ approximately equals the MC average:

$$O_{ii} := \langle E_i|\hat{O}|E_i\rangle \simeq \langle \hat{O}\rangle_{\mathrm{MC}}, \tag{1}$$

which is also referred to as the diagonal ETH, because it is written with the diagonal elements. In the same manner, the off-diagonal version of the ETH has been also investigated [2]. The off-diagonal ETH states that

$$O_{ij} := \langle E_i|\hat{O}|E_j\rangle \simeq 0. \tag{2}$$

In this study, we have investigated the (off-)diagonal ETH in disordered quantum spin chains, which exhibit many-body localization transition [3] between the ergodic and the nonerdogic phases. In the disordered phase, the diagonal ETH is not true.

We have numerically investigated the ETHs by using the numerically exact diagonalization. As the indicator of the diagonal ETH, we adopt r defined in Ref. [3]. For the off-diagonal ETH, we calculate the following quantity

$$\Delta := \frac{1}{D(D-1)}\sum_{i\neq j}|O_{ij}|, \tag{3}$$

where D is the dimension of the Hilbert space of the energy shell. The summation is taken over the energy shell. We also calculate the statistical distribution of $|O_{ij}|$.

The Hamiltonian is $1d$ quantum XXZ spin chain with disordered magnetic field.

$$H := \sum_i (S_{\mathrm{x},i}S_{\mathrm{x},i+1} + S_{\mathrm{y},i}S_{\mathrm{y},i+1} + S_{\mathrm{z},i}S_{\mathrm{z},i+1}) + \sum_i h_i S_{\mathrm{z},i}, \tag{4}$$

where h_i is sampled uniformly from $[-h, h]$. We consider a very simple observable $\hat{O} = S_{\mathrm{z},1}$.

Fig. 1 shows h-dependence of r. When h is small, r is small, implying that the diagonal ETH is true. As h becomes larger, r becomes large. This implies that the diagonal ETH is false.

Fig. 2 shows h-dependence of Δ. As h becomes larger, Δ becomes smaller. This implies that the off-diagonal ETH is true in the non-ergodic phase. However, we think that this interpretation is not appropriate. The result is inconsistent with the result of the diagonal ETH. This discrepancy is due to the statistical distribution of $|O_{ij}|$.

Fig. 3 shows h-dependence of $|O_{ij}|$. In the ergodic phase with the weaker disorder, The median, upper quartile, and lower quartile decrease in h, probably because the participation entropy in the non-ergodic phase is small [3]. Thus, most of the energy eigenstates do not contribute to Δ. We consider that the maximum value of $|O_{ij}|$ should characterize the MBL transition of the off-diagonal ETH. The reason why the median and quartiles decrease is that most of the elements $|O_{ij}|$ are much

smaller than ones expected from the random matrix theory.

In this report, we have shown the results for the very simple observable. We also calculate other local observables, and they show similar behavior (not shown). Though the off-diagonal elements for other disorder realizations also show similar behavior, we should analyze systematically and quantitatively with more samples. Investigating non-local observables and other models, which exhibit another phase transition, are future issues.

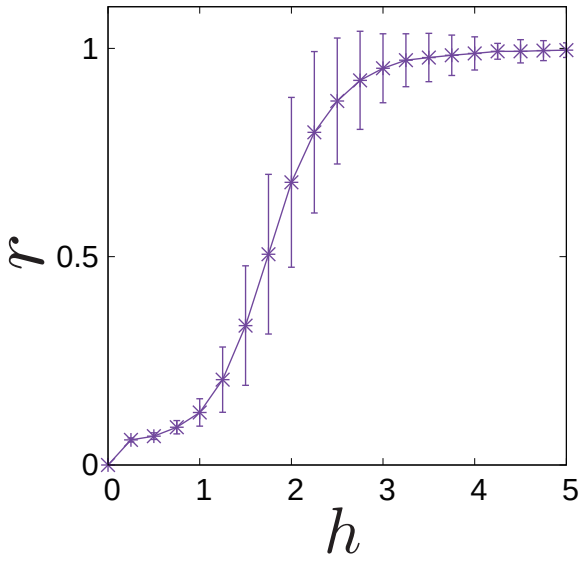

Figure 1: Disorder h-dependence of the diagonal-ETH indicator r. The number of samples is 200.

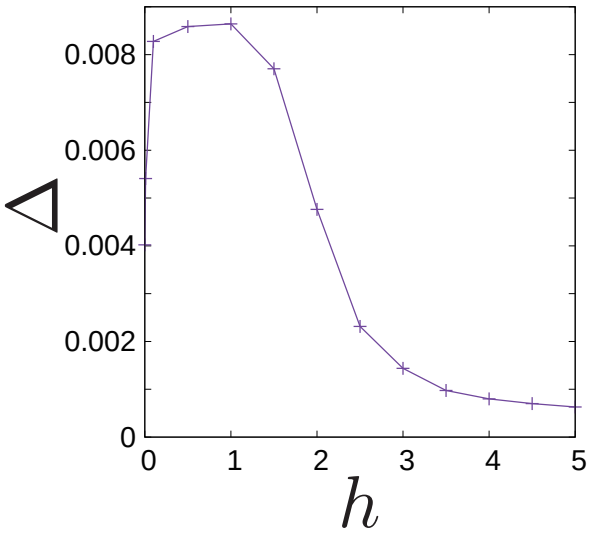

Figure 2: Disorder h-dependence of the off-diagonal-ETH indicator Δ. with single disorder realization.

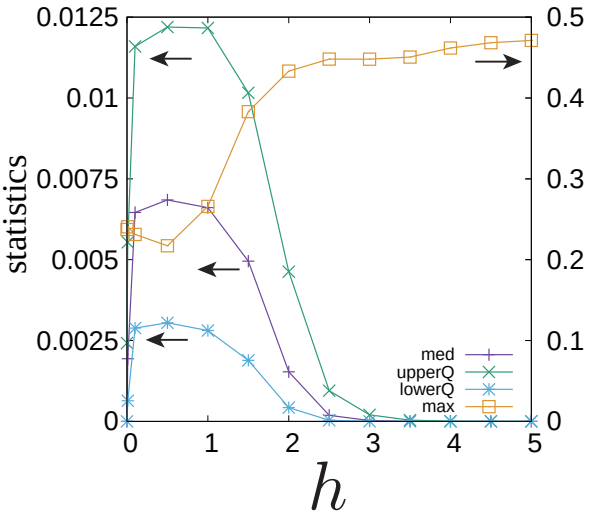

Figure 3: Disorder h-dependence of the median, upper quartile, lower quartile and maximum values of $|O_{ij}|$'s with single disorder realization.

References

[1] M. Rigol, V. Dunjko, and M. Olshanii, Nature **452**, 854 (2008).

[2] R. Mondaini and M Rigol, Phys. Rev. E **96**, 012157 (2017).

[3] D. J. Luitz, N. Laflorencie, and F. Alet, Phys. Rev. B **91**, 081103 (2015).

[4] H. Kim, T. N. Ikeda, and D. A. Huse, Phys. Rev. E **90**, 052105 (2014).

Spinglass transitions in frustrated vector spin models

Hajime YOSHINO
Cybermedia Center, Osaka University
1-32 Machikaneyama, Toyonaka, Osaka 560-0043
(Dated: April 26th,2019)

Possibility of spinglass transitions induced by purely geometrical frustration without quenched disorder has been a long standing issue in the field of frustrated magnets. A prominent candidate [1] is the frustrated antiferromagnet on the pyrochlore lattice such as $Y_2M_2O_7$. Recently we found theoretically [2] that spinglass transitions without quenched disorder occur in a family of exactly solvable vectorial spin models in a large dimensional limit.

In the present project we analyzed static and dynamics properties of an original theoretical model [3] developed for the pyrochlore system performing Monte Carlo simulations. Our model is motivated by experiments which suggest relvance of lattice distortions: we consider classical Heisenberg spins on the vertices of the pyrochlore lattice which deforms dynamically. The lattice distortion induces changes of the magnetic coupling. Contrary to the conventional view point, we do *not* assume static, quenched distortion but allow *dynamic* distortions.

In the figure below we display some of our key findings. We found both the a) lattice and b) spin degrees of freedom exhibit critical slowing down approaching a critical temperature. The non-linear susceptibility c) become negatively large increasing the system size around the critical temperature. On the other hand, the static structure factors d) of the lattice and spin degrees of freedom exhibit no qualitative changes passing the critical temperature. These observations strongly suggest existence of a 2nd order spinglass transition where both the spins and lattice distortions collectively freeze at the same critical temperature.

Our simulations are performed on system B (2,000 points, 24000 node hours, jobclasses: B18acc, F18acc, L18acc). The program code was paralellized within nodes by openmp.

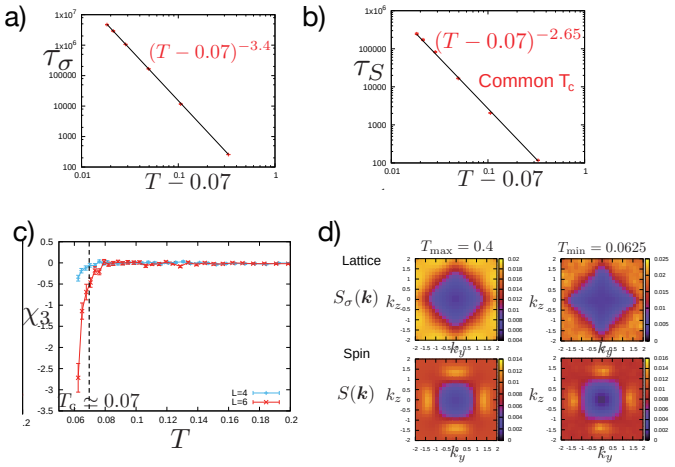

FIG. 1. Results of Monte Carlo simulations. a) and b): relaxation times of the spin and lattice auto-correlation functions. c): the non-linear susceptibility evaluated through the fluctuation formula. d): the static structure factors of the spin and lattice distortions.

[1] M. J. P. Ginsgras, et. al. PRL **78** 947 (1997).
[2] Hajime Yoshino, Disorder-free spin glass transitions and jamming in exactly solvable mean-field models, SciPost Physics, 4(6), 040 (2018).
[3] Kota Mitsumoto, Chisa Hotta, and Hajime Yoshino, in preparation.

Magnetic excitation and spin transport in frustrated quantum spin chain

Hiroaki ONISHI
Advanced Science Research Center, Japan Atomic Energy Agency
Tokai, Ibaraki 319-1195

In a spin-1/2 J_1-J_2 Heisenberg chain with ferromagnetic J_1 and antiferromagnetic J_2 in a magnetic field, there occurs a spin nematic liquid ground state, which is also spin-density-wave quasi-long-ranged. We have studied spin and quadrupole excitation spectra and found that low-energy excitations are governed by bound magnon pairs [1]. Thus we expect that magnon pairs would carry spin current.

To gain an insight into the spin transport property mediated by magnon pairs, we study the spin Drude weight [2]. We perform exact diagonalization with up to 24 sites to obtain all eigenenergies and eigenvectors and evaluate thermal expectation values. Utilizing the total magnetization and the momentum for block-diagonalization, the maximum dimension is 112720, accessible thanks to MPI simulations with ScaLAPACK on the system B of the ISSP supercomputer.

In Fig. 1(a), the temperature dependence of the spin Drude weight at zero magnetic field is presented. Note that data of $N = 4n$ sites and those of $N = 4n + 2$ sites show different behavior, since the system is regarded as two J_2 chains connected by J_1, and each J_2 chain includes even sites for $N = 4n$ and odd sites for $N = 4n + 2$. For $N = 4n$, the spin Drude weight decreases with N at high temperatures, while it increases with N at low temperatures. A crossover temperature separating these two regions seems to approach zero temperature with N. This is suggestive of vanishing spin Drude weight, i.e., diffusive spin transport.

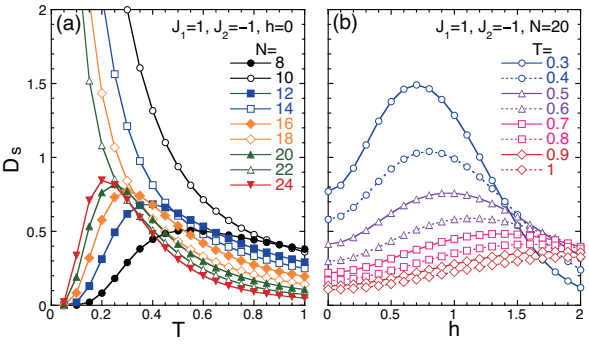

Figure 1: (a) Temperature and (b) magnetic field dependencies of spin Drude weight.

In Fig. 1(b), we show the dependence on the magnetic field at various temperatures. With increasing the magnetic field, the spin Drude weight is enhanced, while it is suppressed after showing a peak. The peak structure is more clearly seen at lower temperatures. Note that the ground state should have contribution to observables at low temperatures. In this sense, the enhancement of the spin Drude weight at low temperatures is regarded as a precursory phenomenon of the formation of magnon pairs at zero temperature, suggesting that magnon pairs would contribute to the spin transport.

References

[1] H. Onishi, J. Phys. Soc. Jpn. **84**, 083702 (2015); J. Phys.: Conf. Ser. **592**, 012109 (2015); Physica B **536**, 346 (2018).

[2] H. Onishi, J. Magn. Magn. Mater. **479**, 88 (2019).

Analysis on Structuring and Dynamics of Ionic Liquid Forming Electric Double Layer at Electrode Interfaces

Ken-ichi FUKUI

Department of Materials Engineering Science, Graduate School of Engineering Science, Osaka University, Machikaneyama, Toyonaka, Osaka 560-8531

Ionic liquids (ILs) are promising electrolytes for electrochemical devices such as secondary battery, capacitor, electric double layer (EDL)-FET, etc., due to their high chemical stability with negligible vaporization. Structuring and dynamics of the interfacial IL faced to charged graphite electrodes were analyzed by molecular dynamics (MD) calculations [1].

The MD simulations were performed with AMBER 11. The graphite substrate consisted of unit cells of linear dimensions 83.0×72.1 ×30.2 Å^3, respectively. Around 800 BMIM-TFSI ion pairs (46000 atoms) were sandwiched between the substrates and a vacuum layer (> 4 nm) (Fig. 1). The systems were equilibrated at a constant volume for 100 ps, followed by a constant volume simulation for 5 ns with fixing all of the substrate atoms. The MD simulations were performed at 300, 350, 400, and 450 K.

Fig. 2 shows the side view of the first-layer ions (z < 6.5 Å) and the total atom number density profiles as a function of the surface charge. The total atom number density profile of the BMIM cation (blue) at pzc (center) indicates a single peak (z = 3.5 Å) with shoulders, whose intensity increases with the negative potential and decrease with the positive potential without changing the overall shape. In contrast, the profile of the TFSI anion (red) at pzc (center) has three peaks at 3.0, 4.0, and 5.5 Å, and its potential dependence is more complicated at negative potential compared to the BMIM cation. These changes reflect a significant difference in the ionic arrangement on the graphite between the checkerboard type at the positive potential and the bilayer type at the negative potential and strongly affect the mobility of interfacial ions.

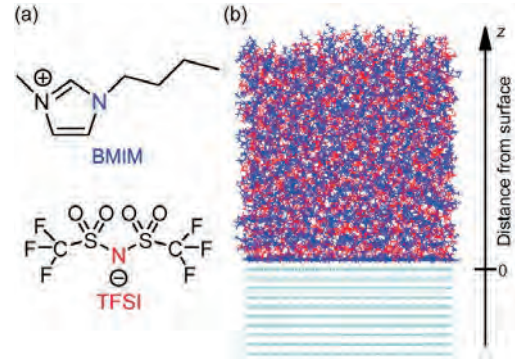

Fig. 1: (a) Ionic liquid (BMIM-TFSI) and (b) a MD snapshot for graphite the interface. BMIM cations and TFSI anions are represented by blue and red colors, respectively.

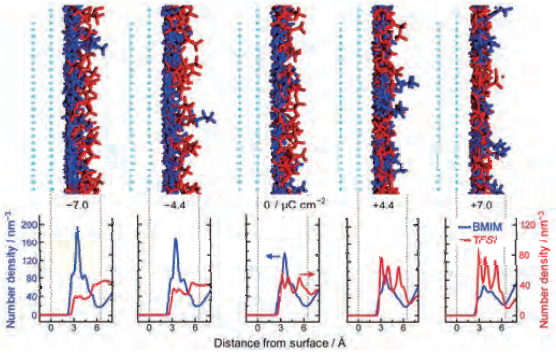

Fig. 2: (top) Side-view snapshots of the first layer ions (z < 6.5 Å) and (bottom) the total atom number density profiles for the indicated charge density of on the graphite electrode. BMIM cations and TFSI anions are represented by blue and red colors, respectively. Each cyan-colored dot represents a carbon atom in the graphite substrate.

Reference

[1] H. Miyamoto, Y. Yokota, A. Imanishi, K. Inagaki, Y. Morikawa, K. Fukui, *Phys. Chem. Chem. Phys.* **20**, 19408 (2018)

Transferability of machine learning forces to temperature and pressure

Ryo TAMURA
International Center for Materials Nanoarchitectonics,
National Institute for Materials Science,
1-1 Namiki, Tsukuba, Ibaraki, 305-0044

Data-driven techniques are becoming more and more valuable in materials science[1, 2, 3]. One of the important issues in this trend is to predict atomic forces by machine learning (ML). If we can develop a method to predict ML forces having almost the same accuracy as density functional theory (DFT) calculations, the cost of force calculations in molecular dynamics (MD) simulations will be much lower. As a result, we can perform prolonged MD simulations of large systems with DFT-level accuracy, and understanding of materials properties would be deepened.

In our study, we trained a machine-learning model for the Si and Ge single-component systems in order to directly predict the atomic forces at a wide range of temperatures and pressures in the liquid state[4, 5]. Gaussian process regression is adopted as the machine learning technique to predict atomic forces, and we use atomic fingerprints that express the local structure around the target atom. The training and test data are generated by MD simulations based on DFT using a linear-scaling method using the CONQUEST code[6].

We first clarified the accuracy of the ML model when both training and test data were sampled from the DFT-MD simulations at the same temperature. We found that the accuracy becomes the lowest around the phase boundary between the solid and liquid states. However, even in the liquid state, the relative error is smaller than 6.5% for the Si system and 5.2% for the Ge system. ML models with such accuracy are useful for performing MD simulations to calculate the physical properties. Figure 1 shows the prediction results for the Si system at 1200 K (solid state) and 9000 K (liquid state).

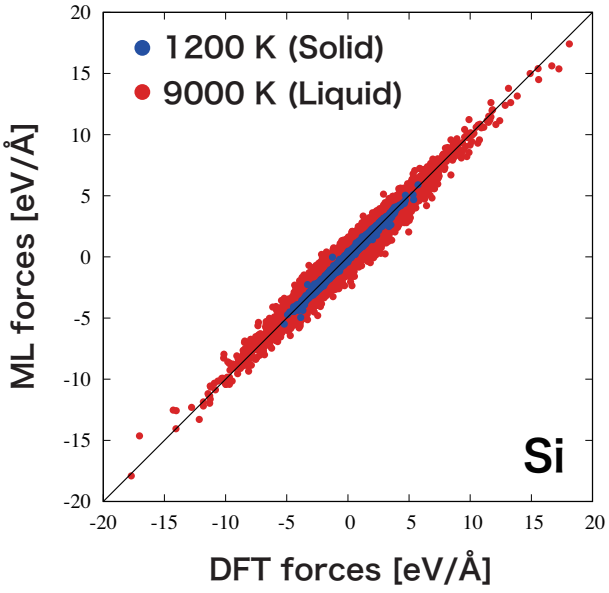

Figure 1: Parity plot of DFT forces versus ML forces for the Si single-component systems.

Next, we investigated the transferability of ML models trained in the liquid state to temperature and pressure. We demonstrated that, if the training is performed at a high temperature and if the volume change is not so large, the transferability of ML forces in the liquid state is sufficiently high, whereas its transfer-

ability to the solid state is very low. Thus, in the liquid state, the ML model using training data generated by the DFT-MD simulations under specific conditions, such as at a high temperature with a standard volume, can be used to accurately predict forces under various conditions without additional or further DFT-MD simulations.

References

[1] K. Shiba, R. Tamura, T. Sugiyama, Y. Kameyama, K. Koda, E. Sakon, K. Minami, H. T. Ngo, G. Imamura, K. Tsuda, and G. Yoshikawa, ACS Sensors **3**, 1592 (2018).

[2] M. Sumita, X. Yang, S. Ishihara, R. Tamura, and K. Tsuda, ACS Central Science **4**, 1126 (2018).

[3] K. Terayama, R. Tamura, Y. Nose, H. Hiramatsu, H. Hosono, Y. Okuno, and K. Tsuda, Phys. Rev. Matererials **3**, 033802 (2019).

[4] T. Suzuki, R. Tamura, and T. Miyazaki, Int. J. Quantum Chem. **117**, 33 (2017).

[5] R. Tamura, J. Lin, and T. Miyazaki, J. Phys. Soc. Jpn. **88**, 044601 (2019).

[6] http://www.order-n.org.

Schmidt-number dependence of phase-separation dynamics of colloidal suspensions

Michio Tateno and Hajime Tanaka
Department of Fundamental Engineering, Institute of Industrial Science, University of Tokyo
4-6-1 Komaba, Meguro-ku, Tokyo 153-8505

Colloidal suspensions are a mixture of large colloidal particles and small solvent molecules, between which there is a huge gap in the characteristic time scales of the motion. It is known that the Schmidt number, $S_c = \nu/D$, is a dimensionless parameter that characterizes the difference between the momentum and material diffusion, where ν is the kinetic viscosity of the solvent and D is the thermal diffusion constant of a free isolated colloid. In typical colloidal systems, these two diffusion coefficients differ by many orders of magnitude (for example, $S_c \sim 10^6$, for μm-size colloids suspended in water at room temperature), and this condition ($S_c \gg 1$) is widely assumed in the physical laws associated with the dynamics of colloids, such as the Stokes-Einstein relation. For such a large Schmidt number, numerically accessing the colloidal dynamics, such as collective colloidal motion, self assembly dynamics, and rheological behavior, starting from molecular-level dynamics, is almost impossible with current computational power. Indeed, in most of simulation studies, the Schmidt number has been set to modest values ($S_c < 10$) [1].

The main purpose of this project is to clarify the Schmidt number dependence on colloidal dynamics, with which we aim to provide a guidance on the minimum S_c that we need to reproduce real colloidal dynamics. In this project, we used a hydrodynamic simulation model, fluid particle dynamics (FPD) method [3, 4], which is based on direct computation of the Navier-Stokes equation. We have shown that this FPD method combined with fluctuating hydrodynamics at $S_c = 8$ can well reproduce the Brownian motion of a free isolated colloid while satisfiying statistical mechanical consistency between colloids and solvent [4]. Below we focus on phase-separation dynamics of colloidal suspensions, which may be regarded as a typical example of nonequilibrium phenomena of colloidal matter.

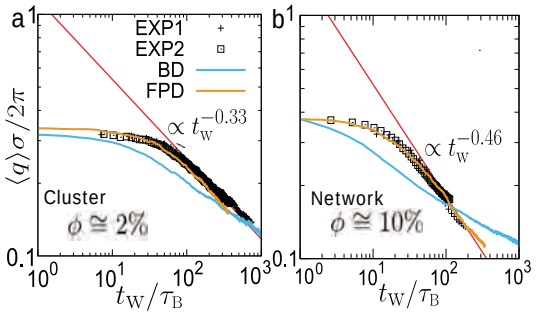

Figure 1: Time evolution of the characteristic wave number $\langle q(t) \rangle$ for two different volume fractions $\phi \simeq 2$ % (a) and 10 % (b). Here we compare two experiments and two simulations: EXP1 (black cross), EXP2 (black square), BD (blue curve) and FPD (brown curve). In FPD simulation, we set the Schmidt number as $S_c = 8$.

We first show the time evolution of the characteristic wave number $\langle q(t) \rangle$, which is approximately inversely proportional to the characteristic domain size of colloidal aggregates. Panel a and b in Fig. 1 corresponds to the results at the colloidal volume fractions of 2% and 10%, where isolated clusters and space-spanning network structure of the colloid-rich

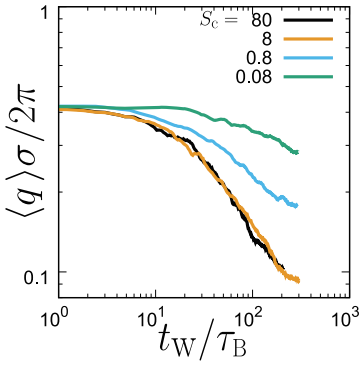

Figure 2: The temporal change of the characteristic wave number $\langle q \rangle$ during phase separation at $\phi \simeq 10$ % for four different Schmidt numbers.

phase are observed respectively. To evaluate the validity of the simulation results, here we compare them to experimental results obtained by three-dimensional (3D) confocal microscopy observations (black cross and black square). In the figure, we can cleary see that results obatined by the FPD simulation with $S_c = 8$ almost perfectly reproduce the experimental results (EXP1 and EXP2: see Ref. [5] on the detail of experiments). BD in Fig. 1 corresponds to simulation results by Brownian dynamics without hydrodynamic interactions, and obviously fails to reproduce the experimental results. These results clearly indicate the fundamental importance of many-body hydrodynamic interactions in colloidal phase separation.

Next we check under what condition the agreement in the time development of $\langle q \rangle$ during phase separation between EXP and FPD can be attained. In Fig. 2, we show the temporal change of the characteristic wave number $\langle q \rangle$ at $\phi \simeq 10\%$ for four different Schmidt numbers: $S_c = 0.08, 0.8, 8, 80$. We can clearly see that $\langle q \rangle$ is almost identical when the Schmidt number satisfies $S_c \geq 8$.

Here we consider why we can see such a good agreement even with a rather moderate Schmidt number $S_c \sim 10$. The key time scale is the characteristic time required for the momentum of the solvent to diffuse over a characteristic distance l_c from a particle, which is given by $\tau_\nu(l_c) \cong l_c^2/\nu$. Denoting the colloid diameter as σ and the Brownian time as $\tau_B = (\frac{\sigma}{2})^2/6D$, then $\tau_\nu/\tau_B \cong 24(l_c/\sigma)^2 S_c^{-1}$. This means that how far the momentum diffuses away within the time scale of τ_B depends on the value of S_c. For $S_c \sim 10$ and $\tau_\nu/\tau_B \sim 1$, for example, we obtain $l_c/\sigma \sim 1$, implying that a flow field around a particle is established by momentum diffusion at least up to a distance of about the particle diameter from that particle. This indicates that, for $S_c \sim 10$, our method can properly describe near-field many-body hydrodynamic interactions, which is expected to play a dominant role in the aggregation process of colloids undergoing Brownian motion.

In summary, we study the Schmidt number dependence of phase separation dynamics of colloidal suspensions, and found that our hydrodynamic simulation model (FPD method) with a moderate Schmidt number (i.e., $S_c \sim 10$) is able to precisely reproduce experimental results observed by confocal microscopy. Our result provides a guidance on the parameter setting required for proper hydrodynamic simulations of colloidal suspensions.

References

[1] F. B. Usabiaga, X. Xie, R. Delgado-Buscalioni and A. Donev : J. Chem. Phys. **139** (2013) 214113

[2] A. Furukawa and H. Tanaka: Phys. Rev. Lett. **104**, (2010) 245702.

[3] H. Tanaka and T. Araki: Phys. Rev. Lett. **85**, (1999) 1338

[4] A. Furukawa, M. Tateno and H. Tanaka: Soft Matter **14** (2018) 3738

[5] M. Tateno and H. Tanaka: npj Computational Materials **5** (2019) 40

Numerical study of collective motion transition of crowding cells with anisotropic shape.

Katsuyoshi Matsushita
Depertment of Biological Science, Osaka University
Machikaneyama 1-1, Toyonaka, Osaka 560-0043

Collective motion of cells is a fundamental phenomenon for development of organisms, wound healing, and immune response [1]. This motion usually be driven by pseudepod formation and is associated by the elongation of the cell shape due to the pseudepods. Therefore, the cell shape is correlated to the cell motion. The clarification of the correlation effects is an important issue for the understanding of physical mechanisms of these collective motion.

Even in crowding environments in organism bodys, these cells move with with this elongation. The elongation is expected to induce another correlation between motion and shape because the cell shape affects the excluded volume interaction and subsequently the interaction affects the motion. This composite effect is not clear today. To get insight into the composite effect on collective motion in crowding cells, we tried to model this situation and numerically investigated the shape dependence on the collective motion on the model.

For this purpose, we employed the Cellular Potts model and its Kinetic Monte Carlo simulation [2]. This model have used to appropriately represent the motion of cells through flexible shape changes in tissues, which is expected for collective motions under cell crowding in organism bodys [3]. Furthermore, this model can easily express the excluded volume of cells as a surface free energy. These properties help us to express the above crowding cells with collective motion.

We further constructed model elongated cells with correlating its motion by using the cell model with the spatial polarization in F-actin density [4]. We simulated the cells with elongation and showed that the elongation of the model cells stabilize their collective motion. This result implies the steric interaction effect due to the elngated excluded volume between cells. Namely, the steric interaction stabilizes the nematic ordering of the elongated cell shape and also thereby aligns cell motion in the elongation direction of cells.

In contrast, when the elongation due to F-actin is weaken and the cell shape exhibits isotoropy, the collective motion is destabilized. This is because the stabilization effect of steric interaction in cell shape is absent in the isotropic cell. In this case, the cells collectively exhibits large fluctuation in their motion and the direction of motion frequently changes in time advance. This result implies the function of the cell elongation for stabilization of the collective motion in organism bodys.

References

[1] C. J. Weijer: J. Cell Sci. 122 (2015) 3215.

[2] F. Graner and J. A. Glazier: Phys. Rev. Lett. 69 (1992) 2013.

[3] A. J. Kabla, J. R. Soc. Interface 9 (2012) 3268; K. Matsushita: Physical Review E 95 (2017) 032415.

[4] K. Matsushita: Proc Sympo. Simul. Traffic flow 23 (2017) 37.

Computer-simulated eight-beam and 18-beam X-ray pinhole topographs based on the Ewald-Laue dynamical theory and FFT

Kouhei OKITSU

Institute of Engineering Innovation, School of Engineering,

The University of Tokyo, 2-11-16 Yayoi Bunkyo-ku Tokyo 113-8656

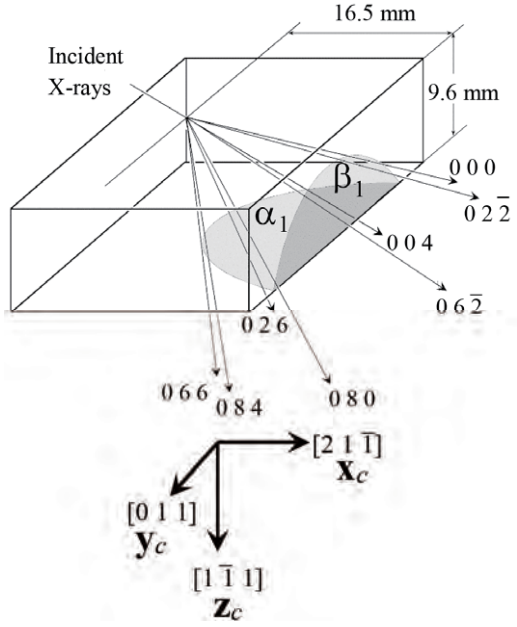

Fig. 1 Schematic drawing of the geometry of the eight-beam pinhole topographs [1].

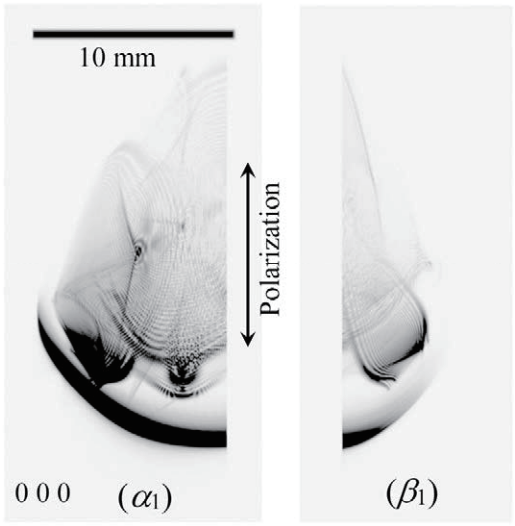

Fig. 2 Pinhole topograph of 0 0 0 forward-diffracted X-rays computer-simulated separately for α_1 and β_1 of Fig. 1. (α_1) and (β_1) were linked to obtain Fig. 3 [S_v(E-L)] [1].

Experimentally obtained and computer simulated eight-beam and 18-beam pinhole topographs were compared and agreed with each other.

In the eight-beam case, the experimental setup used when taking the topographs and assumed in the computer simulation is as shown in Fig. 1. (α_1) and (β_1) in Fig. 2 were computer-simulated pinhole topographs. These were separately calculated under the assumptions of [1 -1 1]-oriented silicon crystal with a thickness of 9.6 mm, and of [2 1 -1]-oriented one with a thickness of 16.5 mm, respectively. Figs. 2 (α_1) and 2 (β_1) were obtained by fast Fourier-transforming the amplitude of forward-diffracted or transmitted-reflected X-rays calculated based on the Ewald-Laue dynamical diffraction theory. This method (E-L FFT simulation) was reported by Kohn and Khikhlukha (2016) and Kohn (2017) for a symmetric six-beam case for the first time. However, the present eight-beam case is an asymmetric case for a silicon crystal whose shape is not single planar. Figs. 2 (α_1) and 2 (β_1) were linked to obtain Fig. 3 [S_v(E-L)] that are in excellent agreement with Fig. 3 [E_v] experimentally obtained.

On the other hand, experimentally obtained 18-

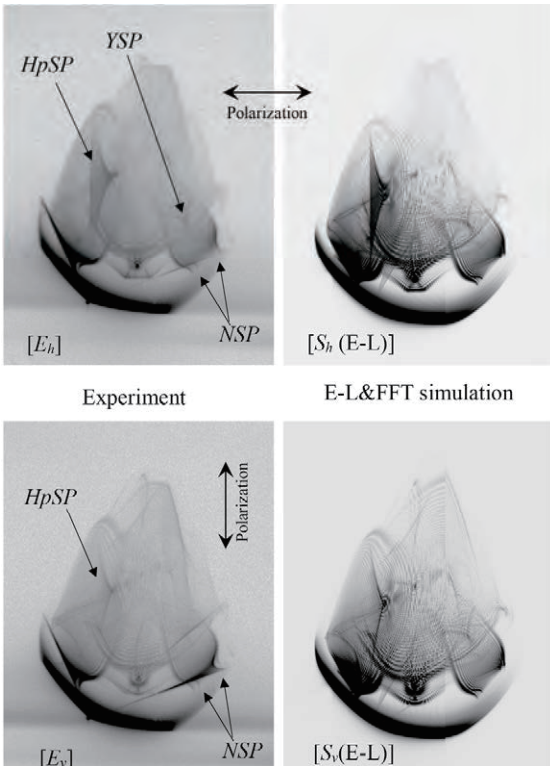

Fig. 3 [E_x] and [S_x(E-L)] (x is h or v; polarization state of the incident X-rays) are experimentally obtained and computer-simulated topographs [1].

beam pinhole topographs as shown in Fig. 4 (a) were also in good agreement with Fig. 4 (b). In this 18-beam case, reciprocal lattice nodes giving the Bragg reflections for inner six images and outer 12 ones do not exist on a circle in reciprocal space (non-circular case).

From the agreement between the experimentally obtained pinhole topographs and those obtained with the computer simulation, it has been revealed that the E-L FFT simulation is effective even when the crystal has a complex shape and/or the reciprocal lattice nodes simultaneously giving the Bragg reflections do not ride on a single circle in reciprocal space. This situation is the case for multiple reflection (widely known as the Renninger effect) in crystal structure analysis in general.

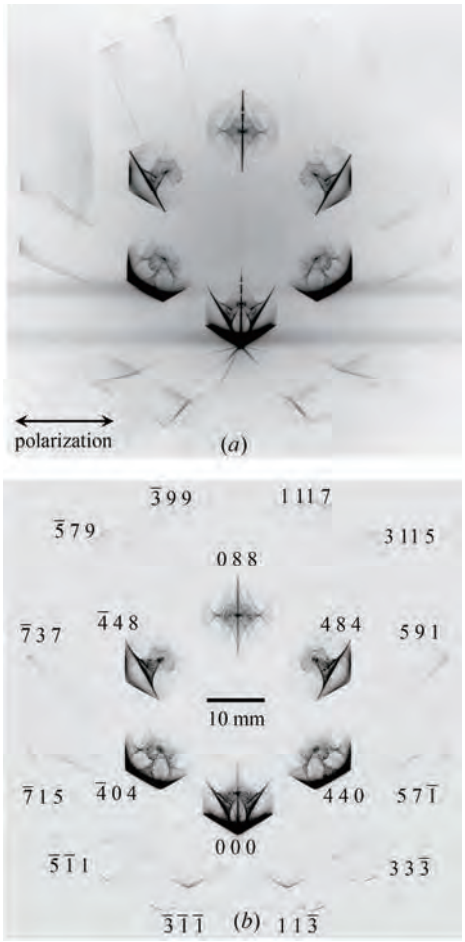

Fig. 4 (a) and (b) are experimentally obtained and computer-simulated 18-beam pinhole topographs [2].

The present author has a hypothesis that too large R factor for macro molecules is caused by multiple reflection and bankruptcy of the two-beam approximation that has been used for over 100 years. The present author has prepared to verify this hypothesis concerning the too large R factor of macro molecule crystals by estimating it with multiple-beam approximation in place of the conventional two-beam approximation.

References

[1] K. Okitsu, Y. Imai, Y. Yoda and Y. Ueji: *Acta Cryst.* **A75** (2019) In Press in Advanced Section.

[2] K. Okitsu, Y. Imai, and Y. Yoda: *Acta Cryst.* **A75** (2019) In Press in Advanced Section.

Calculation of ordered structures and their optical properties of soft materials

Jun-ichi FUKUDA

Department of Physics, Kyushu University, Motooka 744, Nishi-ku, Fukuoka 819-0395

We have made use of the supercomputer facility of ISSP in part to investigate particularly the ordered structures of a chiral liquid crystal under strong spatial confinement between two parallel plates. Last year we showed that such a thin system of a chiral liquid crystal exhibits various exotic ordered structures [1], including a hexagonal lattice of half-Skyrmions (a swirl-like structure of orientational order without singularities at the center) and a thin slice of bulk three-dimensional structure known as cholesteric blue phase. We also calculated their microscope images in excellent agreement with experimental ones.

This year, based on the solutions of the Maxwell equations for light wave utilized for the construction of numerical microscope images, we constructed numerical Kossel diagrams exhibited by the above-mentioned ordered structures [2]. Kossel diagrams are made up of straight or elliptic lines (Kossel lines) visualizing the directions of strong reflections of monochromatic light incident onto the sample from different directions within a certain solid angle. Kossel diagrams are commonly used to investigate the symmetry of bulk crystal structures exhibiting strong Bragg reflections. How Kossel diagrams should be interpreted for a thin system was not clear. We compared numerical Kossel diagrams again with experimental ones, and they showed good agreement with each other on the locations and intensities of Kossel lines. We further showed that Kossel lines of a thin system should be attributed not to Bragg reflections but the coupling between different guided modes through the periodic structure of the system. The locations of the Kossel lines deduced from the above theoretical argument are in perfect agreement with those of numerical Kossel lines. We demonstrated that Kossel diagrams are useful not only for the determination of bulk crystal symmetry but also for the investigation of the structural properties of a thin system.

References

[1] A. Nych, J. Fukuda, U. Ognysta, S. Žumer and I Muševič, Nature Phys. **13**, 1215 (2017).

[2] J. Fukuda, A. Nych, U. Ognysta, S. Žumer and I Muševič, Scientific Reports **8**, 17234 (2018).

Coherent Control of Nonadiabatic Wavepacket Dynamics of Electron-phonon-photon Systems

Kunio ISHIDA

Department of Electrical and Electronic Engineering, School of Engineering, Utsunomiya University, 7-1-2, Yoto, Utsunomiya, Tochigi 321-8585

Recent experiments on diamond showed the possibility of phonon-mediated coherence between qubits via Raman scattering processes[1]. In this case, entanglement between electrons, phonons, and photons plays an important role, which means that fully quantized theory of interaction between irradiated light and materials is necessary to reveal and/or design the control methods for them.

In order to study the quantum dynamics of those systems, we numerically solved the time-dependent Schödinger equation for electron-phonon-photon systems described by the Hamiltonian[2]:

$$\mathcal{H} = \omega a^{\dagger}a + \sum_{i=1}^{n} \Omega_i {c_i}^{\dagger} c_i + \{\mu(a^{\dagger} + a) + \varepsilon\}\frac{\sigma_z + 1}{2} + \left\{\sum_{i=1}^{n} \nu_i({c_i}^{\dagger} + c_i) + \lambda\right\}\sigma_x,$$

where n is the number of photon modes, and a and c_i denote the annihilation operators of phonons and the photons of the i-th mode, respectively. σ_i corresponds to the Pauli matrices which operate on the electronic states denoted by $|g\rangle$ ground state) and $|e\rangle$ excited state). ω and Ω_i are the angular frequencies of phonon and the i-th mode photon, while ν and μ_i give the strength of the electron-phonon coupling and the dipole interaction, respectively. λ is the nonadiabatic coupling between electronic states, and ε is the energy difference between $|g\rangle$ and $|e\rangle$. The initial state of the i-th mode photon is a coherent state parameterized by α_i. Since not only the phonon mode but also three photon modes are quantized, the dimension of the Hilbert space of electron-phonon-photon systems is as large as 10^8. Hence, numerical calculations require a lot of computational resources, and hybrid parallelization is made on the source code for the System B.

As an example of coherent dynamics of the system, we show the calculated results of control by external light field, we show that the relative phase between photons affects the created phonon states. Figure 1 shows the number of phonons $N_n(t) = \langle\Phi(t)|a^{\dagger}a|\Phi(t)\rangle$ for $\Delta\phi = -\pi, -\frac{\pi}{2}, 0, \frac{\pi}{2}$ and π, where $\Delta\phi$ denotes the phase difference between Stokes/anti-Stokes mode and the pump mode, i.e., $\alpha_2 = |\alpha_2|e^{i\Delta\phi}$ and $\alpha_3 = |\alpha_3|e^{-i\Delta\phi}$. Since the wavepacket

trajectory varies with $\Delta\phi$, different phonon states are created in the material, which shows that the number of phonons is able to be modified by $\Delta\phi$.

We have been studied the dynamical properties of a single electron-phonon system so far, and these results will be a basis to study various types of non-classical correlations between noninteracting systems mediated by incident light, e.g., creation of phonon entanglement in spatially separated diamond crystals[3].

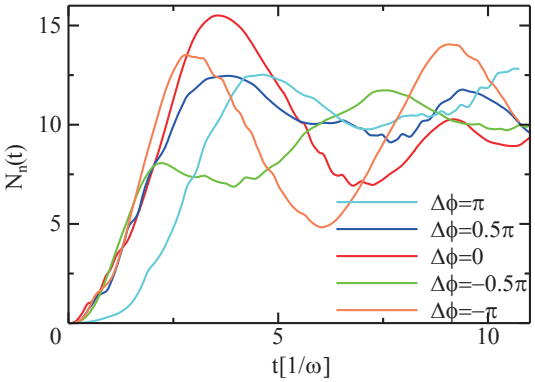

Fig.1 The average number of phonons $N_n(t)$ for $\alpha_1 = 5, \alpha_2 = \alpha_3 = 3.16, \lambda = 1.5$ with different values of $\Delta\phi$.

References

[1] D. G. England, *et al*., Phys. Rev. Lett. **117**, 073603 2016).

[2] K. Ishida, Eur. Phys. J. D, doi: 10.1140/epjd/e2019-09485-5.

[3] K. C. Lee, *et al*., Science **334**, 1253 2011).

Transport properties of the classical antiferromagnetic Heisenberg model on the triangular lattice

Kazushi AOYAMA
Department of Earth and Space Science, Graduate School of Science, Osaka University
Machikaneyama-cho, Toyonaka-shi, Osaka 560-0043

The ground state of the nearest neighbor(NN) antiferromagnetic Heisenberg model on the triangular lattice is the non-collinear 120° Neel state, so that the order parameter space has the $SO(3)$ symmetry. On the two-dimensional lattice, a point defect, namely, a vortex excitation, in the SO(3) manifold is characterized by the topological number of $\mathbf{Z}_2$. In contrast to a conventional vortex having an integer topological number $\mathbf{Z}$, less is known about how the $\mathbf{Z}_2$ vortices affect magnetic properties of the system. In this work, we investigate transport properties of the triangular-lattice Heisenberg model, putting emphasis on the role of the $\mathbf{Z}_2$-vortex excitation.

The spin Hamiltonian of the present system is given by

$$\mathcal{H} = -J \sum_{\langle i,j \rangle} \mathbf{S}_i \cdot \mathbf{S}_j \qquad (1)$$

where $\mathbf{S}_i$ is a classical Heisenberg spin at a lattice site i. From the Hamiltonian (1), one can derive the semiclassical equation of motion for spins as follows,

$$\frac{d\mathbf{S}_i}{dt} = \Big(-J \sum_{j \in N(i)} \mathbf{S}_j \Big) \times \mathbf{S}_i, \qquad (2)$$

where $N(i)$ denotes all the NN sites of i. Since Eq. (2) is a classical analogue of the Heisenberg equation for the spin operator, all the static and dynamical properties intrinsic to the Hamiltonian (1) could be described by the combined use of Eqs. (1) and (2).

Within the linear response theory, the conductivities of the spin current $\mathbf{J}_s$ and the thermal current $\mathbf{J}_{th}$ can be obtained by evaluating the thermal average of the time correlations of $\mathbf{J}_s$ and $\mathbf{J}_{th}$ which are respectively given by

$$\begin{aligned} \mathbf{J}_s &= \frac{J}{2} \sum_{\langle i,j \rangle} (\mathbf{r}_i - \mathbf{r}_j)(\mathbf{S}_i \times \mathbf{S}_j)^z, \\ \mathbf{J}_{th} &= \frac{J^2}{2} \sum_{\langle i,j,l \rangle} \mathbf{r}_l \, \mathbf{S}_l \cdot (\mathbf{S}_i \times \mathbf{S}_j) \end{aligned} \qquad (3)$$

with $\mathbf{r}_i$ being the position of a site i.

Starting from temperature-dependent initial spin configurations generated by Monte Carlo (MC) simulations, we numerically integrate Eq. (2) to obtain the time correlations of $\mathbf{J}_s$ and $\mathbf{J}_{th}$. In this work, we perform long-time integration typically up to $t/|J| = 100 - 800$ with time step $\delta t/|J| = 0.01$ and the thermal average is taken as the average of 2000-4000 initial spin configurations which are picked up every 1000 MC sweeps after 10^5 MC sweeps for thermalization. Here, in our MC simulations with linear system size L, one MC sweep consists of 1 Heatbath sweep and successive 10-30 over-relaxation sweeps. Most of the calculation is done by using the facilities of the Supercomputer Center, ISSP, the University of Tokyo.

It is found by performing the above calculations for $L = 24 - 768$ that the longitudinal spin conductivity is significantly enhanced at the $\mathbf{Z}_2$-vortex transition temperature T_v, while the thermal conductivity does not exhibit any clear anomaly near T_v.

Molecular simulation of colloidal suspensions

Takamichi TERAO

Department of Electrical, Electronic, and Computer Engineering,

Gifu University, Yanagido 1-1, Gifu, 501-1193

The self-assembly of colloidal particles is a fundamental topic in material science, and diverse colloidal composites are applied in various industries. The industrial applications include photonic crystals with bandgaps that prevent the propagation of light within a certain frequency range. Polymer–nanoparticle composites, also known as spherical polymer brushes, are a typical example of a soft colloidal system. Spherical polymer brushes contain an inner core particle that cannot overlap another core particle.

Recently, spherical dendritic brushes, which have many dendrons grafted onto the spherical surface of a core particle, have been investigated. By virtue of the stronger entropic repulsion between dendrons in the spherical than in the linear configuration, spherical polymer brushes improve the colloidal stability and their structural formation has roused great interest.

We have examined the self-assembly of colloidal particles with spherical dendritic brushes. The effective interaction between these particles was studied in Monte Carlo simulations of the Kremer–Grest model (Fig.1). Results confirmed the transferability of the effective potential at different temperatures. Using the potential of mean force obtained from Monte Carlo simulations, the structural formation of the system was studied in a three-dimensional system. The system is a crystalline state in the intermediate density range and exhibits re-entrant melting at much higher densities. Based on generalized local bond order analysis, a refined numerical method has been proposed for analyzing the structural formation of colloidal particles in three-dimensional systems [1].

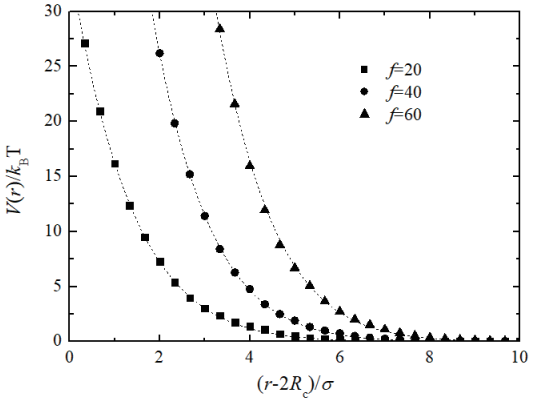

Fig. 1: Effective potential between a pair of spherical dendritic polymer brushes.

References

[1] R. Mizuno, K. Okumura, J. Oguri, and T. Terao: Mol. Simul. **45** (2019) 743.

Ground-State Phase Diagram of an Anisotropic $S=1$ Ferromagnetic-Antiferromagnetic Bond-Alternating Chain

Takashi Tonegawa

Professor Emeritus, Kobe Univ. and Visiting Professor, Osaka Prefecture Univ.

This report aims at exploring the ground-state phase diagram of an anisotropic $S=1$ ferromagnetic-antiferromagnetic bond-alternating chain by using mainly numerical methods. We express the Hamiltonian which describes this system as

$$\mathcal{H} = \sum\nolimits_j \{h^{\rm F}_{2j-1,2j} + h^{\rm AF}_{2j,2j+1} + D_2 (S^z_j)^2\}, \quad (1)$$

$$h^{\rm F}_{j,j'} = -J_{\rm F}(S^x_j S^x_{j'} + S^y_j S^y_{j'} + \Delta_{\rm F} S^z_j S^z_{j'}), \quad (2)$$

$$h^{\rm AF}_{j,j'} = J_{\rm AF}(S^x_j S^x_{j'} + S^y_j S^y_{j'} + \Delta_{\rm AF} S^z_j S^z_{j'}). \quad (3)$$

Here, S^μ_j ($\mu = x,\ y,\ z$) is the μ-component of the spin-1 operator $\vec{S}_j$ acting on the jth site; $J_{\rm F}(>0.0)$ and $J_{\rm AF}(\geq 0.0)$ denote, respectively, the magnitudes of exchange intereraction constants for the ferromagnetic and antiferromagnetic bonds; $\Delta_{\rm F}$ and $\Delta_{\rm AF}$ are, respectively, the parameters representing the XXZ-type anisotropies of the former and latter interactions.

Our motivation for treating this system is as follows. As we will concretely discuss in the next paragraph, this system can be mapped onto an anisotropic spin-2 chain, when $J_{\rm F}$ is sufficiently larger than $J_{\rm AF}$. In the ground-state phase diagram of the latter system, on the other hand, the intermediate-D (ID) phase, which is a typical example of the symmetry protected topological (SPT) phase received recently much attention, appears [1-8]. Thus, we are interested in how the ID phase appears in the ground-state phase diagram of the present anisotropic $S=1$ ferromagnetic-antiferromagnetic bond-alternating chain.

Discussing the mapping of the present anisotropic $S=1$ ferromagnetic-antiferromagnetic bond-alternating chain onto the anisotropic spin-2 chain, we perform lowest perturbation calculations by taking the unperturbed Hamiltonian as $\mathcal{H}_0 = -J_{\rm F}\sum_j \vec{S}_{2j-1}\cdot\vec{S}_{2j}$. Then, straightforward calculations lead to the result,

$$\tilde{\mathcal{H}} = \tilde{J}_{\rm AF}\sum\nolimits_j \left(T^x_j T^x_{j+1} + T^y_j T^y_{j+1} + \Delta_{\rm AF} T^z_j T^z_{j+1}\right) + \sum\nolimits_j \left\{\tilde{D}_2 \left(T^z_j\right)^2 + \tilde{D}_4 \left(T^z_j\right)^4\right\}, \quad (4)$$

where T^μ_j is the μ-component of the spin-2 operator $\vec{T}_j$ at the jth site, and $\tilde{J}_{\rm AF} = J_{\rm AF}/4$, $\tilde{D}_2 = \{7D_2 - 2J_{\rm F}(\Delta_F - 1)\}/6$, $\tilde{D}_4 = -D_2/6$. It is noted that these results are valid when $J_{\rm F} \gg J_{\rm AF} > 0.0$, $J_{\rm F} \gg |D_2|$, and $\Delta_{\rm F} \sim 1.0$.

There exist five interaction parameters, $J_{\rm F}$, $J_{\rm AF}$, $\Delta_{\rm F}$, $\Delta_{\rm AF}$, and D_2 in our Hamiltonian $\mathcal{H}$. Since we are much interested in the ID phase, we choose the values of these parameters under the condition that this phase appears as widely as possible when we perform the numerical calculations of the phase diagram. It is now known that in the ground-state phase diagram of the anisotropic spin-2 chain governed by $\tilde{\mathcal{H}}$, positive values of $\tilde{D}_4$ stabilize the ID phase [6,7]. Thus, referring to the above results of the perturbation calculations, we fix our attention upon the case where $J_{\rm F} = 1.0$ ($J_{\rm F}$ is the unit of energy), $\Delta_{\rm F} = 0.8$, and $D_2 = -1/30$, and numerically determine the phase diagram on the $J_{\rm AF}$ versus $\Delta_{\rm AF}$ plane. Note that the above values of $\Delta_{\rm F}$ and D_2 give $\tilde{D}_2 = 1/36$ and $\tilde{D}_4 = 1/180$, if we respectively use the above equations for $\tilde{D}_2$ and $\tilde{D}_4$.

Figure 1 shows our final result for the ground-state phase diagram on the $J_{\rm AF}$ versus $\Delta_{\rm AF}$ plane, which has been determined by using a variety of numerical methods based on the exact diagonalization calculation. This phase diagram consists of six phases, which are the $XY1$, large-D (LD), ID, Haldane (H), spin-1 singlet dimer (SD), and Néel (N) phases. Among these, the LD, H, and SD phases are the trivial phases, and the ID phase is the SPT phase. Interestingly, the former three are smoothly connected without any quantum phase transitions between the LD and H phases and between the H and SD phases, and therefore they belong to the same phase. It is also emphasized that the ID phase appears in a wider region compared with the case of the phase diagram of the anisotropic spin-2 chain for $\tilde{D}_4 = 0.0$ [2-5].

We now briefly discuss how to estimate numerically the phase boundary lines in the phase diagram shown in Fig. 1. We denote, respectively, by $E^{\rm P}_0(L,M)$ and $E^{\rm P}_1(L,M)$, the lowest and second-lowest energy eigenvalues of the Hamiltonian $\mathcal{H}$ under the periodic boundary condition within the subspace characterized by N and M, where $N(=4,\ 8,\ 12,\ 16)$ is the total number of spins in the system and $M(=0,\ \pm1,\ \cdots,\ \pm N)$ is the total magnetiza-

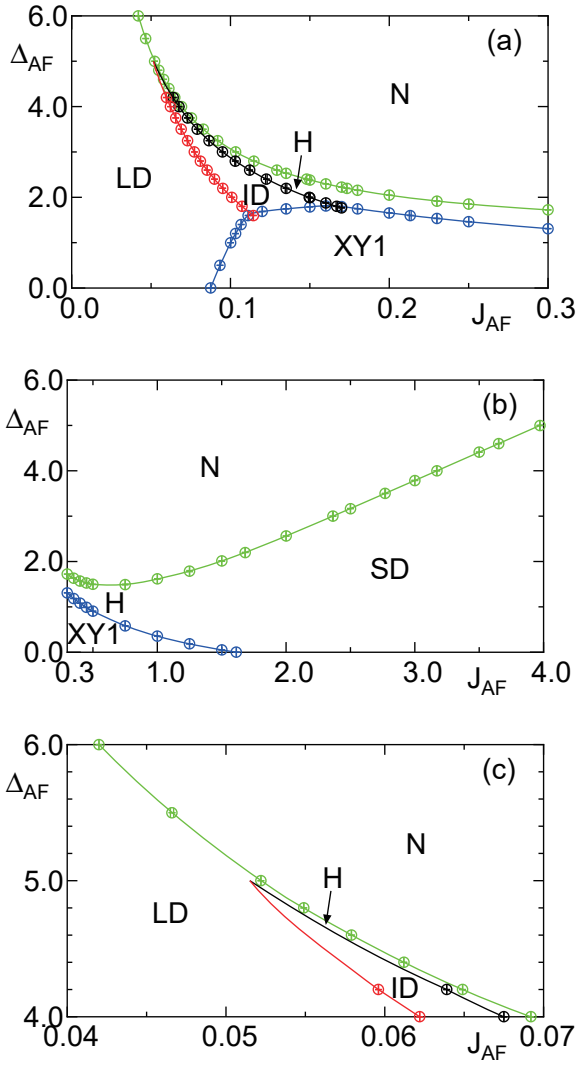

Figure 1: The ground-state phase diagram on the $J_{\rm AF}$ versus $\Delta_{\rm AF}$ plane for $J_{\rm F}=1.0$, $\Delta_{\rm F}=0.8$, and $D_2=-1/30$, obtained in the present work; (a) $0.0\le J_{\rm AF}\le 0.3$, (b) $0.3\le J_{\rm AF}\le 4.0$, in (c) part of (a) is enlarged.

tion. We also denote by $E_0^{\rm T}(L,M,P)$ the lowest energy eigenvalue of $\mathcal{H}$ under the twisted boundary condition within the subspace characterized by N, M, and P, where $P(=+1,-1)$ is the eigenvalue of the space inversion operator with respect to the twisted bond. We numerically calculate these energies by means of the exact-diagonalization method. In the following way, we evaluate the finite-size critical values of $J_{\rm AF}$ (or $\Delta_{\rm AF}$) for various values of $\Delta_{\rm AF}$ (or $J_{\rm AF}$) for each phase transition. Then, the phase boundary line for the transition is obtained by connecting the results for the $N\to\infty$ extrapolation of the finite-size critical values.

Firstly, the phase transition between the LD and ID phases and that between the ID and H phases are of the Gaussian type. Therefore, as is well established, the phase boundary lines can be accurately estimated by Kitazawa's level spectroscopy (LS) method [9]. That is to say, we numerically solve the equation,

$$E_0^{\rm T}(N,0,+1)=E_0^{\rm T}(N,0,-1) \qquad (5)$$

to calculate the finite-size critical values. It is noted that, at the $N\to\infty$ limit, $E_0^{\rm T}(N,0,+1)>E_0^{\rm T}(N,0,-1)$ in the ID phase and $E_0^{\rm T}(N,0,+1)<E_0^{\rm T}(N,0,-1)$ in the LD and H phases.

Secondly, the phase transitions between one of the LD, ID, ID, and SD phases and the $XY1$ phase are the Berezinskii-Kosterlitz-Thouless type. Then, the phase boundary line can be accurately estimated by the method developed by Nomura and Kitazawa [10]. Thus, we solve the following equation to calculate the finite-size critical values:

$$E_0^{\rm P}(N,2)=E_0^{\rm T}(N,0,P)\,, \qquad (6)$$

where $P=-1$ or $P=+1$ depending upon whether the transitions are associated with the ID phase or with the LD, ID, and SD phases.

Lastly, since the phase transitions between one of the LD, H, SD phases and the N phase are the 2D Ising-type transition, the phase boundary line between these two phases can be estimated by the phenomenological renormalization group method [11]. Then, the finite-size critical values for this transition are calculated by solving the equation,

$$N\,\Delta_{00}^{\rm P}(L,0)=(N+4)\,\Delta_{00}^{\rm P}(L+4,0)\,, \qquad (7)$$

where $\Delta_{00}^{\rm P}(L,0)=E_1^{\rm P}(L,0)-E_0^{\rm P}(L,0)$.

This work has been done in collaboration with K. Okamoto, M. Kaburagi, and T. Sakai.

[1] M. Oshikawa, J. Phys.: Condens. Matter **4**, 7469 (1992).
[2] T. Tonegawa, K. Okamoto, H. Nakano, T. Sakai, K. Nomura, and M. Kaburagi, J. Phys. Soc. Jpn. **80**, 043001 (2011).
[3] K. Okamoto, T. Tonegawa, H. Nakano, T. Sakai, K. Nomura, and M. Kaburagi, J. Phys. Conf. Ser. **302**, 012014 (2011).
[4] K. Okamoto, T. Tonegawa, H. Nakano, T. Sakai, K. Nomura, and M. Kaburagi, J. Phys. Conf. Ser. **320**, 012018 (2011).
[5] Y.-C. Tzeng, Phys. Rev. B **86**, 024403 (2012).
[6] J. A. Kjäll, M. P. Zaletel, R. S. K. Mong, J. H. Bardarson, and F. Pollmann, Phys. Rev. B **87**, 215106 (2013).
[7] K. Okamoto, T. Tonegawa, T. Sakai, and M. Kaburagi, JPS Conf. Proc. **3**, 014022 (2014).
[8] K. Okamoto, T. Tonegawa, and T. Sakai, J. Phys. Soc. Jpn. **85**, 063704 (2016).
[9] A. Kitazawa, J. Phys. A **30**, L285 (1997).
[10] K. Nomura A. and Kitazawa, J. Phys. A **31**, 7341 (1998).
[11] M. P. Nightingale: Physica A **83** (1976) 561.

Study on quantum annealing from a viewpoint of statistical mechanics

Shu TANAKA

Green Computing Systems Research Organization,

Waseda University, Waseda-cho, Shinjuku, Tokyo 162-0042

Quantum annealing is a promising calculation technique to perform combinatorial optimization [1,2]. We studied two topics on quantum annealing toward the construction of high-performance quantum annealing.

The first one is the quantum annealing on singular value decomposition. Hashizume et al. considered the adiabatic limit of the quantum annealing on the singular value decomposition [3]. Based on the previous study by Hashizume et al. [3], we studied dynamical properties of quantum annealing on singular value decomposition of random matrices. We investigated the performance of quantum annealing on the singular value decomposition up to five singular values depending on the energy gap at $t=0$ (initial state), the annealing time, and the selection of bases [4].

The second one is the quantum annealing on the Wajnflasz-Pick model which is a generalization of the Ising model [5]. In the model, the first-order quantum phase transition point is passed when we consider a usual quantum annealing using the time-dependent transverse field. It is known that a bottleneck of quantum annealing is the first-order quantum phase transition. We constructed a method to avoid the bottleneck by introducing a transverse *interaction* type quantum fluctuation [5].

References

[1] T. Kadowaki and H. Nishimori: Phys. Rev. E **58** (1998) 5355.

[2] S. Tanaka, R. Tamura, and B. K. Chakrabarti: “Quantum Spin Glasses, Annealing and Computation” Cambridge University Press, (2017).

[3] Y. Hashizume, T. Koizumi, K. Akiyama, T. Nakajima, S. Okamura, and M. Suzuki: Phys. Rev. E **92** (2015) 023302.

[4] Y. Hashizume, S. Tanaka, and R. Tamura: in preparation.

[5] Y. Seki, S. Tanaka, and S. Kawabata: J. Phys. Soc. Jpn. **88** (2019) 054006.

Transport properties of one-dimensional interacting electron systems by a quantum Monte Carlo method

Takeo KATO

Institute for Solid State Physics,

The University of Tokyo, Kashiwa-no-ha, Kashiwa, Chiba 277-8581

Effect of Coulomb interaction on electronic transport via nanoscale devices has been one of important problems in mesoscopic physics. It is still a challenging problem to evaluate electronic conductance in the presence of Coulomb interaction, in particular, at finite temperatures. In the present project, we considered interacting electron systems on a finite-size one-dimensional lattice, and tried to calculate a conductance in the one-body scattering problem by the quantum Monte Carlo method.

We first formulated the conductance by using the linear response theory, in which the current-current correlation function is related with the conductance [1,2]. Then, we considered the spinless Fermion chain with nearest-neighbor repulsive interaction with a local impurity one-body potential. Since this model is effectively described by the Tomonaga-Luttinger model [3], the model is convenient for consistency check of our formulation.

We employed the stochastic series expansion (SSE) method, which is one kind of the quantum Monte Carlo, to evaluate the current-current correlation function. On the supercomputer (system B), we have used simple parallelization method in the Monte Carlo sampling. We checked that the numerical results reproduce the conductance of the noninteracting electron systems, which is purely determined by the reflection probability. Furthermore, the numerical results show that the conductance is reduced from the one expected from the bare transmission probability. This behavior is consistent with the theory based on the Tomonaga-Luttinger model [3].

In order to obtain the conductance in more realistic situations, we need larger SSE simulations, which are left for the future important problem as well as improvement of our naive formulation based on the linear response theory.

References

[1] N. Shimada, Master Thesis (The University of Tokyo, 2018).

[2] N. Shimada and T. Kato, in preparation.

[3] C. L. Kane and M. P. A. Fisher, Phys. Rev. Lett. **68**, 1220 (1992)

Fast Algorithm for Generating Random Bit Strings

Hiroshi Watanabe
Institute for Solid State Physics, University of Tokyo
Kashiwa-no-ha, Kashiwa, Chiba 277–8581

Suppose we want to generate a bit string with length N in which each bit is set with arbitrary probability p. If we adopt the simple algorithm, which repeats check for each bit, we need to generate N random numbers. However, we can reduce the number of random number generations by adopting more sophisticated algorithms [1, 2]. We proposed three algorithm, the Binomial-Shuffle (BS), the Poisson-OR (PO), and the finite-digit algorithms.

The Binomial-Shuffle algorithm is an algorithm that first calculates how many bits are set and then shuffles them. Adopting Walker's alias method and Floyd's sampling method, it is possible to generate a random bit string with $pN+1$ random number generations. The Poisson-OR algorithm generates k bit strings with one of the bits is set randomly and takes the logical OR of them. This is a special case of the algorithm proposed by Todo and Suwa [3]. The average number of the random number generations is $-N\log(1-p)+1$. The finite digit method is effective when the probability p can be represented by a finite digit in the binary notation. When the probability p can be expressed by n digits in the binary notation, we can generate a random bit string with that probability by generating n bit strings in which each bit is set with a probability 1/2 and properly taking the logical operations. Therefore, the finite-digit algorithm with n digits involves the random number generates n times.

We constructed a hybrid algorithm, i.e., which first generates a bit string with probability $\tilde{p}$ close to p with the finite digit algorithm and corrects the difference $\tilde{p}-p$ by the Binomial-Shuffle or Poisson-OR algorithms. The expected number of random numbers generated to generate a string in which each bit is set with arbitrary probability is at most 7 for the 32-bit case and 8 for 64-bit case. Employing the developed algorithm, we applied the multispin coding technique to the one-dimensional bond-directed percolation and obtained a factor of 14 speed-up.

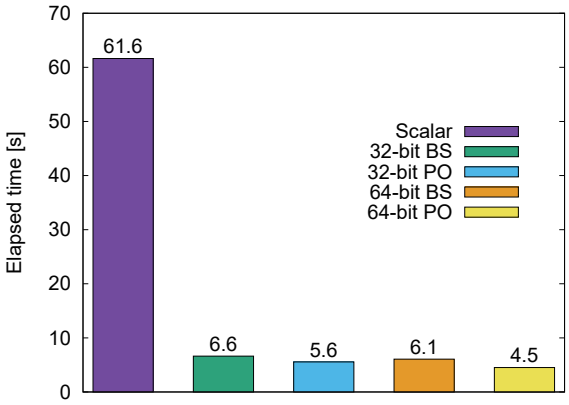

Figure 1: Multi-spin coding of the directed-percolation. Times required for the simulations with 32768 steps and 1000 independent samples with L = 32768.

References

[1] H. Watanabe, S. Morita, S. Todo, and N. Kawashima, J. Phys. Soc. Jpn. 88, 024004 (2019)

[2] `https://github.com/kaityo256/rbs`

[3] S. Todo and H. Suwa, J. Phys.: Conf. Ser. 473, 012013 (2013).

Dynamics of structure formation in charged colloids

Kyohei Takae and Hajime Tanaka
Institute of Industrial Science, University of Tokyo
4-6-1 Komaba, Meguro-ku, Tokyo 153-8505, Japan

We investigate non-equilibrium dynamics in charged colloidal suspensions. In numerical simulations of colloidal suspensions, an efficient computational methods called Fluid-Particle-Dynamics (FPD) method is often applied to study hydrodynamic effects in structure formation kinetics and responses to external field. In previous studies of charged colloidal solutions, it is assumed that the surface charge of the colloids are constant both in space and time. However, it is widely recognized that the surface charge becomes inhomogeneous under heterogeneous environment such as colloidal solutions in binary solvents and solutions under external fields. The surface charge also varies in time under nonequilibrium conditions. In these cases, surface charges relaxes to satisfy electrochemical equilibrium at the surface. This effect is called *charge regulation*, and is of great interest in chemistry and biology. We construct theoretical framework of electrohydrodynamics in colloidal solutions with charge regulation and thermodynamic consistency. By performing numerical simulations, we show application of our method to electrostatic and electrokinetic problems, where charge regulation plays an important role. We examine cluster formation of colloid particles where a significant reduction of the electrostatic repulsion between colloids results in the extra stabilization of clusters with a more compact shape. We also a dynamical problem, that is, single colloid particle under an external field. The surface charge of the colloid becomes highly heterogeneous under a strong electric field due to the deformation of the counterion cloud, resulting in the enhancement of electrokinetic mobility. We also examine collective dynamics of charged colloids under external electric field, where they form crystalline ordering in quiescent state.Under strong electric field, particles undergo collective vibration along the field direction, and eventually the crystals melt into disordered state. This is essentially caused by hydrodynamic interaction among the particles. To see this, we also examine the same calculation but neglecting hydrodynamic interaction by solving Brownian limit of our model, where we find no instability, clearly indicating that the instability is due to the electrohydrodynamic coupling. By these examples, we show not only the importance of considering charge-regulation effects in the self-organization of charged systems but also the applicability of our simulation method to more complex problems of charged soft matter systems.

References

[1] K. Takae and H. Tanaka: Soft Matter **14** (2018) 4711.

Calculation of higher-order moments by higher-order tensor renormalization group method

Satoshi MORITA

Institute for Solid State Physics,

The University of Tokyo, Kashiwa-no-ha, Kashiwa, Chiba 277-8581

Tensor networks (TN) are powerful tools for quantum and classical many-body problems. The tensor renormalization group method (TRG) provides an efficient contraction scheme based on coarse-graining TNs. The higher-order tensor renormalization group method (HOTRG) is one of the few TN methods applicable to higher-dimensional systems [1].

We propose a calculation method for higher-order moments of physical quantities based on HOTRG [2]. In TN methods, there are two ways of calculating an expectation value of a physical quantity like the magnetization. One method is numerical differentiation of the free energy with respect to the external field. The other is introduction of the impurity. However, both the methods have some difficulty in calculation of higher-order moments, which are important for analysis of critical phenomena. To resolve this problem, we introduce a coarse-grained tensor which represents summation of all configurations of multiple impurities and derive its update rule based on the systematic summation scheme. We showed that a jump of the Binder ratio precisely determines the transition temperature in the two-dimensional Potts model. The finite-size scaling analysis provides critical exponents and distinguishes the weakly first-order and continuous phase transitions.

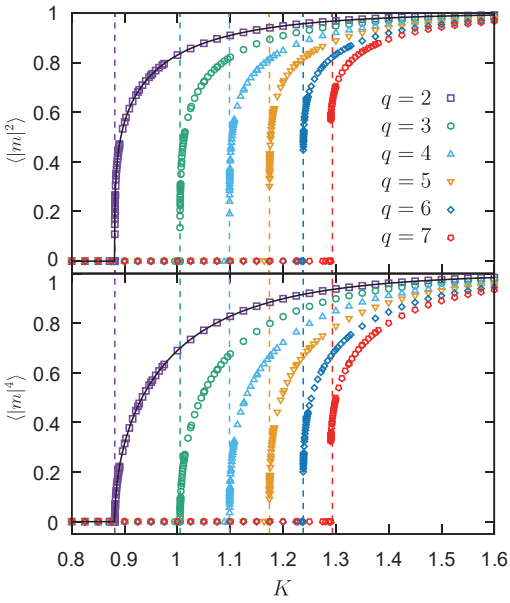

Fig. 1: The 2nd- and 4th-order moments of the magnetization of the q-state Potts model on a $2^{20} \times 2^{20}$ square lattice by HOTRG with $\chi = 48$.

References

[1] Z. Y. Xie, et al., Phys. Rev. B **86**, 045139 (2012)

[2] S. Morita and N. Kawashima, Comput. Phys. Commun, **236**, 65-71 (2019)

Compression behavior and inhomogeneous structure of silica glass in its intermediate state in structural transformations

Daisuke WAKABAYASHI[1] and Fuyuki SHIMOJO[2]

[1]*Photon Factory, Institute of Materials Structure Science, High Energy Accelerator Research Organization (KEK), Tsukuba 305-0801*

[2]*Department of Physics, Kumamoto University, Kumamoto 860-8555*

Silica glass is well known as an archetypal oxide glass and its compression behavior has attracted considerable attention in various fields of physical sciences. Recent small-angle X-ray scattering measurements have revealed the subnanometer-scale inhomogeneity appears in silica glass during the pressure-induced structural transformations [1].

To reveal the detailed structure of subnanometer-scale inhomogeneity, we have to conduct large-scale molecular-dynamics (MD) simulations with a system of ~10,000 atoms. We have confirmed that ab-initio methods can simulate the compression behavior of silica glass accurately [2]. On the basis of the results of ab-initio calculations, we fitted the potential with a machine-learning technique (ANN potential) and applied it for the calculations with an extended system.

To obtain the data for fitting ANN potentials, we conducted ab-initio calculations. The configurations of six-coordinated or densified four-coordinated glasses (corresponding to high-pressure phases of silica glass) were prepared by gradually cooling silica melt from 4,000 K at high pressures, and then the decompression and recompression processes were calculated. There is remarkable agreement between the densities on decompression and recompression. This suggests not only that six-coordinated and densified four-coordinated glasses behave in an elastic manner as a single phase but also that glass in the intermediate state seems to behave like a single phase, which agrees with our model.

We tested the MD simulations with a system of about 30,000 atoms using the ANN potential determined from the data at 40 GPa. The calculations at high temperatures can be made without numerical divergence by setting an appropriate time step. Large-scale simulations of decompression process will be carried out in the near future.

References

[1] T. Sato, N. Funamori, D. Wakabayashi, K. Nishida, and T. Kikegawa: Phys. Rev. B **98** (2018) 144111.

[2] E. Ryuo, D. Wakabayashi, A. Koura, and F. Shimojo: Phys. Rev. B **96** (2017) 05420.

Application of Eigenstate Thermalization Hypothesis to Non-equilibrium steady states

Tatsuhiko SHIRAI
Green Computing Systems Research Organization, Waseda University
Waseda-chou, Shinjuku-ku, Tokyo 162-0042

We have studied steady states of quantum many-body systems in a weak contact with out-of-equilibrium environment [1]. It is found that Gibbs state at a certain effective temperature can describe the steady state in some open quantum systems in spite of the violation of the detailed balance condition. The argument of the realization of the Gibbs state is based on the validity of the perturbation theory on weak system-environment coupling and the eigenstate thermalization hypothesis (ETH).

As for the weak coupling peturbation theory, it is known that the convergence radius of the perturbation series quickly shrinks to zero with the system size in generic open quantum systems [2]. Nevertheless, our numerical calculation of some spin systems suggest that the leading-order perturbative solution well describes the steady state in the thermodynamic limit provided that there is no current of a conserved quantitity in the bulk. This implies that the perturbative expansition is a kind of an asymptotic expansion. Furthemore, it also turns out that the perturbation theory completely fails when there is current in the bulk. We demonstrate the failure of the perturbation theory in a Bose-Hubbard model coupled to environments with different chemical potentials at each end.

As for the ETH, it is recognized as an important property of the Hamiltonian that explains the approach to themal equilibrium in isolated quantum system [3, 4]. With this property, if a density matrix is diagonalized in the basis of energy eigenstates and has a subextensive energy fluctuation, the state is indistinguishable from the Gibbs state at a certain effective temperature as far as we observe local quantities. We argued that in an open quantum system, the leading-order perturbative solution meets the above condition. Therefore, by combining the ETH with the perturbation theory, we can conclude that the steady state is described by the Gibbs state irrespective of the detailed balance condition.

In numerical simulations, we solve a quantum master equation called the Lindblad equation, which describes a time evolution of open quantum systems. Based on the symmetry of the time-evoluation operator of the Lindblad equation, we divide the density matrix into some sectors. We assign the matrix elements in each sector to each core, and perform a parallel simulation using openMPI.

References

[1] T. Shirai, and T. Mori: arXiv:1812.09713.

[2] H. C. F. Lemos, and T. Prosen: Phys. Rev. E **95** (2017) 042137.

[3] M. Rigol, V. Dunjko, and M. Olshanii: Nature **452** (2008) 854.

[4] T. Mori, T. N. Ikeda, and E. Kaminishi, and M. Ueda: J. Phys. B **51** (2018) 112001.

Structural Change of Electrolyte Solution in Nanospaces

Md Sharif Khan and Tomonori Ohba

Graduate School of Science,

Chiba University, 1-33 Yayoi, Inage, Chiba 263-8522

Massive parallel computer simulation has been used to elucidate the structural properties of the organic and aqueous electrolytes confined in the different carbon nanospaces. In nanospaces, molecules show unique properties by changing their structure and dynamics and have the potential applications in future technologies and industries [1]. Electrolytes in nanospaces play an important role in various fields including electrochemistry, biochemistry, biotechnology, and ion channel technology [2]. Various electrolytes such as aqueous electrolytes and organic electrolytes (OEs) have been utilized for their own advantages, however, the performance of those electrolytes can be extensively influenced due to the change of dynamics and structure in nanospaces [3]. The comprehensive understandings of the electrolyte structure and dynamics in the nanospaces are crucial to improve these technologies and develop efficient new technologies. We have been employed fully atomistic simulations to study the behavior of different electrolyte salts and different organic solvents in slit and cylindrical carbon nanopores, to reveal the structure and storage mechanism. Organic solvents with different properties were selected: ethylene carbonate (EC), propylene carbonate (PC) and ethyl methyl carbonate (EMC). We demonstrate, due to the one-dimensional confinement in CNTs there are much fewer ions inserted into the nanotubes than the amount inserted into slit carbon nanopores. Further, linear like structure EMC solvent shows higher performance owing to high cation accessibility rather than cyclic solvents EC and PC **(Fig. 1)** [4].

In addition, we have evaluated the structure

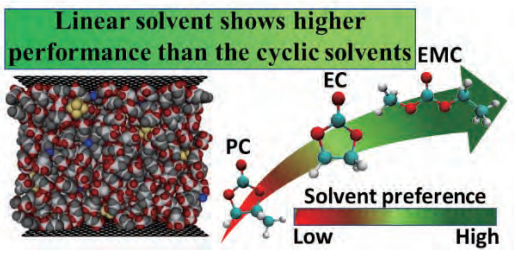

Fig. 1. Organic solvents effect on Na ion storage

of water, NaCl and LiCl aqueous solutions inside the carbon nanotubes with diameter 1 and 2 nm were evaluated by using molecular dynamics simulations and benchmarked the simulation outcomes by X-ray diffraction [5]. The intermolecular distances in aqueous solutions were decreased from that in water system in carbon nanotubes with 1 nm pore, while longer than those in carbon nanotubes with 2 nm pore. Significant hydration formation was observed in 2 nm carbon nanotubes since the elongated nearest neighbor distances were observed. Ions play the dominant role in the anomalous structure in extremely narrow carbon nanotubes.

References

[1] T. Ohba, K. Ideta, K. Hata, S. Yoon, J. Miyawaki: ChemPhysChem. **17** (2016) 3409.

[2] D. A. Newsome, D. S. Sholl: Nano Lett. **6** (2006) 2150.

[3] M. S. P. Sansom, P. C. Biggin: Nature ***414***, (2001) 156.

[4] A. Karatrantos, S. Khan, T. Ohba, Q. Cai: Phys. Chem. Chem. Phys. *20*, (2018) 6307.

[5] S. M. Khan, S. Faraezi, Y. Oya, K. Hata, T. Ohba: Adsorption in press.

Nonequilibrium phase transition and slow dynamics in the dense hard sphere systems

Masaharu ISOBE
Nagoya Institute of Technology
Gokiso-cho, Showa-ku, Nagoya, 466-8555

As one of the simplest model, the hard disk/sphere systems have been investigated in the field of both equilibrium and non-equilibrium statistical physics. In this project, we investigated non-equilibrium phenomena in the hard disk/sphere model system with modern algorithms, especially for Event-Chain Monte Carlo(ECMC) [1] and Event-Driven Molecular Dynamics(EDMD) [2], where we propose the "Hybrid Scheme", namely, ECMC for equilibration and EDMD for calculation of dynamical properties [3, 4].

Physical origin of facilitation in athermal molecular systems on approaching glass transition:

On approaching glass transition, the viscosity of the supercooled liquid would be increased rapidly. It often behaves as solid with disorder structure within an experimental timescale. One of the challenging issues is to understand whether the essential properties of glass forming materials is fundamentally thermodynamic or dynamic in origin. However, the microscopic origin of structural (so-called α) slow relaxation in deeply supercooled liquids at an atomic scale has remained elusive due to the limitation of both electron microscopy experiment and computer simulation. Although many theoretical models have been discussed, one of a perspective that favors a dynamic origin is called Dynamic Facilitation (DF) theory [5, 6, 7]. DF theory was known to explain a wide range of empirically observed dynamical features of thermal supercooled liquids and glasses. Recently, we devoted to investigating the applicability of DF theory to athermal systems, i.e., systems of hard particles where the relevant control parameter is pressure rather than temperature, under "supercompressed" conditions. By employing novel efficient algorithms [1, 2, 3], it was possible to find true equilibrium states and generate the phase diagram of a binary mixture of hard spheres. The novel methodologies allowed studying in detail the equilibrium dynamics of high-density systems. The slow relaxation at these conditions is consistent with the predictions of DF theory generalized to systems controlled by pressure rather than temperature. In such athermal molecular systems under "super-compressed" conditions — where what is facilitated is the ability of the constituent particles to structurally relax — giving rise to correlated and cooperative dynamics, in a manner predicted by theory [8]. In collaboration with the experimental group in Hong Kong, we resolve in detail that colloidal particles undergo a transition from collective "creeping" to the string-like "hopping" motion on approaching the glass transition, and the structural relaxation of the supercooled glass is just caused by string-like escape hopping motion. Furthermore, such a string-like motion has an ultra-high returning hopping probability which is proved to be the leading contribution to the kinetic arrest for slow relaxation. These results are also confirmed by extensive molecular dynamics simulation and show an evidence of the scenario of

DF theory [9].

References

[1] E. P. Bernard, W. Krauth, and D. B. Wilson: Phys. Rev. E **80** (2009) 056704.

[2] M. Isobe: Int. J. Mod. Phys. C **10** (1999) 1281.

[3] M. Isobe: Mol. Sim. **42** (2016) 1317.

[4] M. Isobe: "Advances in the Comutational Sciences — Proceedings of the Symposium in Honor of Dr Berni Alder's 90th Birthday", edited by Eric Shwegler, Brenda M. Rubenstein, and Stephen B. Libby, World Scientific, **Chapter 6** (2017) 83.

[5] D. Chandler and J. P. Garrahan: Annu. Rev. Phys. Chem. **61** (2010) 191.

[6] L. O. Hedges, R. L. Jack, J. P. Garrahan and D. Chandler: Science **323** (2009) 1309.

[7] A. S. Keys, L. O. Hedges, J. P. Garrahan, S. C. Glotzer, and D. Chandler, Phys. Rev. X, **1** (2011) 021013.

[8] M. Isobe, A. S. Keys, D. Chandler, and J. P. Garrahan: Phys. Rev. Lett. **117** (2016) 145701.

[9] C.-T. Yip, M. Isobe et al.: in preparation.

phase field simulation for amoeboid cells

Nen SAITO
Graduate School of Science, The University of Tokyo
7-3-1 Hongo, Bunkyo-ku, Tokyo 113-8656, Japan

Biological systems show variety of dynamic changes in morphology. Specifically in single cell morphodynamics, large deformations, such as membrane internalization (endocytosis) and externalization (exocytosis), occurs constitutively and spontaneously. In such morphological changes, geometry of membrane is not simple and the geometry itself deforms in time, which is quite different from theory of pattern formation via reaction-diffusion equation on a flat surface. How such shapes dynamics emerges in a self-organized manner is an important question not only for cell biology but also for physics.

To address dynamics in morphology of cell, we focus on macropinocytosis. Macropinocytosis is clathrin-independent endocytosis and allows internalization of large volume of extracellular fluid, as is illustrated in Fig1(a). Dictyostelium discoideum and tumor cells show constitutive macropinocytosis for uptake of nutrients from extracellular fluid. With help of recent advance of microscopy for 3D observation, macropinocytosis has been considered to be driven by self-organizing pattern of actin polymerization on the membrane. However, it remains still unknown how macropinositosis cup structure (see Fig1(a)) forms, how it closes and what chemical reactions make it possible.

From theoretical perspective, we introduce a mathematical model based on 3D phase-field method, which enables reaction-diffusion process on the membrane and large membrane deformation simultaneously. Phase field method has been wildly applied for numerical tracking of interface motions such as crystal growth, phase separation, and also 2-dimensional dynamics of amoeba cell [1]. The proposed model with the help of GPU successfully describes a spontaneous large invagination of cell membrane (see Fig1(b)), which is resemble to actual macropinocytosis observed in several experiments. Simulation results indicate that simple reaction-diffusion process on the cell membrane lead to drastic membrane deformation, which results in an engulfment of extracellular fluid [2]. We will continue to perform simulations with different parameters, and to analyze the results.

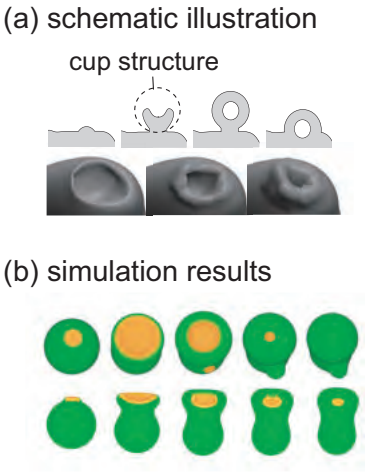

Figure 1: macropinocytosis

References

[1] D. Taniguchi, et al. Proc. Natl. Acad. Sci. U.S.A. 110(13), 5016 (2013) R. Kubo: J. Phys. Soc. Jpn. **12** (1957) 570.

[2] N. Saito and S. Sawai in preparation

Constructing the database of exited states for desigining photosynthetic pigments to absorb the longer wavelength radiation

Yu Komatsu
NINS Astrobiology Center, National Institutes of Natural Sciences
NINS National Astronomical Observatory, National Institutes of Natural Sciences
2-21-1 Osawa, Mitaka, Tokyo, 181-8588

Molecules absorbing longer wavelength radiation is gathering attention in varieties of research fields, e.g.) bioimaging and dye sensitized solar cell. In addition, in order to detect traces of photosynthesis from planets outside our solar system, it has been significant to learn limitations of photosynthesis from the red molecules or pigments. Here, starting with natural photosynthetic pigments, the database of excited states of pigments are being constructed for these applications. As an attempt through the construction of the database, the effect of the central metal of the pigments is examined. Bacteriochlorophyll *b* is a natural photosynthetic pigment which has the reddest absorption band. Like the other chlorophyll-type pigments, it has a tetrapyrrole-ring, which includes a central metal ion as Mg. With the tetrapyrrol, possessing metal ions has a significant benefit to adopt to changing environments and to have various functions.

Here, to focus on the ring, the effect of the central metal in bacteriochlorophyllide *b* (M-Bchl *b*) was investigated at DFT level. With CAM-B3LYP/Def2tzvp//B3LYP-D3/6-31G(d), the excited and ground states of M-Bchls *b* were estimated; M=2H, Mg, Ca, Ni, Zn, Sr, Pd, Cd, Pt, Hg and Pb. For M=Mg, 2H and Zn, the estimated energies in the first excited states are 757.03, 722.66, 737.46 nm, respectively. The energy for M=Pb is 771.60 nm as the longest wavelength absorption, while that for M=Pt is 698.24 nm as the lowest (73.36 nm difference). Moreover, elec-

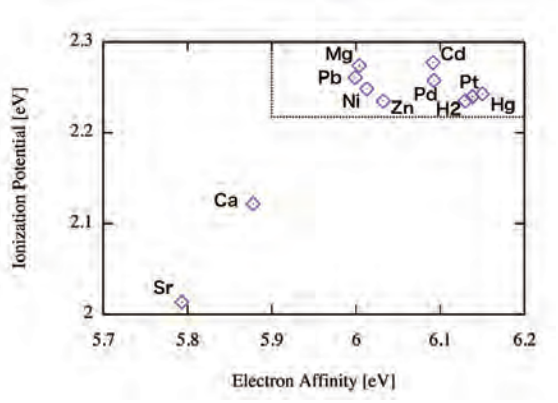

(a)

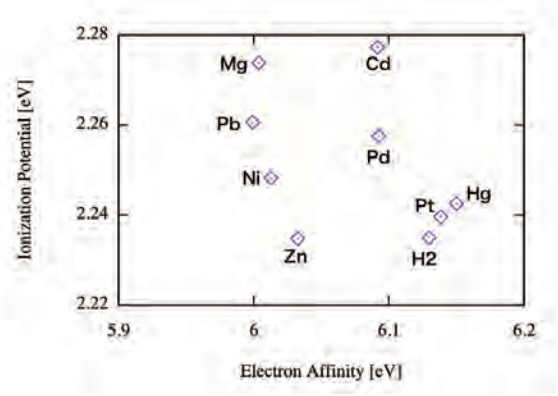

(b)

Figure 1: (a) Electron affinities and Ionization potentials for M-Bchl *b*. (b) The enlarged figure from the top right part of (a).

tron affinities and ionization potentials for M-Bchls *b* are shown in the Figure 1. The pigments for M=Ca and Sr do not seem to be alternative to original because of being apart from the others and their large atomic radius.

With the supercomputer in ISSP, NWChem 6.6 was used to make the model selection, including functionals and basis functions. The main calculations were performed with the supercomputer in NAOJ.

Realization and Manipulation of Topological States by Nanostructures

Toshikaze Kariyado

International Center for Materials Nanoarchitectonics,

National Institute for Materials Science, Namiki, Tsukuba, Ibaraki 305-0044

The main focus of this project was on (i) orbital magnetism in topological semimetals, and (ii) electronic states of graphene with nanostructure, where the supercomputing resources are required mainly for ab-initio simulations and model construction on top of that, and occasionally for massive parallelization in k-point sampling in computation of response functions.

For (i) orbital magnetism in topological semimetals, a Dirac material Sr_3PbO is analyzed as a typical example. After a little consideration, it turned out that some minor details of the band structure details of the band structure may have sizable effects on the magnetic susceptibility. Then, we first construct a model reflects features of the first-principle band structure using the maximally localized Wannier function method. By optimizing the number of relevant orbitals, we could successfully construct an improved model comparing with the previous work [1]. Using the improved model, the magnetic susceptibility is calculated using the Green's function based formula. In order to capture the contribution from Dirac electrons, or band singularities, a fine mesh is required for the k-point sampling. For this, we applied massive parallelization on the k-point sampling for numerical efficiency. The obtained results show fairly good agreement with experiments.

For (ii) graphene with nanostructure, we explored possible topological states in graphene nanomesh. We have established that by changing the hole alignment in nanomesh, the topological character can be tuned [2]. The topological characterization was done through the interface states, and also through the inspection of the irreducible representation of the relevant bands derived through the first-principles calculation.

References

[1] T. Kariyado and M. Ogata, J. Phys. Soc. Jpn. **81** (2012) 064701.

[2] T. Kariyado, Y.-C. Jiang, H. Yang, and X. Hu, Phys. Rev. B **98** (2018) 195416.

Quantitative Analysis of the Influence of Pulley Effect on the Strain-Hardening of Slide-Ring Gels.

Koichi Mayumi[1], Yusuke Yasuda[1], Masatoshi Toda[2], Hideaki Yokoyama[1], Hiroshi Morita[2], and Kohzo Ito[1]

[1] *Dept. of Advanced Materials Science, Graduate School of Frontier Sciences, the University of Tokyo, 5-1-5 Kashiwa-noha, Kashiwa, Chiba 277-8561.* [2]*National Institute of Advanced Industrial Science and Technology (AIST), 1-1-1, Umezono, Tsukuba, Ibaraki 305-8568.*

Slide-ring (SR) gel is a kind of supramolecular polymer network that does not have direct cross-links between polymer chains, but topological constraint by figure-of-8 shaped cross-linking molecules between them. [1] The unique feature of SR gel is that it has large deformability and toughness. [2]

The molecular origin of this deformability has been explained by a hypothesis, "pulley effect" [1]. In SR gels, movable cross-links act like pulleys and prevent stress-concentration on short chains in the networks. However this hypothesis has not been verified, because the visualization of the cross-linking points is experimentally difficult.

In the previous project, we fabricated a coarse-grained model of SR gels and conducted a uni-axial deformation simulation by means of molecular dynamics simulation technique, and succeeded in visualizing the pulley effect (Fig. 1(b).), and unexpected orientations of figure-of-eight cross-links (Fig. 1(a).), suggesting there is another mechanism contributing to stress relaxation of SR gels under deformation. (Fig. 1(c).)

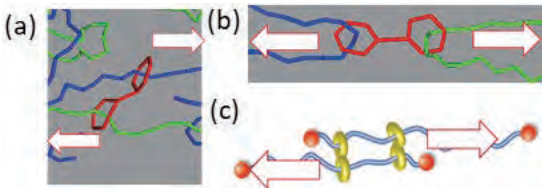

Fig. 1. (a) Unexpected orientation of figure-of-eight crosslinks (b) the orientation expected from pulley effect (c) the stress relaxation mechanism considered from orientation (a)

In this project, we visualized stress distribution in SR gels under deformation and analyzed local stress applied to the cross-links and polymer chains separately. Based on the results, we discuss which orientation of the cross-links shown in Fig.1 is dominant in SR gels.

We fabricated coarse-grained models of SR gel and fixed-crosslinking (FC) gel with the same crosslinking density using beads-spring model [3]. 20,000 and 35,000 beads system was used

for FC and SR gel, respectively. For simulation, we conducted Langevin dynamics equilibration simulation for $1.0 \times 10^7\,\tau$. Then we tried elongation simulation at an elongation speed of $4.37 \times 10^{-4}\,\sigma/\tau$ up to maximum elongation ratio $\lambda = 11$. The molecular dynamics simulations were performed using COGNAC engine in OCTA system, and LAMMPS.

Fig.2 shows stress distribution of FC and SR gels under large deformation. The chains loading more than $70\epsilon/\sigma$ force are colored in red, shown in Fig. 2. In FC gels, fully-stretched chains are percolated from end to the other end at a starch ratio of $\lambda = 5.5$. On the other hand, there is almost no fully stretched chain in SR gels at a stretch ratio of $\lambda = 7$, indicating that there is a stress relaxation mechanism owing to the effect of slidable cross-links in SR gels.

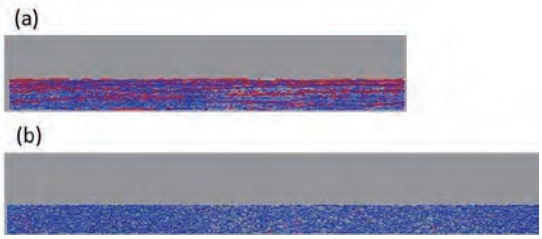

Fig. 2. Visualization of stretched bond by coloring the bonds loading force over $70\epsilon/\sigma$ in red for (a) FC gel at $\lambda = 5.5$ and (b) SR gel at $\lambda = 7$.

Next, Fig. 3 shows the stretch ratio dependence of loaded forces on cross-linking points and main chains in FC and SR gels. From Fig. 3(a), the averaged force loaded on both the main chains and cross-linking points increases with stretch ratio λ. The force loaded on the cross-linking points are larger than that on the main chains, suggesting the stress concentration at cross-linking point occurs under deformation in FC gels. Differently in the case of SR gels, only the stress on axial chains increases with deformation. Conversely, the stress on cross-linking points in SR gels hardly increases. If pulley effect was the main stress-relaxation mechanism of SR gels, stress would concentrate on both the cross-linking points and main chains in the same way as FC gels. Thus, these results suggest that the major molecular origin of the stress relaxation in SR gels is not the pulley effect (Fig. 1(a)), but the unexpected orientation of the cross-links perpendicular to deformation (Fig. 1(b)).

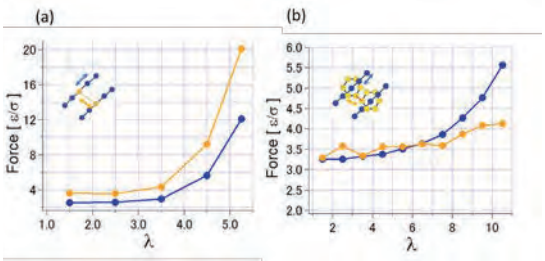

Fig. 3. Averaged forces loaded on crosslinking bond (yellow) and main chain (blue) for (a) FC gels and (b) SR gels.

References

[1] Y. Okumura, and K. Ito: *Adv. Mater.* **13** (2001) 485.

[2] K. Ito: *Polym. J.* **39** (2007) 489

[3] K. Kremer, G. S. Grest: *J. Chem. Phys.* **92** (1990) 5057.

Numerical study of vortices in ferromagnetic superconductor

Hirokazu TSUNETSUGU

The Institute for Solid State Physics,

The University of Tokyo, Kashiwa-no-ha, Kashiwa, Chiba 277-8581

This project has targeted a numerical study on the effects of domain structure on spatial configuration of supercurrent and vortices in ferromagnetic superconductors. A few uranium-based compounds exhibit a superconducting transition within their ferromagnetic phase, and two orders coexist. This is a very interesting system in that two different types of spontaneous symmetry breaking correlate. Domain walls of magnetic structure and vortices of superconducting current are two types of topological defects in ferromagnetic superconductors, but their interplays and correlations have not been well understood yet.

The possibility of self-induced vortex lattice has been pointed out as a distinguishing characteristic of ferromagnetic superconductors. We planned two stages of numerical investigation into this topic. The first stage employs a phenomenological Ginzburg-Landau model, and the second stage proceeds to target a microscopic tight-binding model of electrons with ferromagnetic electron-electron interactions. These interactions are treated by local mean-field approximation that converts the Hamiltonian into a Bogoliubov-de Gennes model. In these analyses, superconducting order parameters as well as electrons couple to magnetic field, which follows Maxwell's equations and are generated by electric currents.

Magnetic field is represented by vector potential, and this vector potential attaches the Peierls phase to electron hopping amplitudes in the microscopic model in the second stage. We plan to introduce ferromagnetic order and domain structure by a proper setting of their corresponding local order parameters.

We investigated the system with torus geometry and magnetic domain extends along its circumference direction, and found emergent supercurrent flowing parallel to the domain wall. We also found that the current direction depends on whether the magnetic domain wall is either Ising or Bloch type.

A big challenge in computations is the search of self-consistent solutions of the Bogoliubov-de Gennes and Maxwell equations. This is needed for understanding self-induced vortices in the microscopic level, and it is interesting to examine the difference in the local electronic structure between near and far from a vortex core.

Estimation of the density of states using Maximum entropy method and Sparse modeling

Yasuhiro H. MATSUDA

Institute for Solid State Physics,

The University of Tokyo, Kashiwa-no-ha, Kashiwa, Chiba 277-8581

We have studied a Shastry-Sutherland antiferromagnet $SrCu_2(BO_3)_2$[1] using massive parallel computer simulations. We have used a numerical solver HPhi[2] for calculation by thermal pure quantum states[3].

For obtaining field dependence of magnetic entropy, several calculations have been done with various fields. The calculation by thermal pure quantum states have reproduced substantially the magneto-caloric effect measurements on $SrCu_2(BO_3)_2$ (Fig. 1).

References

[1] Y. H. Matsuda *et al.*,: Phys. Rev. Lett. **111** (2013) 137204.

[2] M. Kawamura *et al.*,, Comp. Phys. Commun. **217** (2017) 180.

[3] S. Sugiura and A. Shimizu, Phys. Rev. Lett. 108 (2012) 240401.

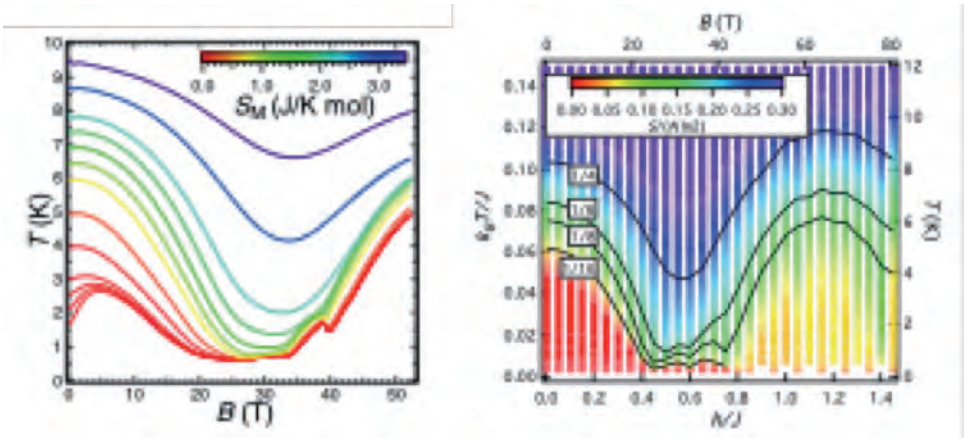

Fig.1 (Left) Temperature variation of $SrCu_2(BO_3)_2$ with various initial temperature due to Magneto-caloric effects. The colors of the lines show the magnetic entropy.
(Right) Color map of magnetic entropy of Shastry-Sutherland lattice system.

Theoretical studies on kagome antiferromagnets and related systems

Yoshiyuki Fukumoto
Department of Physics, Faculty of Science and Technology, Tokyo University of Science
2641 Yamazaki, Noda, Chiba 278-8510

We made, in this year, finite-temperature calculations of the spin-1/2 spherical kagome cluster and exact-diagonalization calculations for the orthogonal dimer system.

In the study of the spherical kagome cluster, taking Dzyaloshinskii-Moriya (DM) interactions into account, we study effects of thermal fluctuations on the magnetization process and magnetic field effects on the specific heat. The usage of the supercomputer is vital to carry out the present calculations, because (i) the dimension of the Hilbert space amounts to $2^{30} \simeq 10^9$ for our model with thirty spins and DM interactions and (ii) the present calculation contains two sampling procedures concerned with initial vectors of thermal pure quantum states and magnetic-field directions. Several years ago, we calculated specific heat under magnetic fields for spherical kagome cluster without DM interactions [1]. Recently, Kihara *et al.* made an experimental study on the low-temperature specific heat of a spherical kagome material $\{W_{72}V_{30}\}$ [2]. They reported that the total number of singlet states below the first triplet excitation is consistent with the theoretical result [1], but the curves of specific heat are different from each other qualitatively. In particular, the experimental specific heats show no magnetic-field dependence, although the theoretical specific heats depend on it. The DM interactions are expected to affect specific heat at low temperatures. However, the present calculations indicates that the DM interactions can not resolve the discrepancy between the theory and experiment. Thus, we have to explore other mechanisms.

As for the orthogonal dimer system, recently, Nakano *et al.* used the exact diagonalization method to find a new phase in the ground state phase diagram [3]. The main purpose of the present study is to clarify the nature of this new phase. In the present calculation, we consider extended models with (a) plaquette structures, (b) dimer structure, or (c) Ising-type anisotropy to study the adiabatic connection between the new phase and each of limits in (a)-(c). These extended models were used in series expansion studies [4, 5]. The first series expansion study, for the extended model of (a), suggested the existence of the plaquette phase [4]. A successive series expansion study reported that the ground state energy via the plaquette expansion is higher that via the dimer expansion [5]. However, it is not clear what these series expansion results mean. We hope the present exact-diagonalization study to shed light on this issue.

References

[1] N. Kunisada *et al.*, PTEP 2014, 41I01 (2014).
[2] T. Kihara *et al.*, PRB 99, 064430 (2019).
[3] H. Nakano *et al.*, JPSJ 87, 123702 (2018).
[4] A. Koga *et al.*, PRL 84, 4461 (2000).
[5] W. Zheng *et al.*, PRB 65, 014408 (2001).

Theoretical study for superconductivity in multilayer cuprates with two-particle self-consistent approach

Kazutaka NISHIGUCHI
Graduate School of Engineering Science, Osaka University,
Toyonaka, Osaka 560-8531
Graduate School of Science, Technology, and Innovation, Kobe University,
Nada-ku, Kobe 657-8501

In this report, the main result of "Theoretical study for superconductivity in multilayer cuprates with two-particle self-consistent approach" in 2018 fiscal year with using the supercomputer at ISSP is presented.

Superconductivity arising from layer differentiation in multilayer cuprates [1]

One salient feature in cuprate superconductors is that, if we look at representative homologous series, e.g., Hg-based multi-layer cuprates $HgBa_2Ca_{n-1}Cu_nO_{2n+2+\delta}$ [called Hg-12$(n-1)n$], where n is the number of CuO_2 layers within a unit cell and δ is the doping, the superconducting (SC) transition temperature T_c becomes the highest for multi-layer cases, which possess the highest T_c ($\simeq$ 135 K for Hg-1223) to date at ambient pressure. The CuO_2 plane can be described by the Hubbard model with on-site Coulomb repulsion along with electron hopping, where a competition between the itinerancy and localization of electrons takes place due to electron correlations. If we look more closely at the n-layer cuprates, T_c systematically depends on n for each homologous series: T_c increases for $1 \leq n \leq 3$ and decreases slightly and saturates for $n \geq 3$. To explain the superconductivity and other electronic properties, several pictures for the multi-layer superconductor have been theoretically proposed so far.

Recently, we have studied normal properties (carrier concentrations and magnetism) of OP and IP by investigating the three-layer Hubbard model as an effective model for Hg-1223, where we have employed the two-particle self-consistent (TPSC) approach for multi-layer systems [2]. When we applied this to the trilayer system, we first found that the concentration of hole carriers tends to be larger in OP than in IP with increasing on-site Coulomb repulsion, which is an electron correlation effect. Then the AF instability in the IP is shown to be always larger than in the OP. These results are consistent with the NMR results on the antiferromagnetism and carrier concentrations in OP and IP mentioned above. In particular, the many-body charge transfer between the OP and IP can be called a *self-doping effect*.

These have motivated us here to investigate the superconductivity itself in the multi-layer cuprates. Thus the present paper theoretically identifies the factors governing superconductivity in multi-layer cuprates with a three-layer Hubbard model in the TPSC approach. By solving the linearized Eliashberg equation for the gap function in a matrix form to examine the role of OP and IP, we shall show for the trilayer strongly correlated system that OPs dominate in the $d_{x^2-y^2}$-wave superconductivity, while IP dominates in the antiferromagnetism. This is caused by electron correlations because the crucial factor for the differentiated doping rates between OPs and IP, i.e. the self-doping effect, takes place in intermediate and strong correlation regimes.

Physically, the self-doping makes the strengths

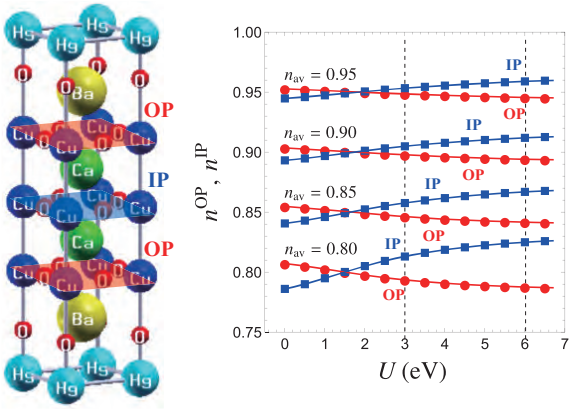

Figure 1: (Left) Crystal structure of Hg-1223 with two OPs and one IP in an unit cell. (Right) TPSC result for the layer fillings in the OP and IP, respectively, against the on-site Hubbard interaction U for various values of the average filling n_{av} = 0.95-0.80.

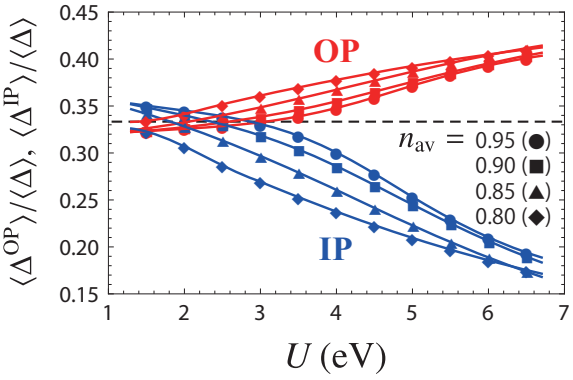

Figure 2: Weights of the OP and IP gap functions, $\langle\Delta^{OP}\rangle/\langle\Delta\rangle$ (red symbols) and $\langle\Delta^{IP}\rangle/\langle\Delta\rangle$ (blue), against the on-site Hubbard interaction U for various values of the average filling n_{av} = 0.95–0.80. The black horizontal line marks 1/3.

of electron correlation different between OP and IP: the AF spin fluctuations in the IP are stronger than in the OP due to the layer filling closer to half-filling in the IP, while the quasiparticle density of states (DOS) is reduced for the same reason around the antinodal regions in the IP, suppressing the $d_{x^2-y^2}$-wave superconductivity. We also show that, although the off-diagonal (inter-layer) elements in the gap function matrix are tiny, the inter-layer pair scattering processes are actually at work in enhancing T_c by comparing the results when these processes are turned on and off. We further reveal that the trilayer system has higher T_c than the single-layer system in the weak and intermediate correlation regimes due to the differentiation between OP and IP in a regime of the on-site Hubbard interaction U that includes those estimated for the cuprates. The present results are qualitatively consistent with NMR experiments in multi-layer cuprates superconductors.

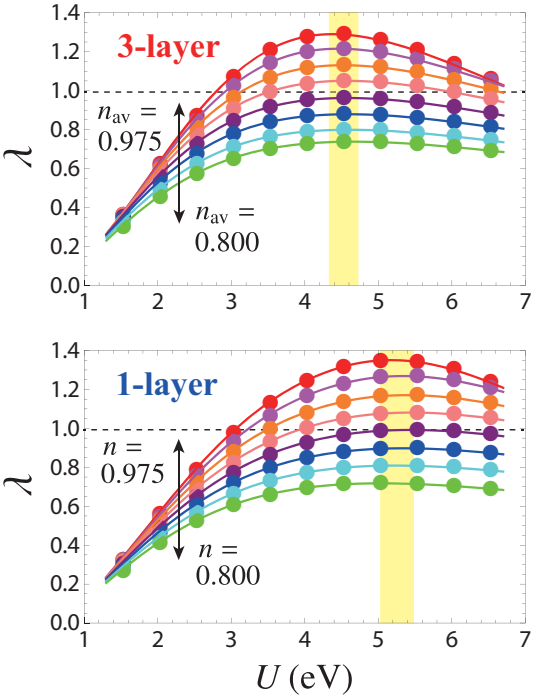

Figure 3: Eigenvalue λ of the linearized Eliashberg equation against the Hubbard interaction U for three-layer and single-layer Hubbard models for various values of the average filling $n_{(av)}$ = 0.800–0.975. Peak positions are marked with a yellow shading in each panel.

References

[1] K. Nishiguchi, S. Teranishi, K. Kusakabe, and H. Aoki: Phys. Rev. B **98** 174508 (2018).

[2] K. Nishiguchi, S. Teranishi, and K. Kusakabe: J. Phys. Soc. Jpn. **86** 184707 (2017).

Numerical Study of One Dimensional Frustrated Quantum Spin Systems

Kazuo HIDA
Professor Emeritus, Division of Material Science, Graduate School of Science and Engineering Saitama, Saitama 338-8570

1 Model

We investigate the ground state phases of spin-1 distorted diamond chains described by the following Hamiltonian:

$$\mathcal{H}_{\rm B} = \sum_{l=1}^{N}\Big[(1+\delta)\boldsymbol{S}_l\boldsymbol{\tau}_l^{(1)} + (1+\delta)\boldsymbol{\tau}_l^{(1)}\boldsymbol{S}_{l+1} + (1-\delta)\boldsymbol{S}_l\boldsymbol{\tau}_l^{(2)} + (1-\delta)\boldsymbol{\tau}_l^{(2)}\boldsymbol{S}_{l+1} + \lambda\boldsymbol{\tau}_l^{(1)}\boldsymbol{\tau}_l^{(2)}\Big], \quad (1)$$

where $\boldsymbol{S}_l$, $\boldsymbol{\tau}_l^{(1)}$, $\boldsymbol{\tau}_l^{(2)}$ are spin-1 operators. The lattice structure is depicted in Fig. 1.

The overall ground state phase diagram is discussed in the activity report of last year. Also, the undistorted case is discussed in detail in ref. [1]. These works show that this model has a nonmangetic ground state in the appropriate range of parameters. In the present work, we show that this phase consists of at least two topologically distinct phases based on analytical and numerical calculations.

2 Weak distortion regime ($\delta \simeq 0$)

In the absence of distortion, the ground state for $1.0727 \lesssim \lambda \lesssim 2.5773$ is a Haldane phase[1]. The ground state remains in the Haldane phase for weak distortion, since nondegenerate gapped states are generally robust against weak distortions. This phase is a symmetry protected topological phase with half-integer edge spins.

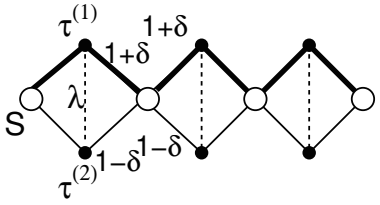

Figure 1: Structure of the distorted diamond chain (1).

3 Strong distortion regime ($\delta \simeq 1$)

For $\delta = 1$ and $\lambda = 0$, the whole system is decomposed into two parts. One is a single spin-1 chain of length $2N$ consisting of $\boldsymbol{S}_l$ and $\boldsymbol{\tau}_l^{(1)}$ with exchange constant $2J$ described by the Hamiltonian

$$\mathcal{H}_0 = \sum_{i=1}^{2N} 2J\boldsymbol{\sigma}_l\boldsymbol{\sigma}_{l+1}, \quad (2)$$

where $\boldsymbol{\sigma}_{2l} = \boldsymbol{\tau}_l^{(1)}$ and $\boldsymbol{\sigma}_{2l+1} = \boldsymbol{S}_l$. The ground state of the Hamiltonian (2) is a Haldane state. The remaining part is N isolated spins $\boldsymbol{\tau}_l^{(2)}$.

For small $1-\delta$ and λ, the spins $\boldsymbol{\tau}_l^{(2)}$ interact with each other mediated by the fluctuation in the chain (2). We estimate the effective interaction $J_{\rm eff}$ using eigenvalues and eigenvectors of the finite length spin-1 chains (2) with $2N = 8, 10$ and 12 obtained by numerical diagonalization. After the extrapolation to $N \to \infty$, we find that $J_{\rm eff}$ is positive for

$$0.594 \gtrsim \frac{1-\delta}{\lambda} \gtrsim 0.416. \quad (3)$$

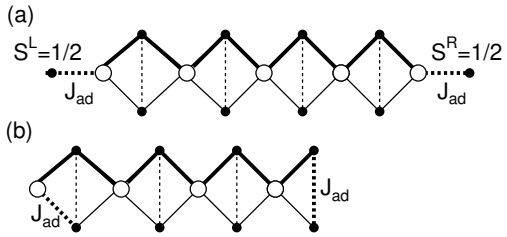

Figure 2: Structures of the distorted diamond chains used for the calculation of the energy gaps (a) $\Delta_{\rm H}$ and (b) $\Delta_{\rm DH}$ in the nonmagnetic phase.

Hence, the ground state of the chain consisting of spins $\boldsymbol{\tau}_l^{(2)}$ is a nonmagnetic Haldane state in the region (3). As a whole diamond chain, this corresponds to a double Haldane state[2, 3] that consists of two coupled chains each with Haldane ground state. This ground state is topologically trivial.

4 Numerical calculation

To distinguish these two phases, we carry out the finite size DMRG calculation to estimate the energy gap with structures H and DH depicted in the Figs. 2(a) and (b), respectively. Then, the energy gap $\Delta_{\rm H}$ in the Haldane phase should be finite for the structure H, and the energy gap $\Delta_{\rm DH}$ in the double Haldane phase should be finite for the structure DH.

The numerical results for $\delta = 0.5$ and 0.6 are shown in Fig. 3(a) and (b), respectively. We set the edge coupling $J_{\rm ad} = 1$. In the nonmagnetic phase, the scaled gaps $N_{\rm s}\Delta_{\rm H}$ and $N_{\rm s}\Delta_{\rm DH}$ are shown for several values of $N_{\rm s}$ by open symbols where the $N_{\rm s}$ is the number of spins including the additional spins. In the ferrimagnetic phases, the spontaneous magnetization per spin m is plotted for $N_{\rm s} = 72$.

For $\delta = 0.5$, the whole nonmagnetic phase belongs to the Haldane phase, since the scaled gap $N_{\rm s}\Delta_{\rm H}$ increases with the system size as shown in Fig. 3(a). On the other hand, for $\delta = 0.6$, the whole nonmagnetic phase belongs to the double Haldane phase, since the scaled gap $N_{\rm s}\Delta_{\rm DH}$ increases with the system size as shown in Fig. 3(b).

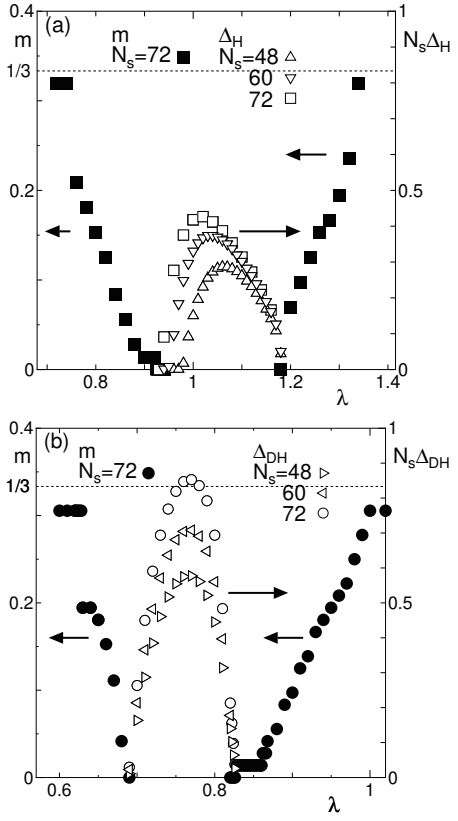

Figure 3: Spontaneous magnetization m, scaled energy gaps $N_{\rm s}\Delta_{\rm H}$ and $N_{\rm s}\Delta_{\rm DH}$ for (a) $\delta = 0.5$ and (b) $\delta = 0.6$.

References

[1] K. Hida and K. Takano: J. Phys. Soc. Jpn. **86**, 033707 (2017).

[2] T. Hikihara, J. Phys. Soc. Jpn. **71** 319 (2002) and references therein.

[3] A. K. Kolezhuk and U. Schollwöck, Phys. Rev. B **65**, 100401 (2002) and references therein.

Theory of multiple spin density waves and magnetic skyrmions in frustrated itinerant magnets

Takashi UCHIDA
Hokkaido University of Science
4-1, 7-15, Maeda, Teine-ku, Sapporo 006-8585

Magnetic skyrmions are topologically stable vortex-like magnetic structures with the spin directions distributing in all directions. Typically, the magnetic skyrmions emerge as 3Q multiple helical spin density waves in the Dzyaloshinskii-Moriya (DM) interaction driven systems under magnetic field. Recently, frustrated systems without the DM interaction have been found to reveal magnetic skyrmions [1, 2]. In order to explore theoretically the possibility of magnetic skyrmions in the frustrated itinerant systems without the DM interactions, we have applied the molecular spin dynamics (MSD) method [3] to the triangular-lattice single-band Hubbard model.

The MSD method is based on the functional integral method for the spin fluctuation theories and the isothermal molecular dynamics method. The method allows us to find automatically the magnetic structure of a large system with thousands of atoms in a unit cell at finite temperatures. Starting from the Hamiltonian expressed in terms of the locally rotated coordinates and by adopting the static approximation to the functional integral technique, the MSD method reduces to the generalized Hartree-Fock approximation at the ground state.

In the numerical calculations the most time-consuming process is the magnetic force calculation at each time step, where the local electronic structures are calculated in real space by means of the recursion method. We have adopted the automatic parallel calculation scheme and found it to be effective in saving both computing time and CPU resources.

We have performed the magnetic structure calculations on the supercell with $n \times n$ ($n = 20, 40$) triangular lattice, which is embedded in a large cluster consisting of 3×3 supercells, each of which are connected by the periodic boundary condition. Under zero magnetic field and the fixed value of the temperature $T/t = 0.001$, we have changed the Coulomb interaction strength U/t and the electron number n. For $n = 0.80 \sim 1.10$, the 120°-structure based complex magnetic structures were found. Of these, the main components for $U/t = 5$ and $n = 0.95$, $U/t = 6 \sim 8$ and $n = 0.95 \sim 1.05$, $U/t = 9$ and $n = 0.95$, $U/t = 10$ and $n = 1.05$ were found to be 3Q states, where the three Q vectors are directed along the axes of the triangular lattice. Although the skyrmion-like features can be seen in these 3Q states, the skyrmion lattice was not detected in the present results. In order to investigate the possibility of realizing the skyrmion lattice, the magnetic structure calculations near the ferromagnetic boundary ($n \sim 1.3$) are now in progress.

References

[1] T. Okubo, S. Chung, and H. Kawamura: Phys. Rev. Lett. **108** (2012) 017206

[2] Y. kakehashi, D. Koja, T. Olonbayar, and H. Miyagi: J. Phys. Soc. Jpn. **87** (2018) 094712.

[3] Y. Kakehashi, S. Akbar, and N. Kimura: Phys. Rev. B**57** (1998) 8354.